TKK Dissertations 111
Espoo 2008

MAGNETODYNAMIC VECTOR HYSTERESIS MODELS FOR STEEL LAMINATIONS OF ROTATING ELECTRICAL MACHINES

Doctoral Dissertation

Emad Ali Dlala

Helsinki University of Technology
Faculty of Electronics, Communications and Automation
Department of Electrical Engineering

TKK Dissertations 111
Espoo 2008

MAGNETODYNAMIC VECTOR HYSTERESIS MODELS FOR STEEL LAMINATIONS OF ROTATING ELECTRICAL MACHINES

Doctoral Dissertation

Emad Ali Dlala

Dissertation for the degree of Doctor of Science in Technology to be presented with due permission of the Faculty of Electronics, Communications and Automation for public examination and debate in Auditorium S4 at Helsinki University of Technology (Espoo, Finland) on the 11th of April, 2008, at 12 noon.

Helsinki University of Technology
Faculty of Electronics, Communications and Automation
Department of Electrical Engineering

Teknillinen korkeakoulu
Elektroniikan, tietoliikenteen ja automaation tiedekunta
Sähkötekniikan laitos

Distribution:
Helsinki University of Technology
Faculty of Electronics, Communications and Automation
Department of Electrical Engineering
P.O. Box 3000
FI - 02015 TKK
FINLAND
URL: http://sahko.tkk.fi/en/
Tel. +358-9-4511
E-mail: emad.dlala@tkk.fi

ISBN 978-951-22-9276-9
ISBN 978-951-22-9277-6 (PDF)
ISSN 1795-2239
ISSN 1795-4584 (PDF)
URL: http://lib.tkk.fi/Diss/2008/isbn9789512292776/

TKK-DISS-2448

Picaset Oy
Helsinki 2008

ABSTRACT OF DOCTORAL DISSERTATION	HELSINKI UNIVERSITY OF TECHNOLOGY P.O. BOX 1000, FI-02015 TKK http://www.tkk.fi

Author: Emad Ali Dlala

Name of the dissertation:
Magnetodynamic Vector Hysteresis Models for Steel Laminations of Rotating Electrical Machines

Manuscript submitted 3 December 2007	Manuscript revised 28 February 2008

Date of the defense 11 April 2008

☐ Monograph ☒ Article dissertation (summary + original articles)

Faculty: Faculty of Electronics, Communications and Automation
Department: Electrical Engineering
Field of research: Electrical Machines
Opponent(s): Prof. Oriano Bottauscio
Supervisor: Prof. Antero Arkkio
Instructor: Dr. Anouar Belahcen

Abstract

This thesis focuses on the modeling and prediction of iron losses in rotating electrical machines. The aim is to develop core loss models that are reasonably accurate and efficient for the numerical electromagnetic field analysis. The iron loss components, including hysteresis, classical eddy-current, and excess losses, are determined by modeling the dynamic hysteresis loops, whereby the incorporation of the core losses into the field solution is feasible and thus the influence of the core losses on the performance of the machine is investigated.

The thesis presents a magnetodynamic vector hysteresis model that produces not only an accurate, overall prediction of the iron losses, but also explicitly models the magnetization behavior and the loop shapes. The model is found to be efficient, stable, and adequate for providing accurate predictions of the magnetization curves, and hence iron losses, under alternating and rotating flux excitations. It is demonstrated that the model satisfies the rotational loss property and reproduces the shapes of the experimental loops. In addition, a more simplified, efficient, and robust version of the magnetodynamic vector hysteresis model is introduced.

The thesis also aims to analyze the convergence of the fixed-point method, examine the barriers behind the slow convergence, and show how to overcome them. The analysis has proved useful and provided sound techniques for speeding up the convergence of the fixed-point method.

The magnetodynamic lamination models have been integrated into a two-dimensional finite-element analysis of rotating electrical machines. The core losses of two induction motors have been analyzed and the impact of core losses on the motor characteristics has been investigated. The simulations conducted reveal that the models are relatively efficient, accurate, and suitable for the design purposes of electrical machines.

Keywords: iron loss, vector hysteresis, ferromagnetic, magnetodynamic, eddy currents, electrical steel, finite element, rotating electrical machines

ISBN (printed) 978-951-22-9276-9	ISSN (printed) 1795-2239
ISBN (pdf) 978-951-22-9277-6	ISSN (pdf) 1795-4584
Language: English	Number of pages 165p.

Publisher Department of Electrical Engineering, Helsinki University of Technology

Print distribution Department of Electrical Engineering, P.O. Box 3000 FI-02015 TKK, Finland

☒ The dissertation can be read at http://lib.tkk.fi/Diss/2008/isbn9789512292776/

Preface

This research work has been conducted during the period between May 2005 and December 2007 at the Laboratory of Electromechanics, Helsinki University of Technology (Laboratory of Electromechanics has recently become part of the Department of Electrical Engineering, Faculty of Electronics, Communications and Automation). First of all, I would like to thank God for giving me the health and strength to do this work and for having made it possible to finish this thesis.

I would like to express my sincere gratitude to my supervisor, Prof. Antero Arkkio, for his constructive supervision, devoted expertise, and critical comments. The support and encouragement of the head of the laboratory, Prof. Asko Niemenmaa, are highly appreciated. I gratefully thank Dr. Anouar Belahcen for constant help, shared knowledge, and unforgettable discussions. I would also like to acknowledge the role played by Dr. Julius Saitz at the beginning of my research. Thanks go to all the staff members of the laboratory for creating a warm atmosphere and for their cheerful assistance. In particular, I am thankful to Mr. Ari Haavisto and Mrs. Marika Schröder for their help in various matters.

From outside the laboratory, I wish to thank Prof. Sergey Zirka for the beneficial discussions we had during my visit to the Wolfson Centre for Magnetics, University of Cardiff, UK. I also thank the staff members of the Seventh of April University, Libya for motivating me to carry out the doctoral degree. I am grateful to the following organizations for their financial support: the Fortum Foundation, the Finnish Cultural Foundation, and the Academy of Finland.

I owe the completion of this thesis to many people in my life. My friends here in Finland, Libya, and elsewhere have been notable for their sharing of experience, knowledge, and nice sense of humor. They are too numerous to name and I simply owe a debt of gratitude to all of them.

My deep thanks go to all the members of my dear family. Even though they were distant, they were amazingly helpful and likewise made tremendous contributions. I am especially grateful to my mother, Shaalia, and father, Ali, who greatly motivated me and provided real non-stop sacrifices; without them I could never have made it through the tough times. My dearly beloved brothers, sisters, nephews, nieces, cousins, and all my relatives are wholeheartedly acknowledged for their continuous support, kindness, and care.

Finally, I would like to deeply thank two people who are very special to me: my wife, Widad, and my daughter, Hayat. Their love, smiles, and support have been a wonderful source of inspiration and challenge.

Espoo, March 2008
Emad Dlala

Contents

List of Publications

This thesis consists of an overview and of the following publications:

P1. Dlala, E., Saitz, J., Arkkio, A., "Hysteresis modeling based on symmetric minor loops", *IEEE Transactions on Magnetics*, Vol. 41(8): 2343-2348, August 2005.

P2. Dlala, E., Saitz, J., Arkkio, A., "Inverted and forward Preisach models for numerical analysis of electromagnetic field problems", *IEEE Transactions on Magnetics*, Vol. 42(8): 1963-1973, August 2006.

P3. Dlala, E., Arkkio, A., "Measurement and analysis of hysteresis torque in a high-speed induction machine", *IET Electric Power Applications*, Vol. 1(5): 737-742, September 2007.

P4. Dlala, E., Belahcen, A., Arkkio, A., "Magnetodynamic vector hysteresis model of ferromagnetic steel laminations", *Physica B: Condensed Matter*, Vol. 403(2-3): 428-432, February 2008.

P5. Dlala, E., Belahcen, A., Arkkio, A., "Efficient magnetodynamic lamination model for two-dimensional field simulation of rotating electrical machines", *Journal of Magnetism and Magnetic Materials*, to be published, in press, January 2008.

P6. Dlala, E., Belahcen, A., Arkkio, A., "Locally convergent fixed-point method for solving time-stepping nonlinear field problems", *IEEE Transactions on Magnetics*, Vol. 43(11): 3969-3975, November 2007.

P7. Dlala, E., Belahcen, A., Arkkio, A., "A fast fixed-point method for solving magnetic field problems in media of hysteresis", *IEEE Transactions on Magnetics*, to be published, in press, January 2008.

P8. Dlala, E., Arkkio, A., "Analysis of the convergence of the fixed-point method used for solving nonlinear rotational magnetic field problems", *IEEE Transactions on Magnetics*, to be published, in press, January 2008.

Author's Contribution

Throughout this research, the author of the thesis shared numerous valuable discussions with Prof. Antero Arkkio and Dr. Anouar Belahcen. At the beginning of the research, the author received assistance from Dr. Julius Saitz on the topic of hysteresis modeling. The author improved the finite-element code written by Dr. Saitz in Matlab. Thereafter, because of its great simplifications and the slow speed of Matlab, the author abandoned the Matlab code and turned to a more specialized and efficient finite-element code of rotating electrical machines. The code is written in Fortran and known as FCSmek. It was originally developed by Prof. Arkkio and is continuously being improved by various researchers in the Laboratory of Electromechanics. Before the start of this thesis, only single-valued magnetization curves were available in FCSmek. In order to incorporate hysteresis and eddy-current models, the author had to modify FCSmek and change its Newton-Raphson formulation to the fixed-point formulation. In the early stages, Dr. Belahcen and Prof. Arkkio assisted the author in modifying FCSmek. The hysteresis and eddy-current models were implemented solely by the author of the thesis.

The ideas and background of the published articles are mainly attributed to the first author, and they can be summarized as follows:

P1. The paper was developed and written by the first author. The co-authors contributed to the paper through shared discussion and comments.

P2. The paper was developed and written by the first author. The second co-author contributed to the paper by commenting on an earlier draft. The third co-author imparted his knowledge and expertise in the field of electrical machines.

P3. The paper was developed and written by the first author. The co-author contributed to the paper by sharing knowledge and providing assistance in the measurements.

P4. The paper was developed and written by the first author. The second co-author contributed by sharing work in the implementation of the one-dimensional finite-element model. The third co-author contributed by giving valuable comments.

P5. The paper was developed and written by the first author. The second and third co-authors contributed by providing critical comments. The third co-author also provided the experimental data on the core losses of the induction machine.

P6. The paper was developed and written by the first author. The co-authors contributed to the paper by giving valuable comments.

P7. The paper was developed and written by the first author. The co-authors contributed to the paper by giving valuable comments.

P8. The paper was developed and written by the first author. The co-author contributed to the paper by revising it.

List of Notations

Symbols

$\boldsymbol{A}$	magnetic vector potential
A	z-component of the magnetic vector potential
$\boldsymbol{a}_\mathrm{n}$	nodal values of the magnetic vector potential of the 2D finite-element method
$\boldsymbol{a}$	magnetic vector potential of the 1D model
a_φ	magnetic vector potential in the direction of $\boldsymbol{e}_\varphi$
a_0, a_1, a_2	polynomial coefficients of the function v
$\boldsymbol{B}$, B	magnetic flux density
B_φ	geometric projection of $\boldsymbol{B}$ in the direction of $\boldsymbol{e}_\varphi$
B_m	peak of the magnetic flux density
B_s	saturation value of the magnetic flux density
B_x	magnetic flux density component of the x-axis
B_y	magnetic flux density component of the y-axis
B_z	magnetic flux density component of the z-axis
$\boldsymbol{b}$	input of multidimensional iterative function
$\boldsymbol{C}$	matrix associated with the circuit equations of electrical machines
C	convergence factor of the fixed-point iteration
C_0	fitting parameter of the excess loss
$\boldsymbol{D}$	matrix associated with the circuit equations of electrical machines
d	thickness of the lamination
$\boldsymbol{E}$, $\bar{\boldsymbol{E}}$	matrices associated with the circuit equations of electrical machines
E	Everett function
$\boldsymbol{e}_\varphi$	unit vector along φ
F_dy	dynamic hysteretic function for the magnetodynamic vector hysteresis model
F_st	static hysteretic function for the vector hysteresis model
f	frequency
$\boldsymbol{G}$	multidimensional iterative function
$\boldsymbol{H}$, H	magnetic field strength
H_φ	magnetic field strength component in the direction of $\boldsymbol{e}_\varphi$
H_st	static hysteretic function

H_x	magnetic field strength component of the x-axis
H_y	magnetic field strength component of the y-axis
H_z	magnetic field strength component of the z-axis
h_a	increasing magnetic field input of the Preisach operator
h_b	decreasing magnetic field input of the Preisach operator
$\boldsymbol{i}$	current of the stator phases
$\boldsymbol{K}$	matrix associated with the connection of electrical machines
k	iteration index
$\boldsymbol{M}$, M	magnetization or magnetization-like quantity
m	number of real dimensions
N	number of directions in the vector hysteresis model
N_e	number of finite elements in the lamination model
N_n	total number of nodes in the 2D mesh
n	time-stepping index
$\boldsymbol{P}$	column associated with the fixed-point formulation of the 2D finite-element method
P	element in the column $\boldsymbol{P}$
P^c	average power core loss
P^in	average input power of the stator
P^out	average output power of the shaft
$P_\mathrm{r}^\mathrm{res}$	average resistive power loss of the rotor cage
$P_\mathrm{s}^\mathrm{res}$	average resistive power loss of the stator winding
p	parameter related to the dependency of the excess loss on frequency
Q	coefficient associated with the identification of the magnetodynamic model
r	magnetic resistivity of the excess loss
$\boldsymbol{S}$, $\bar{\boldsymbol{S}}$	global coefficient matrix of the 2D finite-element method
S	element in the global coefficient matrix $\boldsymbol{S}$
s	slip
T	time period
t	time
$\boldsymbol{u}$	voltages of the rotor circuit
$\boldsymbol{V}$	line voltages of the stator
v	function controlling the classical eddy-current loss
W_cl	classical eddy-current energy loss
W_ex	excess energy loss
W_hy	hysteresis energy loss
W_tot	total iron energy loss
w	parameter responsible for the loop shapes in the vector hysteresis model

α	phase lag between the vectors $\boldsymbol{H}$ and $\boldsymbol{B}$
β	contraction factor
δ	switching operator in the vector hysteresis model
δ_{e}	switching operator in the simplified magnetodynamic model
η	scaling factor of the first-order reversal curves
γ	relay operator of the Preisach model
Λ	shape function
λ	eigenvalue of the matrix $\boldsymbol{G}$
μ	distribution function of the Preisach model
ν_{FP}	fixed-point coefficient
Ω	cross-section of the machine geometry
ψ	phase shift in the projections of the vector hysteresis model
ρ	spectral radius of the matrix $\boldsymbol{G}$
σ	electrical conductivity
τ	constant used in the analysis of the fixed-point method
θ_B	polar angle that specifies the direction of $\boldsymbol{B}$
φ	angle between the directions of the vector hysteresis model

Abbreviations

GCM	global-coefficient method
LCM	local-coefficient method
MDVH	magnetodynamic vector hysteresis
NRM	Newton-Raphson method
PWM	pulse-width modulation

List of Figures

List of Tables

Chapter 1

Introduction

The characteristics of magnetic materials are important to the performance and efficiency of electrical devices. In practice, this importance is given considerable attention and is well recognized. It is no surprise, therefore, that the analysis of iron losses in electrical machines has been investigated over many decades.

The magnetic flux patterns appearing in an electrical machine are complicated and, thus, hinder the development of adequate methods. Traditionally, the complexity has been grossly reduced to the use of highly simplistic techniques for the prediction of the iron loss. These techniques are widely believed to provide reasonable results, but their limitations and imperfections in generally obtaining accurate results are commonly acknowledged.

Despite the great amount of research done into the problem, achieving accurate prediction of iron losses remains difficult and distant. The key factors that emerge as profound barriers to success are the complicated microstructure of the magnetic materials, the interdependency of various physical phenomena, and the lack of reliable experimental data. These factors have directly influenced the discovery of suitable methods for predicting iron losses and have rather led to the use of simple techniques. The popular approach adopted for calculating iron losses conventionally employs a post-processing formula of the magnetic field solution. This approach is often based upon an empirical procedure to separate the three main loss phenomena: the hysteretic properties of the material, macro eddy currents induced by a varying magnetic flux, and the mechanism responsible for the excess loss.

On the other hand, it is well known that obtaining accurate estimation of iron losses requires the development of models that are able to predict the magnetization curves and loop shapes accurately, whereby the iron loss is simply determined from the loop area. This thesis is developed from the latter notion. The goal is to develop advanced methods for the prediction of the magnetodynamic vector hysteretic behavior observed in the cores of electrical machines. The new methods are identified and validated with experimental results.

1.1 Aim of the Thesis

The general aim of the thesis is to develop adequate methods for the prediction of the magnetodynamic vector hysteresis behavior observed in the cores of electrical machines, using the numerical electromagnetic field analysis. The methods to be developed are aimed to predict the core losses accurately as well as incorporate the core losses into the magnetic field analysis. The stability and efficiency of the developed methods are carefully considered.

1.2 Scope of the Research

With the aid of more powerful computers, advanced numerical techniques have been exploited to analyze and study electromagnetic field problems. The suitable numerical technique that is presently prevalent is the finite-element method. This mathematical tool is utilized to discretize Maxwell equations in order to solve the magnetic field in complicated geometries such as electrical machines. The progress in research has also made it possible to incorporate iron losses into the overall modeling of the magnetic field. However, as a result of the complexity of the iron loss phenomena, the problem of the loss determination has not yet been satisfactorily solved and remains a challenging task.

Electrical machine cores are usually made of laminated materials in order to limit the eddy-current loss induced. The eddy-current loss in the lamination intrinsically creates a three-dimensional (3D) problem, which can be reduced to a 1D problem for the lamination depth if the edge effects are neglected. The 3D analysis is not considered here because of its high computation time, especially if magnetic material models are used.

Practically, it is difficult to deal with iron losses in a rotating electrical machine because of the complicated geometry and the unwanted phenomena that occur. The steel laminations of the electrical machine can be provided by the manufacturer in order to study them conveniently. In principle, any model developed for estimating the iron loss of the lamination can be applied to electrical machines. The flux patterns that occur in an electrical machine must be investigated.

Because the core loss phenomena are interdependent and cannot be simply kept apart, an accurate and systematic approach would employ a magnetodynamic model that physically links the three loss phenomena. Such a model is seemingly ideal; however, it is difficult to develop under complicated magnetic field conditions. Moreover, modeling vector hysteresis is still regarded as a new subject and one that is subject to much speculation, even under quasi-static fields. Therefore, modeling the magnetodynamic losses under rotational fields creates a problem of considerable difficulties.

From the designer's point of view, the accurate but inefficient modeling of core losses is usually undesirable. Machine designers must find the material modeling capabilities of the software packages adequate for most of their everyday design purposes, or else they would not be so interested in using these packages. These goals may conflict, however.

For example, a rapidly convergent method for solving nonlinear field problems may not be stable for certain problems. On the other hand, a robust method may also be the slowest. Trade-offs between accuracy, robustness, and speed are central issues in numerical analysis. They receive careful consideration in this thesis.

1.3 Scientific Contributions

This thesis has made scientific contributions in various aspects of the areas of magnetic material modeling and the electromagnetic field analysis of electrical machines. The main new findings and contributions are summarized as follows:

1. A new magnetodynamic vector hysteresis model for predicting the characteristics of the magnetic material is introduced. The model is based upon the well-known Mayergoyz model. Unlike the Mayergoyz model, the new model satisfies the rotational loss property, can be applied in a wide range of frequencies, and reproduces the experimental data of the loop shapes. A simple identification method is also proposed for the model [P4].

2. An efficient magnetodynamic lamination model for the 2D finite-element analysis of rotating machines is proposed. The model consists of two coupled iterative procedures [P5].

3. A simplified version of the magnetodynamic vector hysteresis model is proposed that is more efficient, stable, and accurate. The simplified model requires no solution of the 1D diffusion equation.

4. Three static hysteresis models and their inverted versions are discussed. Unlike the conventional models, the models studied compute the output quantity (the magnetic field strength) directly, and thus, they can be conveniently incorporated into a finite-element method [P1-P3].

5. A novel method for accelerating the convergence of the fixed-point technique is proposed. The method secures a locally convergent iteration and enforces a small contraction factor for fast convergence [P6-P8].

6. The aforementioned models are implemented in finite-element analysis of electrical machines. The models are validated by measurement where the core losses of two induction motors are predicted [P2,P3,P5].

Most of these scientific contributions have been published in journals [P1-P8]. Recently, the magnetodynamic vector hysteresis model and its simplified version have been further extended in the thesis. Two articles about these extensions, to be submitted to a journal, are still under way.

1.4 Outline of the Thesis

The thesis is organized in the following manner:

- Chapter 1 forms an introductory part to the thesis and ponders the scope and aim of the research. The question why this work has been carried out is answered. The main scientific contributions of the thesis are highlighted.
- Chapter 2 provides background to the topics of hysteresis modeling, eddy-current effects, and iron loss estimation. The chapter is intended to review and analyze the research relevant to the thesis.
- Chapter 3 introduces the magnetodynamic model of the lamination, one of the central topics of the thesis. The development of the models and their mathematical formulations and conditions are given. The identification problem and the accuracy of the models are discussed. The simulations and numerical results of iron losses are presented.
- Chapter 4 focuses on modeling the magnetic material behavior of rotating electrical machines. The 2D finite-element analysis of electrical machines is briefly described. The incorporation of the lamination model into the machine model and the resulting iterative procedure are dealt with. The convergence of the fixed-point method is analyzed. The numerical results of two induction motors are provided.
- Chapter 5 concludes the work of the dissertation. The ideas, aspects, and applications of the work are discussed and assessed.

Chapter 2

Review and Analysis of Relevant Research

This chapter provides a review of the articles written on the topics of hysteresis modeling, eddy-current effects, and iron loss estimation. The review is divided into three categories, each of which will treat a particular area. The first category discusses the behavior of iron losses and the simple techniques used for their prediction. The second category reflects on the advanced hysteresis and eddy-current models that are becoming increasingly employed. In the third category, the incorporation of the hysteresis and eddy-current models into the finite-element analysis of electrical machines is considered. There is a large number of published works in each area and it is impossible to go through all of them. Thus, only those that are fruitful and relevant to the thesis are selected.

2.1 Introduction

Magnetic field variation in ferromagnetic materials causes energy dissipation, a mechanism that is traditionally known as iron loss. The phenomenon has been observed since the eighteenth century [Bozorth (1951)], but, curiously, it has remained an object of study until today. Although there have been rather clear explanations of what seems to be a peculiarity, a definite procedure to determine iron losses is still not even near to being created. The complexity of the magnetization process makes the understanding of the energy profiles a tremendous challenge.

The inherent complexity of the magnetization process is a key factor affecting the invention of adequate models. The hypothesis of subdividing the magnetic material into magnetic domains interfaced through domain walls was successful in describing the magnetization process. The domains have been experimentally observed and thus they are there, but finding a perceptible explanation of the mechanisms responsible for the observed iron losses remains a challenge.

When the material is magnetized by the applied field, its state remains in local free energy minima and it cannot reach thermodynamic equilibrium; thus, hysteresis occurs and

the observation of hysteresis loops is the most distinctive fingerprint that characterizes hysteresis [Bertotti (1998)]. The lag between the applied magnetic field $\boldsymbol{H}$ with respect to the magnetization $\boldsymbol{M}$ appears as a result of ferromagnetic hysteresis, which causes energy dissipation. For more than a century, engineers and scientists have been conducting experimental work to interpret the phenomenon [Steinmetz (1984), originally published in 1890]. Meanwhile, several hysteresis models based on an understanding of physical or mathematical properties in a specific system of interest have been developed.

The microscopic structure of the material requires a search for meticulous mathematical approaches that, it is hoped, will bring successful results [Neel (1944); Fiorillo et al. (2002)]. However, the stochastic picture of the phenomenon is vague, and the idea of tackling the problem directly without the need to know much about the detailed descriptions appears to be productive [Bertotti (1998)].

Since ferromagnetic materials are conductive, eddy currents will be present wherever there is flux variation. An accurate description of the eddy-current loss needs to be based on a quantitative theory of domain wall dynamics [Bishop (1973)]. However, microscopic models may be useful for physicists but are difficult to apply for solving engineering problems, because of the large computation time.

2.2 Simple Models of Iron Loss

In practice, iron losses are often estimated empirically using methods that can be applied with caution [Steinmetz (1984); Lavers et al. (1978); Bertotti (1988); Fiorillo and Novikov (1990)]. In such a case, a post-processing formula is applied to the field solution for the loss calculation. In typical situations, the iron losses can be divided into either two or three components. The two-component methods split the total iron loss into hysteresis, W_{hy}, and eddy-current, W_{ed}, contributions [Jordan (1924); Lavers and Biringer (1976); Lavers et al. (1978); Amar and Kaczmarek (1995)]. The three-component methods of the statistical loss theory separate the eddy currents into classical, W_{cl}, and excess, W_{ex}, dynamic losses in addition to the hysteresis loss [Bertotti (1988); Fiorillo and Novikov (1990); Barbisio et al. (2004); Zirka et al. (2006b)].

The input data of the post-processing methods are the measured values of specific tests. Commonly, the materials are measured under a 1D alternating magnetic flux. The term "alternating" refers to the notion that the flux in the magnetized body is pulsating with time in one direction (unidirectional). The measurement techniques under an alternating flux are standardized and the relevant power loss figures of ferromagnetic materials are normally provided by the manufacturers (e.g. the Epstein test or single-sheet tester under sinusoidal excitation). These types of tests can provide reasonable results only in certain cases. For instance, in the core of a single-phase transformer, the magnitude of the local flux density vector varies with time in one direction. In other applications, such as in the cores of a rotating electrical machine and in the T-joints of a multi-phase transformer, the local magnetic flux density vector rotates within the electrical steel lamination plane. This

type of flux is known as the 2D rotating flux. Moreover, in more complex topologies, e.g. claw pole and transverse flux machines, the magnetic field may rotate in a real 3D space [Guo et al. (2005)].

The statistical loss theory of Bertotti (1988) states that under sinusoidal magnetization at frequency f, the behavior of the total loss in unit volume per cycle, $W_{\rm tot}$, follows the law

$$\begin{aligned} W_{\rm tot} &= W_{\rm hy} + W_{\rm cl} + W_{\rm ex} \\ &= W_{\rm hy} + \frac{\sigma d^2 \pi^2 B_{\rm m}^2}{6} f + C_0 B_{\rm m}^{1.5} f^{0.5} \end{aligned} \tag{2.1}$$

where $B_{\rm m}$ is the peak value of the flux density, d is the thickness of the lamination, σ is the electrical conductivity of the material, and C_0 is a fitting parameter. The classical term of (2.1) is resulted from Maxwell equations assuming a perfectly homogenous body with a unform flux distribution over the sheet. Thus, (2.1) holds only for low frequencies or low conductivities [Bertotti (1998)]. The quasi-static hysteresis loss $W_{\rm hy}$ can either be obtained experimentally or estimated.

However, the practical magnetic cores of electrical machines are subjected to a non-sinusoidal flux. In general, the main source of the flux distortion is the slotting and in other instances, such as in variable speed motors supplied by means of pulse-width-modulated (PWM) voltages, the driving circuit itself generates a non-sinusoidal flux. The two-component methods were modified to consider arbitrary flux waveforms and minor loops [Lavers et al. (1978); Amar and Kaczmarek (1995)]. Fiorillo and Novikov (1990) generalized the statistical loss law (2.1) by considering the dependence of the classical and excess losses on the magnetic flux derivative

$$W_{\rm tot} = W_{\rm hy} + \frac{\sigma {\rm d}^2}{12} \int_0^T \left(\frac{{\rm d}B}{{\rm d}t} \right)^2 {\rm d}t + C_0 \int_0^T \left| \frac{{\rm d}B}{{\rm d}t} \right|^{3/2} {\rm d}t \tag{2.2}$$

where T is the time period of the fundamental frequency component. Fourier analysis can also be performed on the flux density waveform in order to consider the contributions of the high harmonics. In the more recent work of Barbisio et al. (2004), a further generalization of (2.2) has been introduced to allow the prediction of iron losses in the presence of local minima (minor loops) by studying the time dependence of the flux. The efforts exerted on improving the separation loss principle are numerous [Atallah et al. (1992); Boglietti et al. (1998); Barbisio et al. (2004)], and valuable summaries of several of them can be found in [Saitz (1997); Ionel et al. (2006); Zirka et al. (2007)].

The prediction of core losses in electrical machines using the two-component methods and the three-component methods is a common practice. However, because of their limitations in the accurate prediction of rotational losses, the methods have been further generalized.

It has long been known that the behavior of iron losses under a rotating flux is quite different from that under an alternating flux. Baily carried out the first experimental work

on rotational hysteresis losses [Bozorth (1951)]. He was the first to observe the difference in the behavior of the measured quantities between the alternating and rotational losses. It was found that the rotational hysteresis loss increased with an increase in the peak of the flux density until some value near saturation, when it started to decrease quickly. After a long period, a qualitative analysis of the phenomenon based on the Weiss domain theory was given by Brailsford (1938), where disk samples and a torque-meter were used for the measurement.

Even though the statistical loss theory was originally derived for alternating field excitation, it has also been applied to the prediction of rotational losses, with the introduction of some correcting factors for the hysteresis loss [Fiorillo and Rietto (1990); Bertotti et al. (1991); Zhu and Ramsden (1998)]. The dynamic loss components are summed up for the x- and y-directions with certain modifications of the loss coefficients. It is not entirely clear how such an approach is applicable at a given rotational flux vector, since the characteristics of the core materials under various rotational magnetization patterns are complex and should be properly investigated.

2.3 Advanced Models of Magnetic Materials

The idea of the loss separation theory of iron losses is useful only in certain applications in which these losses are unimportant for the field analysis. In other words, in order to investigate the influence of the iron losses on the field solution, the incorporation of the losses into the field equations is needed. The accuracy of the calculation of iron losses is the second and more important objective of using advanced models. However, achieving these objectives requires models that can track the $\boldsymbol{B}$-$\boldsymbol{H}$ behavior accurately so that the iron losses are determined from the loop area. Following this path will guarantee not only the accuracy of the modeled core losses but also the accuracy of the modeled overall performance of the electrical device.

In the early period of the technical application, L. Rayleigh proposed a well-treated but simple model built upon basic analytical parameters [Bozorth (1951)]. P. Weiss made a more general description that even today is very useful in connection with the domain theory [Bozorth (1951)]. He hypothesized that a ferromagnetic material is composed of elementary dipoles, tiny polarized particles which orient themselves according to the field applied. Regions of similarly oriented dipoles form domains of polarization, and the overall magnetization depends on the relative extent of the positive and negative domains.

The Weiss theory was supported by Barkhausen, whose discovery led to the understanding of the irregularities of the magnetization process, known as the Barkhausen effect [Bozorth (1951)]. During a change in magnetization, a jump (noise) caused by the movement of magnetic domains or avalanches was recorded. Similar results obtained by Bozorth, Williams, and Shockley made visible for the first time the domain boundaries characteristic of unstrained iron [Bozorth (1951)].

Preisach (1935) developed a model for hysteresis in magnetic materials which strad-

dles the boundary between physics and mathematics. The mathematical properties of the model have been investigated by Brokate (1989) and Visintin (1994), and many extensions and variations have been proposed. These extensions are often associated with the scientists Della Torre and Mayergoyz [Della Torre (2000); Mayergoyz (1991b)]. On the other hand, scientists such as Bertotti and Jiles have conducted significant research into the physics of hysteresis and micromagnetism [Bertotti (1998); Jiles (1998)].

It is difficult to divide hysteresis models into groups because the subject is heterogeneous and interconnected. For instance, when the magnetic field varies at a quasi-static rate, the models considered are referred to as rate-independent. This case, therefore, is reflected in the study of static and dynamic models of hysteresis, a subject that is especially investigated in this thesis. On the other hand, the treatment of magnetic hysteresis under alternating and rotational excitations generates another particular and important category of models often referred to as scalar and vector hysteresis models. In this thesis, those two categories, the vector models and the dynamic models, are studied, developed, and experimentally tested, and are one of the central goals of the thesis.

2.3.1 Static and Dynamic Iron Losses

It is common to use the word hysteresis to describe rate-independent (static) hysteresis only. Among several branches of hysteresis, rate-independent hysteresis has been the most studied subject because it is basic and more understandable. The term rate-independent hysteresis implies that the magnetization curves are independent of the field rate, which means that only the past input extrema leave their marks on the shape of the hysteresis curve. The rate of the applied field, however, plays an important role in changing the energy profiles of the system through the eddy-current losses, which modify the shape of the hysteresis loop and enlarge its area [Bertotti (1998)]. The magnetic losses are calculated from the loop area and, therefore, tracing the B-H behavior is of vital importance.

The measurement of a hysteresis loop is commonly conducted at low frequency (less than 1 Hz) and is sometimes referred to as DC, or quasi-static measurement. The aim is to segregate the hysteretic effects from the dynamic ones concerning the eddy-current and excess losses. The dynamic loop, however, is obtained as a result of conducting the measurement at a finite rate of excitation. In the modeling stage, using a static hysteresis model will ensure that the modeled loop is purely the hysteresis loop, not including the dynamic losses. On the other hand, modeling the dynamic loop will require the development of a rate-dependent (dynamic) hysteresis model. There is virtually no need for fields that vary quasi-statically to include the rate-dependent effects, i.e., the rate-independent theory is sufficient.

If the magnetization process is assumed to occur over a large scale in time and space, the classical eddy-current component can be obtained from the solution of Maxwell equations with the appropriate boundary conditions. When the material is linear and the

flux varies sinusoidally, this problem can be solved rather easily analytically [Gillott and Calvert (1965); Bertotti (1998)]. However, the introduction of arbitrary waveforms requires the solution of Maxwell equations numerically in time and space.

The eddy current in the lamination requires 3D formulations [Dular et al. (2003)]. However, if the edge effects are neglected, the problem can be rather simplified [Del Vecchio (1982b)]. In this respect, modeling the magnetodynamic effects of ferromagnetic steel sheets has been, and can be, done in various ways. The simplest way, perhaps, is to solve the diffusion equation (resulting from Maxwell equations) by assuming uniform flux distribution along the lamination depth [Bertotti (1998)]. Such an approach can easily lead to under- or overestimated results [Barbisio et al. (2004)]. An improved approach would model the eddy currents by solving the diffusion equation using single-valued reluctivity while neglecting the excess and hysteresis losses [Pippuri and Arkkio (2006)]. However, this approach is far from completion, because the core loss phenomena are interdependent and cannot be simply kept apart. The most accurate way achieved thus far solves the diffusion equation numerically and applies the hysteretic nonlinearity directly in the solution [Basso et al. (1997); Dupre et al. (1999); Serpico et al. (2000); Bottauscio et al. (2000a); Zirka et al. (2006b); Dlala et al. (2008c)].

Static hysteresis models

A great majority of the models found in the literature are static in nature, but some of them have been generalized to take the dynamic effects into account. The Preisach model, for example, was meant to account for rate-independent scalar hysteresis. The model was based on the theory of J. Ewing and others of his period [Bozorth (1951)]. It is not only because the Preisach model was a great invention that made it so popular, but what the model inherits and entertains from its physical, mathematical, and phenomenological composition has also impressed experts in the field.

The classical Preisach model represents the magnetization M by the following formula

$$M(t) = \iint\limits_{h_a \geq h_b} \mu(h_a, h_b)\, \gamma_{h_a h_b} H(t)\, dh_a\, dh_b \tag{2.3}$$

where $\gamma_{h_a h_b}$ is the relay operator. Here h_a and h_b correspond to increasing and decreasing values of the magnetic field input $H(t)$. The output $M(t)$ is determined by summing up the individual contributions of each relay operator $\gamma_{h_a h_b}$, weighted by a Preisach distribution function $\mu(h_a, h_b)$ and integrated over suitable values of h_a and h_b. The distribution function imposes an identification problem on the model and is commonly assumed to be the Lorentzian or Gaussian distribution of a few parameters to be adjusted.

The intrinsic characteristic of the model is the fulfilment of the Madelung rules stated by Madelung (1905) and restated by Zirka et al. (2004a): the return-point memory and the wiping-out property. Early in the 1950s and 60s, the Preisach model began to be a topic of interest for many researchers in the field [Bozorth (1951); Everett (1954); Bate (1962);

Biorci and Pescetti (1966)], but the model has experienced numerous developments, especially after the work of Pokrovskii and Kransoselskii (1983), who reconstructed the model in an elegant mathematical formulation. Many works followed latter that utilized the numerical computer revolution for implementing the model.

Mayergoyz attempted to thoroughly investigate the properties of the model, such as the wiping-out and congruency. His significant contribution to the static model was the numerical discrete formulation of the Preisach model with the Everett function. That was followed by a series of publications, such as the nonlinear model and the moving model, all meant to improve the accuracy and relax the congruency problem [Mayergoyz (1988b)]. The works of Mayergoyz and his collaborators led to the production of a reference book on the Preisach model [Mayergoyz (1991b)]. The book addresses many of the problems generally associated with mathematical models: identification techniques and numerical implementation, as well as the necessary and sufficient conditions for the representation of the Preisach model. More recently, the original well-known book, Mayergoyz (1991b), has been slightly expanded and updated in a new book, Mayergoyz (2003).

The static Preisach model, known as the classical Preisach model, has been extensively studied in the literature. Many of these studies have been associated with identifying the model, using various methods to improve the accuracy of the model [Wiesen and Charap (1988)]. In the work of Della Torre (1966), a moving Preisach model was proposed to generalize the congruency property. Kadar and Della Torre (1987) modified the classical Preisach model and introduced the Product model to improve the non-congruent observed curves. Later, the work of Kadar and Della Torre (1987) was expanded in several articles [Della Torre (2000)]. The congruency problem has been thoroughly explored by Zirka et al. (2004a). It is stated that as a result of the complexity of the problem, most of the existing techniques have not been consistently successful in overcoming the problem.

The modeling accuracy of the experimental Preisach model identified by the experimental reversal curves has been analyzed by Zirka et al. (2004a), Dlala et al. (2005), and Dlala et al. (2006). The experimental Preisach model is generally sensitive to the position of the reversal points and the model does not produce closed minor loops. These problems are associated with the identification method, specifically with the technique that employs the first-order reversal curves. On one hand, the classical Preisach model is endorsed by the return-point memory, but still it cannot reproduce the major loop or the first-order reversal curves accurately. On the other hand, the experimental Preisach model lacks the return-point memory but still reproduces the major loop and the first-order reversal curves exactly.

The rule of the return-point memory is often of more importance to the stability of the model. However, the magnetization behavior of all magnetic materials may deviate slightly from the rule as it is observed in experiments, where the Madelung rules hold true only to a certain extent. The latter phenomenon is known as accommodation. In the works of Della Torre (1987) and Della Torre (1994), a model of accommodation was proposed.

Naidu (1990) made a significant simplification that permitted the identification of the

static Preisach model from a major hysteresis loop, rather than measuring the first-order reversal curves. Recently, it has been demonstrated that the identification process of the Preisach distribution function can be accomplished with the aid of fuzzy logic and artificial neural networks [Adly and Abd-El-Hafiz (1998); Serpico and Visone (1998); Cirrincione et al. (2002); Dlala and Arkkio (2006)].

In spite of the dominance that the Preisach model has enjoyed over many years, there have been other hysteresis models that have shared its success and popularity. A thorough review of several different types of hysteresis models is given in the monograph of Ivanyi (1997).

Jiles and Atherton (1984, 1986) introduced another widely accepted model of hysteresis. The Jiles-Atherton model is based on certain assumptions regarding the domain wall motion and uses the magnetic energy balance, leading to a differential equation with five parameters to identify. The model produces sigmoid-shaped curves but it does not satisfy the Madelung rules because all the modeled curves bend towards saturation. Further attempts made to enforce the model to attain the return-point memory and produce closed minor loops have achieved limited success since they all require a priori knowledge of the field evolution [Jiles (1992)]. During the time when the Preisach model and the Jiles-Atherton model became popular, various publications were written to compare the two models [Philips et al. (1995); Pasquale et al. (1998, 1999); Benabou et al. (2004)]. It is stated that the attractive features of the Jiles-Atherton model are its speed and simplicity, whereas the Preisach model is characterized by accuracy and generality.

Hodgdon (1988) proposed a rate-independent hysteresis model that assumes a constitutive relationship between H and B given by a differential equation. In the work of Ossart et al. (1990), the Hodgdon model was compared with the experimental Preisach model. The Hodgdon model was found to be simple to implement and exhibits the accommodation of minor loops, but it requires a numerical integration and the identification is rather empirical in the choice of its parameters. On the other hand, the Preisach model was found to be more complex but, nonetheless, it reproduces the major loop and the experimental data more accurately.

Recently, Zirka et al. (2004a) proposed a history-dependent hysteresis model that is more accurate and general than all its predecessors. The model is partially analogous to the experimental Preisach model because it also employs a family of first-order reversal curves, and partly to the classical Preisach model because it satisfies the Madelung rules perfectly. It has been shown that the model reproduces the experimental data accurately since it generalizes the congruency problem and significantly improves the accuracy. The model is based on transplanting the particular pattern to be modeled from the first-order reversal curves, and the model stores previous reversals and hence is called the history-dependent hysteresis model. It is distinguished by its search for the pattern to be copied (shifted) over the whole B-H plane, not only in the horizontal direction (or in the vertical direction). The model is accurate but may require a lot of memory when applied in a finite-element code. Nevertheless, the model is efficient since it does not require any

integration. The model has been further generalized to account for accommodation in Zirka et al. (2005a), if needed.

Eddy-current and dynamic hysteresis models

The modeling of electromagnetic devices containing laminated magnetic cores requires an adequate description of the magnetic processes involved. The shape of the dynamic hysteresis loop has to be modeled, and hence the power iron loss is predicted under arbitrary magnetization conditions. This means that an impeccable, systematic procedure that starts from a static hysteresis model must be embraced with Maxwell equations. The excess loss related to the magnetic viscosity, which is also rate-dependent, needs to be included through the dynamization of the static model.

In the works of Bishop (1973, 1985), the effect of the domain arrangement on the eddy-current loss was studied in depth, but no concrete conclusion was reached. The problem is still too complicated to be treated on a microscopic level. Del Vecchio (1982b) stated that for non-oriented materials the iron losses can be well described by the diffusion equation

$$\frac{\partial^2 H}{\partial z^2} = \sigma \frac{\partial B}{\partial t} \tag{2.4}$$

where t is the time and z is the axis along the direction of the lamination depth.

The diffusion equation of the eddy-current problem is difficult to solve because it is nonlinear, hysteretic, and time-dependent. The calculation of iron losses using the diffusion equation (2.4) has been studied throughout recent decades and up until today, with various ideas being devised from a narrow area of research. In general, if the material body is nonlinear or a transient state is studied, the diffusion equation cannot be solved analytically; only numerical solutions are feasible.

In the nineteenth century, Steinmetz solved the eddy-current problem analytically, applying constant reluctivity [Steinmetz (1984)]. In a similar approach to MacLean (1954), Poritsky and Butler (1964) later attempted to approximate the normal magnetization by analytical equations. Gillott and Calvert (1965) introduced a more useful approach, using a numerical time-stepping approach to solve the eddy-current problem. The normal magnetization curve was used and hysteresis was neglected. O'Kelly (1972) investigated the effect of hysteresis on the flux penetration for a ferromagnetic material subjected to a cyclic field, using the concept of complex permeability.

The first work to explicitly incorporate hysteresis in the diffusion equation was that of Del Vecchio (1980). The Preisach model with the Everett integral was employed to model hysteresis and the Gillot-Calvert approach was used to solve the nonlinear time-stepping equation. The excess loss was not considered in the analysis.

During the period when Bertotti was developing his statistical theory on iron losses with an emphasis on the excess loss, Mayergoyz was working on the Preisach model and its extensions to account for various aspects, including the dynamic losses. Mayergoyz (1988a) attempted to generalize the static property of the Preisach model by compelling

the distribution function to be dependent on the time derivative of the output. The model did not receive a resounding success because of its poor accuracy in reproducing the experimental results.

Bertotti (1992), however, used a different, more physical and sound idea for the dynamization of the Preisach model. The method assumes that the elementary Preisach operator switches at a finite rate to account for the dynamic effects. The method has become widely recognized, being applied in various works by Bertotti et al. (1993, 1994) and others. Among the first to test the method was Bergqvist (1994) in his doctoral thesis. He observed that the model can fruitfully model dynamic losses, but it cannot detect fast changes in the system. This observation was later confirmed by Zirka et al. (2004c).

In the works of Philips et al. (1994a,b), the dynamic Preisach model of Bertotti (1992) was used to describe the magnetodynamic hysteresis effects with the effect of minor loops. They applied the finite-element method for the spatial dependency of the diffusion equation and the finite-difference method for the time discretization, and they indicated the influence of hysteresis and eddy currents on the results. Dupre and his group made various experimental studies regarding Bertotti's model and its identification with the 1D lamination problem [Dupre et al. (1996, 1998a,b)].

Basso et al. (1997) carried out a comparison between the conventional approach using the statistical theory (2.1) and the more accurate solution of the magnetodynamic model, combining the dynamic Preisach model with Maxwell equations. The excess loss was found to obey the statistical law up to 400 Hz, depending on the peak flux density.

In a more comprehensive simulation of iron losses, two research groups led by Dupre and Bottauscio compared their numerical procedures to predict the dynamic loops under distorted flux excitations [Dupre et al. (1999)]. The two groups adopted the same physical model, the moving dynamic Preisach model of Bertotti (1992) integrated into the diffusion equation, but different numerical approaches were implemented. Because of the high discretization of the Preisach plane, the moving dynamic Preisach model required significant computation time, more than ninety percent of the total time. The integration of (2.3) has to be performed at every time step and the Everett integral cannot be applied.

In another important class of eddy-current hysteresis models, the excess loss is treated differently, using the notion of magnetic viscosity, which works to increase the lag of the flux density B behind the applied field H. The idea was first proposed by Pirogov and then extensively studied and improved by Zirka et al. (2002, 2004b, 2005b, 2006b). The model is based on the Landau-Lifshitz-Gilbert equation, assuming that the only field acting on the magnetization is the applied field.

The general form of the viscous-type equation can be described by

$$\frac{\mathrm{d}B}{\mathrm{d}t} = r(B)\,\mathrm{sign}[H(t) - H_{st}(B)]^{1/p} \tag{2.5}$$

where the term $H_{st}(B)$ can, in principle, be computed by any inverted static hysteresis model. The dynamic magnetic resistivity r is a material property and the constant p is

related to the dependency of the excess loss on the frequency. Equation (2.5) is substituted in (2.4) and solved numerically. The viscosity-based model has been investigated in several articles [Zirka et al. (2002, 2004b, 2005b, 2006b)]. A time-domain technique was applied for the time discretization and a finite-difference method for the space discretization. The results agreed well with the experimental ones, even in PMW regimes [Zirka et al. (2006b)].

The idea of modeling the classical eddy-current problem by means of a diffusion equation is regarded as fruitful, but not uniquely fruitful. If any approach could model the B-H loop accurately, then it is welcome. The delay in the magnetic flux density B behind the field strength H resulting from the solution of the diffusion equation can be performed differently and more efficiently without its solution. In the work of Fuzi (1999), an illustration of this idea was provided by considering a differential equation that delays its input with respect to the real value [Fuzi and Ivanyi (2001); Fuzi and Kadar (2003)]. Zirka et al. (2006a) extended the viscosity-based model and added the classical eddy-current field component derived from the statistical theory of Bertotti (1988). The model was compared with that of the diffusion equation and found to be reasonably accurate in the case of thin sheets. Another similar method that is based upon two components, hysteresis and eddy currents, applied to grain-oriented materials has been introduced by Matsuo and Shimasaki (2006).

2.3.2 Static and Dynamic Vector Hysteresis

All the models discussed thus far, and a majority of those found in the literature, are scalar in nature. They can be adequate only for modeling unidirectional flux excitations. In order to take the rotation of the flux into account, a vector model is needed. The rotational loss behavior is, however, too complicated a phenomenon to model, and coming up with a general vector hysteresis model remains a question.

Static vector hysteresis models

The behavior of the B-H loops and energy dissipations under rotational flux differs greatly from that under alternating flux. Even when attention is focused on the "static" vector hysteresis models, not mentioning the dynamic ones, the number of models found in the literature can easily be counted.

Stoner and Wohlfarth (1948) proposed a vector hysteresis model that is physically based and uses the concept of the single domain particles with uniaxial anisotropy. The Stoner-Wohlfarth model has been popular and remains so even now. Despite its popularity, which can be attributed to its strong appeal to physical intuition, the Stoner-Wohlfarth model is essentially useful for studying magnetization processes and physical phenomena and not as a suitable modeling tool. The model has been criticized by several researchers [Mayergoyz (2003)], since it is computationally slow and does not yield accurate hysteresis loops. It is inaccurate because it can describe only symmetric loops and it is slow

because the calculation of its output particles requires the solution of nonlinear equations related to the astroid construction. Even though some of the computation difficulties have been circumvented by Koehler (1987), the identification problem of fitting the model to experimental data has not been addressed [Mayergoyz (1988c)]. Relevant investigations of the model and extensions to it have been performed by several scientists [Cullity (1972); Suzuki (1976); Cramer (1990); Charap and Ktena (1993); Ivanyi (1997)].

More recently, following the interest generated by the Preisach model, Mayergoyz (1986) devised a neat idea to model static vector hysteresis. In the Stoner-Wohlfarth model, it was not clear what sort of input history contributes to the future output. Mayergoyz revolutionized the concept by projecting the input data in all feasible directions while using a scalar Preisach model that keeps its history in each direction. In this way, all extremum values of the input leave their mark upon the future, which is crucial to the understanding of the phenomenological nature of vector hysteresis.

The model is widely known as the vector Preisach model. Here, it is preferred to call it the Mayergoyz model, since it can be applied with any scalar hysteresis model, not only with Preisach ones. The identification problem of the isotropic vector models has been based on the condition that the output of the vector model magnetized in one direction must be equal to the output of the scalar model [Mayergoyz (1987)]. In spite of its elegance and appeal both physically and phenomenologically, the Mayergoyz model has been put under scrutiny for describing the rotational losses [Cramer (1990); Pinto (1991); Bergqvist (1994)]. The rotational losses calculated by the model remain high even when the ferromagnetic material is at saturation, which contradicts the experimental observation. The vector fields $\boldsymbol{H}$ and $\boldsymbol{B}$ of the model stay unparallel at saturation because the model still produces a hysteretic behavior inadequately. This problem led Adly and Mayergoyz (1993) to the introduction of a new, supposedly more general version of the Mayergoyz model. The generalized Mayergoyz model was meant to circumvent the problem by increasing the contributions of the projected magnetic field strength. However, the model did not satisfy the rotational loss property and still requires further studies.

Many articles found in the literature center their investigations around the Mayergoyz model [Wiesen and Charap (1987); Wiesen et al. (1990); Gyselinck et al. (1998); Bottauscio et al. (2000b); Fallah and Moghani (2008)]. Matsuo and Shimasaki (2007a) generalized the Mayergoyz model to account for the rotational loss property in the same manner as was done by Adly and Mayergoyz (1993). However, discrepancies in the experimental data were observed by Matsuo and Shimasaki (2007b) and a further modification of the weighting function was needed for improvement. In the recent work of Adly and Abd-El-Hafiz (2006), a vector Preisach model of a Mayergoyz type was constructed from two scalar models based on neural networks.

Along with Mayergoyz, Della Torre and his collaborators made a series of proposals on generalizing the Preisach model to a vector model [Della Torre (1987); Della Torre and Kadar (1988); Della Torre (1998); Kahler and Della Torre (2003)]. The models are still under development and undergoing testing [Della Torre et al. (2006a,b); Loschner et al.

(2007)].

Bergqvist and Engdahl (1994) discussed a phenomenological vector model based on a simple hysteresis operator described by a differential equation.

Useful reviews of several vector hysteresis models and their properties are given in [Bergqvist (1994); Bottauscio et al. (2000b); Dupre and Malkebeek (2003); Kahler et al. (2005)].

Eddy-current and rotational hysteresis models

This is the most general category of magnetic materials models. It combines the magnetodynamic effects, the hysteresis, classical eddy-current, and excess losses in the case of alternating and rotational fields and hence is of paramount importance to the thesis. Because dealing with vector hysteresis has started only recently, little has been done with respect to the simulation of the magnetodynamic effects under rotational excitation. The problem is still new and is considered to be a great challenge.

Although the "rotational eddy-current" phenomenon has been mentioned quite a few times in the literature, it has not, nevertheless, been extensively studied. Only a few researchers, most of whom used analytical methods, have attributed considerable importance to it [Mayergoyz (1998)]. In the 2D case, the governing equations are two coupled diffusion equations of type (2.4) for the x- and y-directions. Del Vecchio (1982a) studied the rotational eddy-current losses by solving the two diffusion equations numerically, using a time-stepping finite-difference method. The algorithm allowed the hysteretic effects to be included, but because of the lack of a suitable vector hysteresis model, only a single-valued magnetization curve was used.

Gyselinck et al. (1998) and Dupre et al. (2000) combined the Preisach model with the resultant 2D Maxwell equations to take the interaction between hysteresis and eddy currents into account. Bottauscio et al. (2000a) introduced another more comprehensive model that is based on the integration of a 1D eddy-current model into a 2D finite-element model, but vector hysteresis was not considered. A comparative investigation was conducted to evaluate the impact of different phenomena, such as hysteresis and eddy currents, on the flux waveforms and iron losses. They later extended their analysis to take the eddy-current rotational losses into account [Bottauscio and Chiampi (2001)]. Other relevant works concerning dynamic vector hysteresis modeling can be found in [Mayergoyz (1991a); Spomic et al. (1996); Henrotte and Hameyer (2006); Dlala et al. (2008c)].

Measurement methods of rotational losses

In the last century, a great deal of research into rotational losses was conducted by a number of researchers. Strattant and Young (1962) devised an experimental apparatus to predict iron losses in elliptically rotating fields. The apparatus consisted of two exciting cores with an air-gap in which the specimen was placed. Two pickup coils were used to measure the flux. To evaluate the precision of the measurement system, Epstein test

results were compared with those obtained by the 2D apparatus with the excitation of one core. The measurement system was then utilized to study the behavior of the rotational iron losses for various frequencies and magnitudes [Young and Schenk (1960, 1966)]. Flanders (1967) developed a multipurpose apparatus based on a rotating sample magnetometer.

Moses and Thomas (1973) measured the rotational iron loss using a cross-sample that was wound by excitation coils. The flux density $\boldsymbol{B}$ was obtained in two directions using sensing coils placed through holes in the center of the sample. The magnetic field $\boldsymbol{H}$, however, was measured through the magnetization current. The cross-sample was then utilized for measuring the rotational loss in a computerized control system [Brix et al. (1982)]. Fiorillo and Rietto (1988) applied a thermometric method to sense the field through the temperature on a fixed disk sample. Cecchitti et al. (1978) measured the rotational losses as a function of frequency for non-oriented and grain-oriented materials using disk samples. A more convenient measuring system was developed by Enokizono et al. (1990), using a square single sheet sample with an adjustable air-gap. Another measuring apparatus using a vertical yoke was also developed by Sievert et al. (1992). In more recent years, the digital era has had an impact on the development of more advanced apparatus for obtaining various shapes of the controlled flux density [Zurek et al. (2005)]. Since then, the investigation of various problems has become easier. The influence of the direction of the rotating flux, whether it is clockwise or anticlockwise, has been studied in [Zurek and Meydan (2006a,b); Maeda et al. (2007)]. Furthermore, Alinejad-Beromi and Moses (1992) showed that it is important to investigate the distance of the H sensing coils from the surface of the sample. A recent review of various measuring systems of the rotational losses is given in [Guo et al. (2008)].

2.4 Electromagnetic Field Computation

The accurate calculation of the magnetic field patterns is essential for assessing the characteristics and performance of electrical devices. At the present time, the development of numerical methods in the determination of electromagnetic fields, as well as the availability of fast computers, has established adequate conditions for the simulation of magnetic materials. The macroscopic properties of the materials are described by phenomenological models and coupled with Maxwell equations to acquire the solution of the magnetic field. In the meantime, the modeling of the magnetic material plays an important role in the accurate prediction of iron losses and in the proper estimation of the performance of an electrical device. Finite-element methods are becoming increasingly used in the magnetic field analysis of electrical machines because they are capable of modeling complicated geometries and solve the field distribution accurately.

In connection with the finite-element analysis of electrical machines, and the interesting mathematical problems that arise, historical reviews and descriptive analyses can be found in [Silvester and Ferrari (1983); Arkkio (1987); Hameyer and Belmans (1999); Salon

(2000); Bastos and Sadowski (2003)].

2.4.1 Incorporation of Hysteresis Models

The inclusion of hysteresis models into the finite-element analysis of electrical machines is still at an early stage, and in most of the published works, the emphasis has been on modeling the steel laminations, as was reviewed in the previous section. A particularly important review of this area of research was conducted by Saitz (2001a).

The analysis of hysteresis motors was one of the essential and long-standing matters that required the consideration of the hysteretic effects, usually by applying the concept of complex permeability [Wakui et al. (1987)].

Nonlinear magnetic field problems require the employment of iterative methods to cope with nonlinearity. Two distinctive methods are typically applied. The fixed-point method has been widely used for solving hysteretic electromagnetic field problems. The method converges stably with a slow rate, exactly opposite to the Newton-Raphson method, which can easily suffer from instability, but which, if it converges, converges remarkably fast [Silvester and Ferrari (1983); Hantila (1975); Chiampi et al. (1980, 1994, 1995); Bottauscio et al. (1999); Hantila et al. (2000); Dlala et al. (2007, 2008b)].

Del Vecchio (1982c) incorporated a hysteresis model into a 2D magnetic field solver. The numerical technique of Del Vecchio (1980), which applied the Preisach model with the diffusion equation, was extended and a time-stepping finite-element method was employed to solve the magnetic field in a rectangular bar with sinusoidal flux. Del Vecchio's article was an inspiration for a few others to follow. Feliachi and Meunier (1985) applied the Stoner-Wohlfarth model to the study of the magnetic recording in storage media using a finite-element method. Friedman and Mayergoyz (1989) used the Mayergoyz model for the calculation of a magnetostatic problem by an integral equation. In the analysis, a time-stepping technique was used to trace the history of the magnetizing process, and the distinctive features of the model in describing non-symmetrical minor hysteresis loops were highlighted.

Ossart and Meunier (1991) integrated a scalar hysteresis model in a 2D finite-element method. The work was dedicated to the simulation of the magnetic recording of longitudinal film. Henrotte et al. (1992) reformulated the constitutive law and inverted a scalar Preisach model by the Regula-Falsi method. The authors applied the hysteresis model to the simulation of a magnetic circuit by the finite-element method and reported problems associated with the convergence of the Newton-Raphson method. Delince et al. (1994) then used the same constitutive law to integrate the Preisach model into a finite-element code with a circuit equation.

In the work of Leonard et al. (1995), a scalar Preisach model linearized by the Newton-Raphson method and integrated in a 3D finite-element model was implemented. Leonard et al. (2006) used a dynamic hysteresis model with a 2D magnetic vector potential finite-element formulation to estimate iron losses. The importance of the efficiency of the static

model was emphasized.

The Belgian research group of Dupre et al. (1998a) and Gyselinck et al. (1998) improved the convergence by using a different approach based on the differential permeability. The Italian research group of Chiampi et al. (1994) and Bottauscio et al. (1995) proposed a numerical technique based on the fixed-point method and especially suitable for modeling time-periodic hysteretic field problems. The formulation was based on the magnetic vector potential, and thus the Preisach model was inverted by the secant method. Saitz (2000) adopted a similar approach based on the magnetic vector potential for modeling induction motors, combining the vector Preisach model with finite-element analysis. A time-stepping scheme was used and a long computation time was reported for the inversion of the Preisach model.

In finite-element formulations that employ the magnetic vector potential $\boldsymbol{A}$ as the unknown, the magnetic flux density $\boldsymbol{B}$ is directly obtained as an output quantity. Hysteresis models, such as the Preisach model and the Jiles-Atherton model, are standardly H-based (forward); thus, they are not suitable for modeling hysteresis when coupled with the finite-element equations because the models have to be inverted in order to be suited to the problem. Iterative methods are typically employed to invert the forward Preisach model in which computing the magnetic field H is based on locally inverting the hysteresis model by means of iteration during the process of simulation [Henrotte et al. (1992); Bottauscio et al. (2000b); Saitz (2001a)]. This mechanism requires substantial amounts of computation to obtain converged solutions and hence the computation of H from B is inefficiently treated.

Other works found in the literature that deal with the magnetic vector potential formulations were dedicated to reformulating the electromagnetic problem with constitutive equations. The first direct approach proposed by Park et al. (1993) to cope with instability can be appropriate for certain problems but is not generally attractive, especially in numerical field problems that involve soft magnetic materials in which the magnetic field $\boldsymbol{H}$ becomes too small compared to the magnetization $\boldsymbol{M}$ [Ivanyi (1997)]. An H-version of the fixed-point technique introduced by Hantila (1975) and further developed by Bottauscio et al. (2000b) is suitable for the formulation of the electromagnetic problem, resulting in the omission of the inversion of the hysteresis model. Another more recent approach introduced by Zhai and Vu-Quoc (2005), called the implicit inverse hysteresis model and based on the Newton-Raphson technique, may not be straightforward to incorporate into simulation programs and is not efficient enough to implement, since it also involves iteration. Further publications on the inverse problem can be found in [Cardelli et al. (2000); Leite et al. (2003); Davino et al. (2008)].

2.4.2 Core Losses of Electrical Machines

Electrical machine designers utilize ferromagnetic materials to keep the flux density high with minimum current density and thus reduce the size and increase the efficiency of the

machine. As the flux in the material varies with time, heat is generated in the machine, partly as a result of the core losses. The localization of the hot spots in transformers and rotating electrical machines has been, and still is, an important problem for machine designers. Having limited energy resources has recently become another important motivation for users and designers to acquire more efficient electrical machines. The energy consumption of electrical machines is enormous, especially at industrial levels. For example, in Finland, Germany, and France, electrical motors consume more than half of the total power generated. It is worthwhile to note that even a small reduction in iron losses at the design stage will be significant. These considerations have had a meaningful impact on studying iron loss phenomena.

In the early days, when analytical design techniques were prevalent, simple empirical formulae, such as those of Steinmetz (1984) and Jordan (1924), were used for the prediction of core losses. Even at present, conventional calculation methods still rely on the use of similar post-processing formulae based on the method of Jordan [Stumberger et al. (2003)]. The magnetization curves of such methods are approximated by a single-valued function. Although the iron losses calculated by the single-valued model are not considered in the field solution and their effects cannot be evaluated, such a technique is the most common tool available nowadays in commercial and research software for the prediction of iron losses in electrical machines.

Bertotti et al. (1991) calculated the core losses of an induction machine, applying the statistical loss theory to account for the rotational losses. The calculation was based on post-processing the finite-element solution of the magnetic field. Binesti and Ducreux (1996) applied a three-component empirical equation to the calculation of the core losses of an induction motor. The loss model was identified by means of an Epstein frame and was used in a 2D time-harmonic finite-element method. The authors associated the discrepancies between the measured and calculated results with the neglecting of the rotational loss component.

The influence of the PWM on the iron losses of an inverter-fed induction motor was tested by Boglietti et al. (1996), also using an empirical equation. The authors generalized their methods by introducing a mathematical relationship between the iron loss contribution and the voltage supply characteristics [Boglietti et al. (2003)]. In more recent comprehensive analyses of electrical machines, core losses were estimated using a two-component equation, taking the effect of minor loops into consideration [Yamazaki (2004); Lei et al. (2003)]. Diaz et al. (2007) proposed an analytical procedure for quantifying the rotational losses in the stator cores of induction motors. The core loss computation was based on the statistical loss theory.

Dupre et al. (1997) were among the first to incorporate an iron loss model into the magnetic field solution of an electrical motor. They included the vector Preisach model and a magnetodynamic model for the loss computation and obtained reasonable results in comparison with the experiment. Their analysis was then extended to study the motor more thoroughly [Dupre et al. (1998c, 2003)].

Arkkio et al. (1998) integrated the vector Preisach model into a time-stepping finite-element code for the computation of hysteresis torque in an induction motor. In the works of Saitz (2000) and Saitz (2001b), the vector Preisach model was incorporated into the 2D time-stepping finite-element analysis of induction motors. The hysteresis effects were considered in the stator while a single-valued function was used for the rotor. The eddy-current and excess losses were omitted in the field analysis and were estimated posteriorly.

Recently, Belahcen and Arkkio (2008) proposed a core loss model based on the statistical loss theory of Bertotti (1988). The model was intended to calculate the core losses of electrical machines as a function of time. The rotational losses were considered in the equations using an additional parameter.

More on the calculation of iron losses in electrical machines can be found in [Findlay et al. (1994); Stranges and Findlay (2000); Takahashi et al. (2005)].

2.5 Conclusions

In this chapter, the published works in the literature that are relevant to the thesis have been discussed. There are many models of static scalar hysteresis that have been proposed whose accuracy, stability, and efficiency vary from one to another. The most common model that is studied and used in various applications is the Preisach model. This model is distinguished by its stability, accuracy, and generality. However, for many researchers, the model is regarded as complex. The Jiles-Atherton model is popular to a certain extent among the engineering community. This model is simpler than the Preisach model but its generality and accuracy are poorer.

The inverse problem needed for obtaining the magnetic field strength as an output quantity is an outstanding obstacle and drawback of most of the hysteresis models, including the Preisach model and the Jiles-Atherton model. Another family of models that are based on predicting the desired curve by interpolating between the experimental first-order reversal curves appears to be more practical because it straightforwardly permits the use of the relations, $H(B)$ or $B(H)$, without conditions.

The eddy current in the lamination is usually treated using the approximation of Maxwell equations, which neglect the structure of domains. The dynamic Preisach model of Bertotti has been incorporated with the diffusion equation to estimate the iron losses in the lamination. It was reported that Bertotti's model is inefficient and cannot respond to fast changes in the input. Furthermore, it is basically restricted only to the Preisach model. Another model of more generality based on the magnetic viscosity has been applied successfully with various hysteresis models.

The rotational magnetic fields impose another difficult modeling problem. The relatively simple concepts of the scalar hysteresis models must be generalized in order to take the vectorial relation between $\boldsymbol{H}$ and $\boldsymbol{B}$ into account. In the literature, little has been done regarding vector hysteresis modeling and far less regarding dynamic vector hysteresis modeling.

Chapter 3

Magnetodynamic Lamination Model

This chapter deals with the magnetic material models of a steel lamination. The behavior of the magnetodynamic losses in the presence of rotational magnetic fields is explored, discussed, and modeled. In the first section, the developments of the models, with their mathematical formulations and conditions, are given. In the second section, the identification problem and the accuracy of the models are addressed. Finally, in the third section, the numerical results of the models and the simulations of iron losses are presented.

3.1 The Lamination Model

Practically, it is more convenient to deal with a steel lamination than a rotating electrical machine. The methods for predicting the behavior of magnetic materials are first established and validated for a lamination model. Then they are applied to predict the core losses of electrical machines. The model is developed for the non-oriented materials that are used for electrical machines.

The combination of the magnetodynamic losses into one model is expedient and manifests itself as an important problem for the thesis. The eddy current in the lamination is a delicate problem that needs to be solved by means of a rigorous approach. The inclusion of the hysteretic behavior in the eddy-current problem is vital, not only for obtaining accurate results but also for validating the numerical model as a whole. The rotational iron loss calls upon a vectorial hysteretic relationship that must, to a certain extent, satisfy the material hysteretic behavior. In the literature, there are a few vector hysteresis models, but the majority of them are either inaccurate or complicated. The vector model proposed by Mayergoyz (1986) is rather convenient, but it does not describe the rotational loss properly. It also involves a tedious identification problem that makes it unattractive. The Mayergoyz model will here be rectified in order to satisfy its rotational loss property and improve its accuracy. Furthermore, a straightforward identification method is proposed for the model.

3.1.1 Governing Equations

The magnetodynamic vector hysteresis (MDVH) problem in the lamination requires the solution of a nonlinear time-dependent equation. If the magnetic flux is rotating in the x-y lamination plane, a general form of (2.4) that results directly from Maxwell equations is needed

$$\nabla \times \nabla \times \boldsymbol{H} = -\sigma \frac{\partial \boldsymbol{B}}{\partial t}. \tag{3.1}$$

If an infinite sheet is assumed, then (3.1) can be reduced to the solution of two 1D coupled equations of type (2.4), for the x- and y-directions

$$\begin{aligned} \frac{\partial^2 H_x(z,t)}{\partial z^2} &= \sigma \frac{\partial B_x(z,t)}{\partial t} \\ \frac{\partial^2 H_y(z,t)}{\partial z^2} &= \sigma \frac{\partial B_y(z,t)}{\partial t}. \end{aligned} \tag{3.2}$$

Although these may appear as separate equations, they are strongly coupled through the vectorial relationship between $\boldsymbol{B}$ and $\boldsymbol{H}$, and also through the boundary conditions [Del Vecchio (1982a)]. The system of equations (3.2) may be solved using a single-valued magnetization curve while assuming a collinear $\boldsymbol{B}$-$\boldsymbol{H}$ relation. In such a case, only the classical eddy currents can be calculated when the effect of the interdependency of the magnetodynamic losses is neglected. However, in this work, the hysteretic effects need to be considered and investigated.

3.1.2 Magnetodynamic Vector Hysteresis Model

The constitutive nonlinear relation can be expressed by the fixed-point method as follows:

$$\boldsymbol{H} = \nu_{\mathrm{FP}} \boldsymbol{B} + \boldsymbol{M} \tag{3.3}$$

where $\boldsymbol{M}$ is a magnetization-like quantity and the fixed-point coefficient ν_{FP} is a reluctivity-like quantity and must be constant. By using (3.3), the nonlinear 1D magnetodynamic problem can be written as

$$\nabla \times \nu_{\mathrm{FP}} (\nabla \times \boldsymbol{a}) + \sigma \frac{\partial \boldsymbol{a}}{\partial t} = -\nabla \times \boldsymbol{M}. \tag{3.4}$$

Here, $\boldsymbol{a}$ is the magnetic vector potential, which is written in small letters for the 1D model as capital letters are commonly reserved for the 2D problem. The 1D and 2D problems are related because the time-varying flux density components of the 2D model are used to set the boundary conditions of the 1D model [Bottauscio et al. (2000a)]. Throughout this chapter, the flux density components are treated as a given.

If the second term in (3.4) is assumed to be negligible ($\sigma \frac{\partial \boldsymbol{a}}{\partial t} = 0$), then the isotropic vector hysteresis relation between $\boldsymbol{H}$ and $\boldsymbol{B}$ can be simply characterized by the Mayergoyz model without the need to solve the nonlinear problem. However, since the formulation (3.4) produces the flux density as output, an inverse model has to be developed. The

Mayergoyz model can be inverted in a straightforward manner, where the applied field strength $\boldsymbol{H}$ is directly calculated as

$$\boldsymbol{H} = \sum_{i=1}^{N} \boldsymbol{e}_{\varphi_i} F_{\mathrm{st}}(B_{\varphi_i}) = \sum_{i=1}^{N} \boldsymbol{e}_{\varphi_i} H_{\varphi_i} \tag{3.5}$$

where N is the number of directions along $\boldsymbol{e}_{\varphi_i}$. The projected flux density components can be calculated by using the so-called "generalized" Mayergoyz model [Adly and Mayergoyz (1993)] as

$$B_{\varphi_i} = |\boldsymbol{B}|\, \delta\, |cos(\theta_B - \varphi_i)|^{1/w}, \quad w \geq 1, \quad i = 1, 2, \ldots, N \tag{3.6}$$

where θ_B is the polar angle that specifies the direction of $\boldsymbol{B}$ and $\delta = \mathrm{sign}[cos(\theta_B - \varphi_i)]$. The coefficient w permits the increase and decrease of the projected components B_{φ_i}. The function F_{st} determines H_{φ_i} through an inverted static hysteresis model that can be identified in such a way that the output of the vector hysteresis model magnetized in one direction is equal to the output of the scalar model.

In the original model of Mayergoyz (1986), the coefficient w is simply not used ($w = 1$). At saturation, the model starts to oscillate around its major loop and the rotational losses remain constant. It will be shown here that the use of $w > 1$ in the generalized Mayergoyz model proposed by Adly and Mayergoyz (1993) does not improve the rotational loss property.

The generalized Mayergoyz model attempts to increase the contributions of the projected magnetic field strength components in a peculiar fashion over the B-H plane. Consequently, the use of the coefficient $w > 1$ causes sort of anisotropy in the model and an exaggeration of its value would result in non-physical behaviors. In other words, the coefficient w changes the characteristics of the isotropic vector model in which the B-H loops and the loci of the magnetic fields become totally dependent on it. For example, if a circular flux was applied to the model and $w = 1$, the loci of the magnetic field strength would be circular. On the other hand, if the same circular flux was applied to the model and $w > 1$, then the loci of the magnetic field strength would not be circular but rather flower-shaped.

In order to control the rotational loss without confronting the latter problem, a constant phase shift ψ is introduced between the directions of the projected B_{φ_i} and the directions of the calculated H_{φ_i}

$$B_{\varphi_i} = |\boldsymbol{B}|\, \delta\, |cos(\theta_B - \varphi_i + \psi)|^{1/w}, \quad w \geq 1 \quad i = 1, 2, \ldots, N \tag{3.7}$$

where $\delta = \mathrm{sign}[cos(\theta_B - \varphi_i + \psi)]$ and the phase shift ψ is associated with the rotational loss property and can be experimentally identified. The angle ψ must be sufficiently small (less than 1^{o}) to ensure that when a unidirectional excitation is applied to the model, no significant excitation is produced in the perpendicular direction.

The new procedure (3.7) leads to the rotation of the system of the H_{φ_i} projections through an angle ψ with respect to the system of the B_{φ_i} projections (see Figure 3.1). Thus, the phase shift ψ compensates the inadequate coupling of the perpendicular components by creating a delay in the vector $\boldsymbol{H}$ so that the vector fields $\boldsymbol{B}$ and $\boldsymbol{H}$ become parallel at saturation. The symmetry and other interesting properties of the Mayergoyz model remain unaffected [Mayergoyz (2003)].

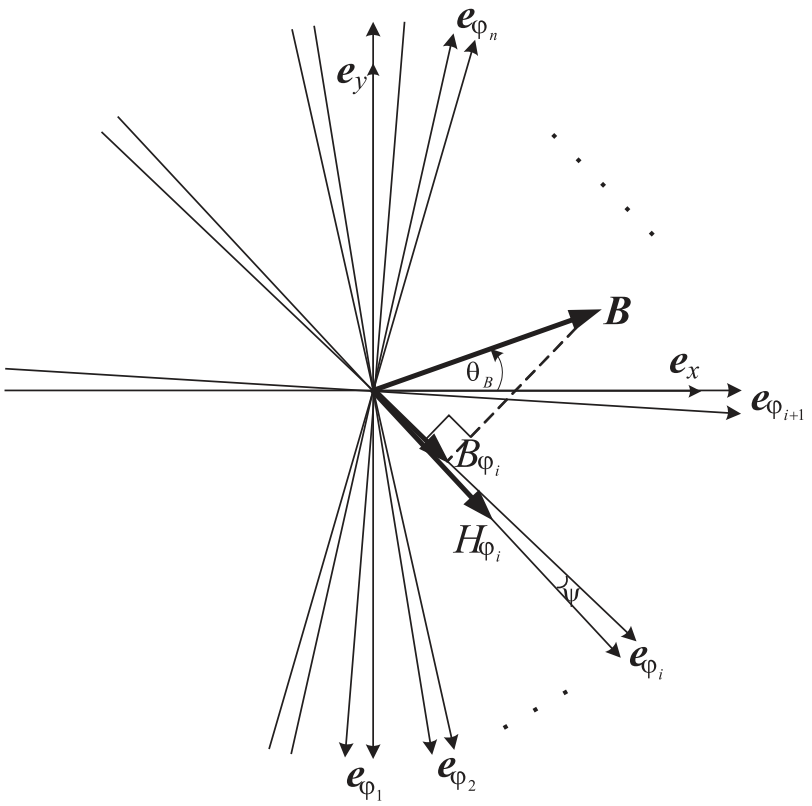

Figure 3.1: The introduction of two projection systems for the vectors $\boldsymbol{B}$ and $\boldsymbol{H}$.

The identification procedure of the Mayergoyz model (3.5) requires the development of lengthy algorithms such as those of Mayergoyz (1987) and Kuczmann (2004). Moreover, if the "magnetodynamic" vector hysteresis property is taken into account ($\sigma \frac{\partial \boldsymbol{a}}{\partial t} \neq 0$), the static, hysteretic function F_{st} must be replaced by a dynamic, hysteretic function F_{dy} and Equation (3.4) must be solved iteratively. The dynamic function F_{dy}, which involves the numerical solution of (3.4), makes the vector model more complicated to identify. Therefore, Model (3.6) needs to be modified to simplify the identification problem

$$\boldsymbol{H} = \sum_{i=1}^{N} \boldsymbol{e}_{\varphi_i} \frac{F_{\mathrm{dy}}(B_{\varphi_i})}{Q(N)} = \frac{1}{Q(N)} \sum_{i=1}^{N} \boldsymbol{e}_{\varphi_i} H_{\varphi_i} \tag{3.8}$$

where Q is a parameter characterizing the MDVH behavior.

Condition 3.1 [Scalar model reduction] *The output of Model (3.8) magnetized along one direction must be equal to the output of the magnetodynamic scalar model.*

Condition 3.2 [Rotational loss property] *The rotational loss of Model (3.8) must drop to zero at saturation when the model is under quasi-static circular flux excitation.*
Condition 3.3 [Loop shape reproducibility] *The shapes of the dynamic hysteresis loops and the loci of the magnetic fields of Model (3.8) must fit the experimental ones.*

The natural simplification in (3.8) lies in two aspects. First, the model utilizes the scalar hysteresis data directly without additional complicated modification, which is not the case when using Model (3.5). In the case of Model (3.8), the scalar hysteresis data are only scaled by a multiplication coefficient, η, in order to satisfy Condition 3.1. Second, the parameter Q can be identified as being unique for a wide range of frequencies. This means that Model (3.5) is no longer needed even in static field conditions.

Applying the MDVH model (3.8) to (3.4) results in N equations that are strongly coupled through the MDVH model

$$\begin{aligned}
\nu_{\mathrm{FP}}\frac{\partial^2 a_{\varphi_1}}{\partial z^2}+\sigma\frac{\partial a_{\varphi_1}}{\partial t} &= -\frac{\partial M_{\varphi_1}}{\partial z}\\
\nu_{\mathrm{FP}}\frac{\partial^2 a_{\varphi_2}}{\partial z^2}+\sigma\frac{\partial a_{\varphi_2}}{\partial t} &= -\frac{\partial M_{\varphi_2}}{\partial z}\\
&\vdots\\
&\vdots\\
\nu_{\mathrm{FP}}\frac{\partial^2 a_{\varphi_N}}{\partial z^2}+\sigma\frac{\partial a_{\varphi_N}}{\partial t} &= -\frac{\partial M_{\varphi_N}}{\partial z}
\end{aligned} \tag{3.9}$$

where the nonlinear problem in the lamination is linearized by defining

$$M_{\varphi_i}(z,t)=H_{\varphi_i}(z,t)-\nu_{\mathrm{FP}}B_{\varphi_i}(z,t),\qquad i=1,2,\ldots,N \tag{3.10}$$

and the dynamic, hysteretic relation is described in the φ_i direction by a viscosity-based model introduced by Zirka et al. (2006b)

$$H_{\varphi_i}(z,t)=H_{\mathrm{st}}(B_{\varphi_i}(z,t))+\delta_{\mathrm{e}}\left|\frac{1}{r}\frac{\mathrm{d}B_{\varphi_i}(z,t)}{\mathrm{d}t}\right|^{1/p},\qquad i=1,2,\ldots,N. \tag{3.11}$$

The first term of (3.11) can be, in principle, calculated by any inverted static hysteresis model. In this thesis, a few static hysteresis models have been tested; they will be discussed in Section 3.1.4. The second term of (3.11) represents the excess field through the time delay of the magnetic flux density behind the magnetic field strength. The switch $\delta_{\mathrm{e}}=\mathrm{sign}(\mathrm{d}B_{\varphi_i}(z,t)/\mathrm{d}t)$ is controlled according to whether the field is increasing or decreasing.

3.1.3 Simplified Magnetodynamic Vector Hysteresis Model

Although the MDVH model is suitable for studying the 1D lamination problem, it becomes a heavy computational burden when it is incorporated into a 2D finite-element

code. The iterative procedure required for the solution of the nonlinear systems of equations (3.9) can be avoided by making certain simplifying assumptions. The idea was originally proposed by Bertotti (1998) and later applied by Zirka et al. (2006a) to determine the eddy-current losses in a simple manner. It is natural to assume that the applied magnetic field strength is composed of three components

$$H_{\varphi_i}(t) = H_{\mathrm{st}}(B_{\varphi_i}(t)) + \frac{\sigma d^2}{12}\frac{\mathrm{d}B_{\varphi_i}(t)}{\mathrm{d}t} + \delta_{\mathrm{e}}\Big|\frac{1}{r}\frac{\mathrm{d}B_{\varphi_i}(t)}{\mathrm{d}t}\Big|^{1/p}, \quad i = 1, 2, \ldots, N. \tag{3.12}$$

where the second term in (3.12) is the classical eddy-current field derived from Maxwell equations assuming a uniform flux distribution. This assumption directly implies that the eddy currents are calculated independent of the magnetization law. It is well known, however, that the eddy-current loss is dependent on the $B(H)$ relation, which means that Equation (3.12) can be applied only in the frequency range where the skin effect is negligible, or to magnetic materials with low conductivities. It is necessary, therefore, to improve the predictions of the method (3.12) in the high-frequency range by enforcing $\mathrm{d}B/\mathrm{d}t$ to be implicitly dependent on the magnetization law in the calculation of the applied magnetic field as

$$H_{\varphi_i}(t) = H_{\mathrm{st}}(B_{\varphi_i}(t)) + \frac{\sigma d^2}{12}\delta_{\mathrm{e}}\Big|\frac{\mathrm{d}B_{\varphi_i}(t)}{\mathrm{d}t}\Big|^{v} + \delta_{\mathrm{e}}\Big|\frac{1}{r}\frac{\mathrm{d}B_{\varphi_i}(t)}{\mathrm{d}t}\Big|^{1/p}, \quad i = 1, 2, \ldots, N. \tag{3.13}$$

An adequate choice of the function v must ensure that the eddy-current field is nonlinearly dependent on $\mathrm{d}B/\mathrm{d}t$, as in the realistic case endured by the MDVH model. It is found that a quadratic dependence of v is rather sufficient to achieve relatively accurate predictions in a wide range of frequencies and flux densities

$$v(B) = \mathrm{a}_0 + \mathrm{a}_1\delta_{\mathrm{e}}\Big(\frac{B}{B_{\mathrm{s}}}\Big) + \mathrm{a}_2\Big(\frac{B}{B_{\mathrm{s}}}\Big)^2 \tag{3.14}$$

where B_{s} is a predefined saturation value of the magnetic flux density. The coefficients a_0, a_1, and a_2 can be estimated by fitting the calculated dynamic loops to the experimental ones. Model (3.13) will be referred to as the *simplified* MDVH model.

3.1.4 Models of Static Hysteresis

The static hysteretic terms in (3.11), (3.13), and (3.12) need an inverse hysteresis model. The accuracy and stability of the hysteresis model is important for obtaining accurate results for the iron losses. In general, hysteresis modeling is complicated because of the non-symmetric multi-valued branching of hysteresis curves. As discussed earlier, in Chapter 2, various hysteresis models have been used to represent hysteresis in ferromagnetic materials. The applicability of these models varies according to several perspectives and the selection of the appropriate model will definitely depend on several criteria. In numerical field analysis, the simplicity, accuracy, and efficiency of the model are considered.

Inverted Preisach model

Among several hysteresis models, the classical Preisach model has been extensively used in various applications. Several methods have evolved to identify the Preisach model. These methods fall into two main groups: interpolative methods and analytical methods. Interpolative methods typically employ experimental data such as first- or higher-order reversal curves. Analytical methods suggest the use of Gaussian or Lorentzian distribution functions of the Preisach plane.

In this thesis, the attention will be focused on the "interpolative methods", since these methods can easily allow for the inversion of the model. The fundamental goal is to obtain the magnetic field H directly from the flux density B. It is imperative to realize that having a monotone Everett function is a necessary condition to make the inverted model work sensibly. The Everett function can be calculated from the input extrema (first-order reversal curves) of the flux density B as

$$E(B^+, B^-) = \frac{1}{2}\big(H_{(B^+B^-)} - H_{B^+}\big) \tag{3.15}$$

where the superscripts $(+, -)$ refer to the increasing and decreasing values of the input B, respectively.

The major loop and the first-order reversal curves, which are used in the identification, are reproduced exactly by the inverted Preisach model. The model is suitable for coping with the congruency problem. The intrinsic property of the Preisach model is the specific (vertical) H-congruency of the modeled curves. On the other hand, the inverted Preisach model predicts curves that are based on the specific (horizontal) B-congruency. The idea of utilizing the B-congruency has proven to be more effective in reproducing curves comparable to those produced in experiments [Dlala et al. (2006)].

History-dependent model

The inverted Preisach model is relatively accurate but can have some discrepancies. Obtaining accurate and general physical modeling of hysteresis requires the development of models that take the H-congruency into account along with the B-congruency: the search for the pattern to be copied (shifted) has to be carried out over the whole B-H plane, not only in the horizontal direction or in the vertical direction. A non-Preisach model of such competence is proposed by Zirka et al. (2004a). The model predicts the particular curve to be modeled from two weighted patterns transplanted from the first-order reversal curves. The model satisfies the wiping-out property and the return-point memory because it stores previous reversals and hence is called the history-dependent hysteresis model. The model requires the solution of nonlinear equations when it searches for the modeled pattern in the two directions.

History-independent model

Although the history-dependent models produce good accuracy, they may still be regarded as approximate ones because of the complicated symmetric and non-symmetric branching of the minor loops. Furthermore, tracking the history by storing the reversal points entails a lot of memory, particularly when a finite-element method of a 2D or 3D geometry is considered.

Because the wiping-out and the return-point memory properties of ferromagnetic materials cannot be regarded as rigorous rules and need not be strictly respected [Zirka et al. (2005a)], evading the history dependence is, to a certain extent, justifiable. Experimental evidence, though rare [Della Torre (1994); Bennett et al. (1996); Zirka et al. (2005a)], shows that the minor loop drifts towards an equilibrium minor loop when an applied field oscillates between two reversal points. This phenomenon, known as accommodation, has prompted us to propose a model that is simple and exhibits stable accommodating minor loops. A similar model was proposed by Dupre et al. (2001).

The model employs a set of first-order reversal curves including the major loop, and thus these curves are reproduced exactly. The model is simple and can be described in a few words. Any intermediate curve of the family can be constructed with the desired accuracy by direct interpolation between the first-order reversal curves obtained by experiment. If the first-order curves are not available, it is possible to create them in the manner outlined by Zirka and Moroz (1999).

3.2 Identification and Validation of the Models

In this section, the MDVH models proposed in Section 3.1 are identified and tested. Since the inverted models are more relevant than the direct models, the focus will be centered around the relation $\boldsymbol{H}(\boldsymbol{B})$. The history-independent model will be identified and integrated into the MDVH models described in Section 3.1. The dynamic function F_{dy} of the vector hysteresis model (3.8) will be represented by two models: either the MDVH model, i.e. the solution of the system of equations (3.9) by the 1D finite-element method, or the use of the simplified MDVH model (3.13).

The models are validated by comparing their outputs with the measured ones. The comparison is done by entering the measured flux density waveform into the model as an input while obtaining the magnetic field strength as an output.

3.2.1 Quasi-Static Testing

The inverted Preisach model and the history-dependent model have been thoroughly investigated by Dlala et al. (2006) and Zirka et al. (2004a), respectively. Therefore, more attention will be paid to the history-independent model. This model is distinguished by its simplicity and speed, but it is important to examine its accuracy and stability. A family of first-order reversal curves was measured on an electrical steel sheet. The bilinear

interpolation technique was used to construct the intermediate curves. At the reversals, the inverse interpolation problem for finding the specific reversal was solved using the method of Muller (1956).

Although the history-independent model can be used individually to predict unidirectionally excited hysteresis loops, the vector hysteresis model (3.8) was used for those predictions where the dynamic function F_{dy} is reduced to the static history-independent model. The first-order reversal curves were scaled so as best fit the calculated major loop to the experimental one. Figure 3.2 illustrates the prediction of the major loop and some minor loops. The flux density B, as an input, was oscillating first between the major loop tips and then around a minor loop, where the stability of the model is tested. The model is found to produce a stable loop accommodating between an input pair and the return-point memory rule is not strictly satisfied. In Figure 3.3, another more complicated input was created to further test the stability of minor loops; the model produced minor loops that are accommodating stably in a controlled manner. A measurement of hysteresis loops

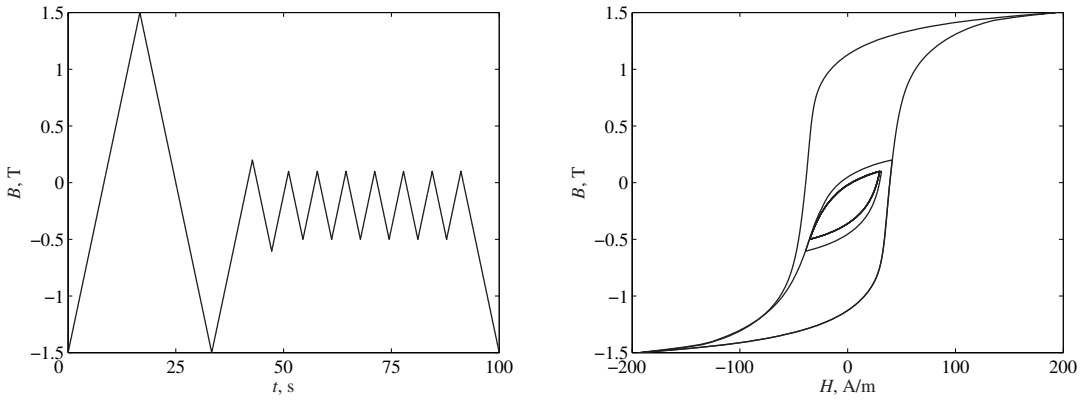

(a) Input of the model

(b) The modeled B-H behavior

Figure 3.2: Testing the history-dependent model against the return-point memory rule and accommodation.

caused by applying a cyclic field was carried out (see Figure 3.4). The measurement is intended to examine the accuracy of the inverted Preisach model, the history-dependent model, and the history-independent model. Since the results of the three models are comparable and are in good agreement with the measurements, the history-independent model is adopted in this work and will be incorporated into the analysis of the magnetodynamic losses.

3.2.2 Identifying the Magnetodynamic Vector Hysteresis Model

To keep the analysis general, all the dynamic hysteresis loops are identified by the use of the MDVH model (3.8), including the unidirectionally excited dynamic hysteresis loops. The system of equations (3.9) is discretized using N_{e} first-order finite elements and solved by the Crank-Nicholson time-stepping scheme. Since the components a_φ are symmetric around the plane $z = 0$, only the segment $[0, d/2]$, instead of $[-d/2, d/2]$, needs to be

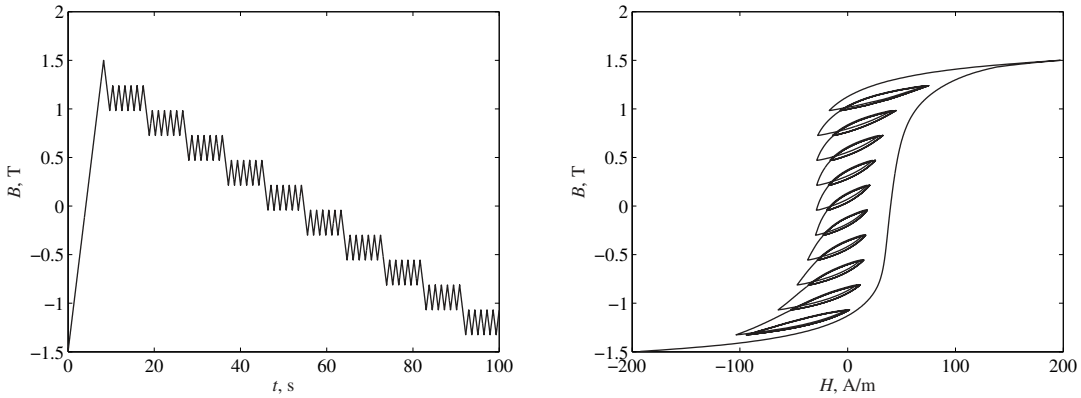

(a) Input of the model (b) The modeled B-H behavior

Figure 3.3: Testing the stability of the history-dependent model in case of complicated flux patterns expected in electrical machine cores.

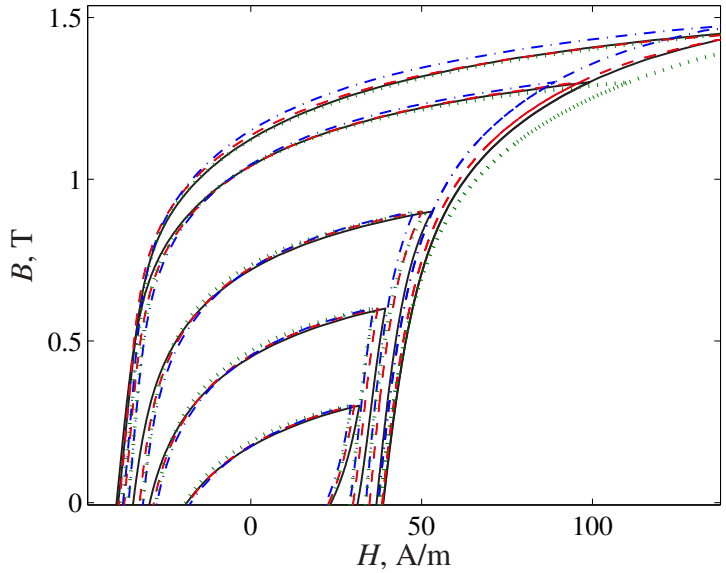

Figure 3.4: Cyclic hysteretic loops predicted by the inverted Preisach model (dotted), the history-dependent model (dashed), the history-independent model (dash-dotted), and compared with experimental data (solid).

discretized, thus saving almost half of the computation time. The 1D model is subjected to a known magnetic flux per unit length $\boldsymbol{\phi} = \boldsymbol{B}d$. The field strength on the surface $H_\varphi(z = d/2, t)$ is used for computing the output of the vector model (3.8).

The identification problem of the MDVH model may be divided into several identification subproblems:

1. Choose the number of directions N.

2. Scale the experimental quasi-static first-order reversal curves by the coefficient η.

3. Adjust the parameter Q using a quasi-static major loop.

4. Refine the excess loss parameters, p and r, using two dynamic loops measured under unidirectional excitation.

5. Identify the coefficient w and the phase shift ψ using experimental data obtained under rotational flux excitations.

These five steps are repeated until the best fit in all cases is found. At the beginning, the identification problem may appear difficult, but using intuition and a macroscopic knowledge of the magnetodynamic rotational phenomena is of remarkable help in achieving the desired results. In other words, the initial guesses for all parameters can be reasonably estimated at the first iteration step. For example, the excess loss parameter p must approximately follow the $f^{0.5}$ law discussed in the statistical loss theory of Bertotti (1988), which means that $p \approx 2$. Additionally, the coefficient w responsible for the loop shapes has to start from a value close to 1 and the phase shift ψ from a value close to zero. The number of directions N can be simply fixed to 8 directions, since this number is found to give relatively accurate results and is rather suitable for the computation time [Saitz (2001a)].

A set of dynamic B-H loops of a ferromagnetic lamination of a thickness $d = 0.5\ \mathrm{mm}$ and conductivity $\sigma = 2.2 \times 10^6\ \mathrm{S/m}$ have been experimentally obtained using a modern digital setup (see Appendix A and Alkar (2007)). Figure 3.5a shows the measured dynamic loops under alternating unidirectional flux excitation and a fundamental frequency of $200\ \mathrm{Hz}$ compared with the predicted loops. The experimental dynamic loops are reproduced relatively accurately by the model. The parameters of the model were further tuned with another set of unidirectional dynamic loops measured at a fundamental frequency of $400\ \mathrm{Hz}$ (see Figure 3.5b.)

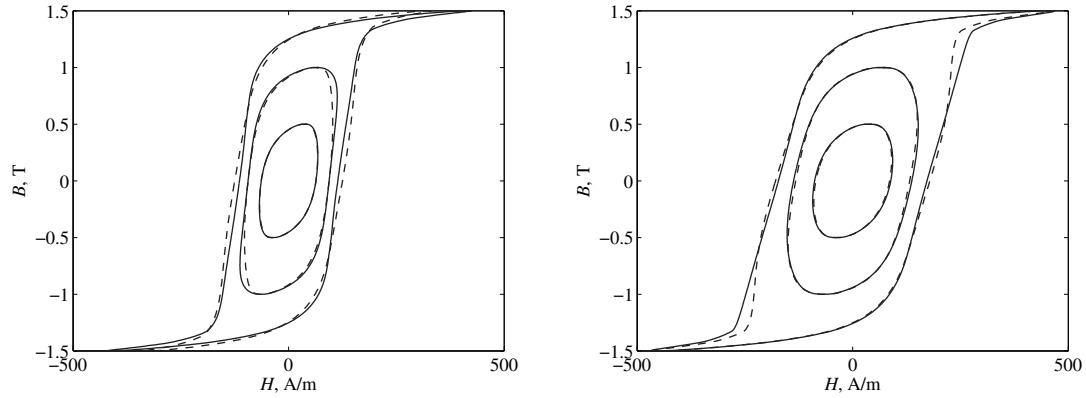

(a) 200 Hz fundamental frequency (b) 400 Hz fundamental frequency

Figure 3.5: The predictions of the unidirectional dynamic loops by the MDVH model (dashed) compared with the experimental loops (solid).

The parameters w and ψ were identified as best fitting the model to the 2D experimental dynamic loops shown in Figure 3.6. The final optimal values of the parameters are summarized in Table 3.1.

Table 3.1: The identified parameters of the magnetodynamic vector hysteresis model.

N	N_e	η	Q	p	r	w	ψ
8	15	1.16	7.54	1.98	0.92	1.12	0.4^o

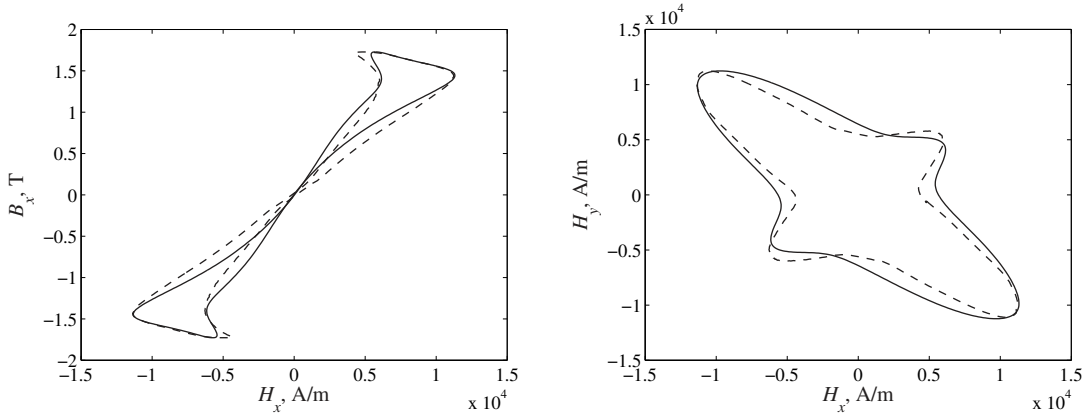

(a) The B_x-H_x dynamic loop (b) The H_x-H_y dynamic loci

Figure 3.6: The 2D dynamic loops predicted by the MDVH model (dashed) and compared with the experimental loops (solid) at a fundamental frequency of 50 Hz .

3.2.3 Identifying the Simplified Magnetodynamic Vector Hysteresis Model

Despite the increase in the number of parameters in the simplified MDVH model, its identification procedure is simpler than that of the MDVH model. Escaping from the iterative solution of (3.9) through the use of the simplified model (3.13) makes the simulations run faster with fewer problems. Further significant numerical advantages will become clearer in Chapter 4.

The identification here needs the same five steps that were used for identifying the MDVH model, with an additional step concerning the coefficients a_0, a_1, and a_2, the optimized values of which are given in Table 3.2. It is interesting to find that all the parameters of the MDVH model shown in Table 3.1 remain the same. The resultant function $v(B)$ is illustrated in Figure 3.7a. The coefficients a_0, a_1, and a_2 of the model were tuned using the same experimental data used to identify the MDVH model. A case of unidirectional dynamic loops measured at a fundamental frequency of 400 Hz is shown in Figure 3.7b. The measured and modeled curves agreed well when $v(B)$ was used (dashed) and disagreed when $v = 1$ (dot-dashed).

Table 3.2: The identified coefficients of the function $v(B)$.

B_s, T	a_0	a_1	a_2
1.7	2.8	0.2	-0.04

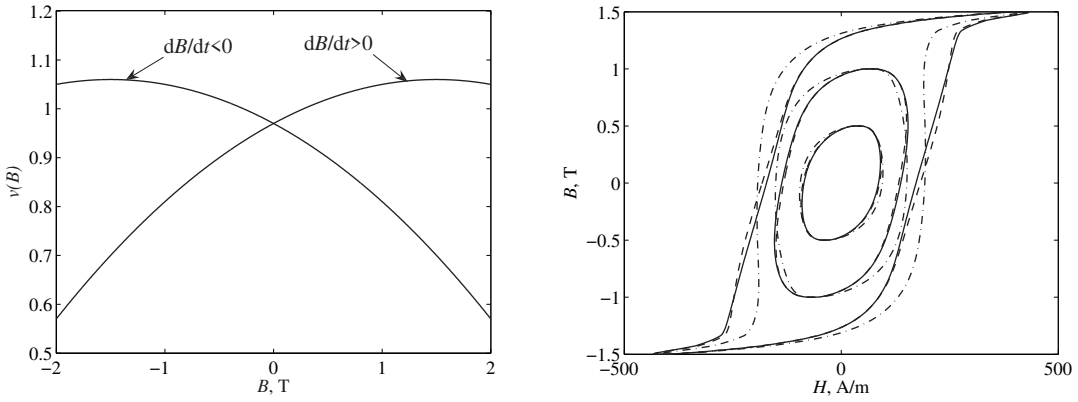

(a) (b)

Figure 3.7: The use of the simplified MDVH model. (a) The identified function $v(B)$. (b) Dynamic loops modeled when $v = 1$ (dot-dashed), $v \neq const$ (dashed), and compared with experimental dynamic loops (solid) at a fundamental frequency of 400 Hz.

3.3 Numerical Results and Discussion

In this section, the properties of the MDVH model are examined by carrying out various simulations. Since the model has shown its ability to reproduce the experimental data, here it will be exploited to study further phenomena that could not be dealt with experimentally during the course of this work. For example, in Figure 3.8, the effect of the harmonics on the iron losses is investigated. In this case, the flux density was forced to be alternating in one direction at a frequency of 50 Hz and magnitude of 1.5 T. When the 25^{th} harmonic was added with a 5% magnitude of the fundamental, the total iron losses increased by 40%, mainly because of the increase in the eddy currents.

Another case, in which the flux was rotational and the frequency was 50 Hz, is investigated next. The loci of the flux density and magnetic field strength, as well as the phase lag α between $\boldsymbol{H}$ and $\boldsymbol{B}$, are shown in Figure 3.9. In the first case (Figures 3.9a and 3.9b), when the flux density was circular with a magnitude of 1.8 T, the phase lag α was small and the vectors $\boldsymbol{H}$ and $\boldsymbol{B}$ were almost parallel. The phase lag α varies with time and takes negative and positive values, depending on whether the vector $\boldsymbol{B}$ lags behind the vector $\boldsymbol{H}$ or is ahead of it. This peculiar phenomenon occurs because w is greater than one; more will be stated about this phenomenon later in this section.

When the flux density was at 1.5 T (Figures 3.9c and 3.9d), the phase lag α was rather high ($\sim 42.5^{\text{o}}$ on average) and always positive, which means that the vector $\boldsymbol{B}$ lags behind the vector $\boldsymbol{H}$. In the case when the flux density was elliptical, with magnitudes ranging between 1.2 T and 0.8 T, the phase lag α oscillated significantly but remained always positive (Figures 3.9e and 3.9f).

In Figure 3.10, the average values of the phase lag α and the ensuing rotational losses in the case when the flux density was circular are plotted as a function of the peak of the flux density at different frequencies. The computations show that the rotational losses

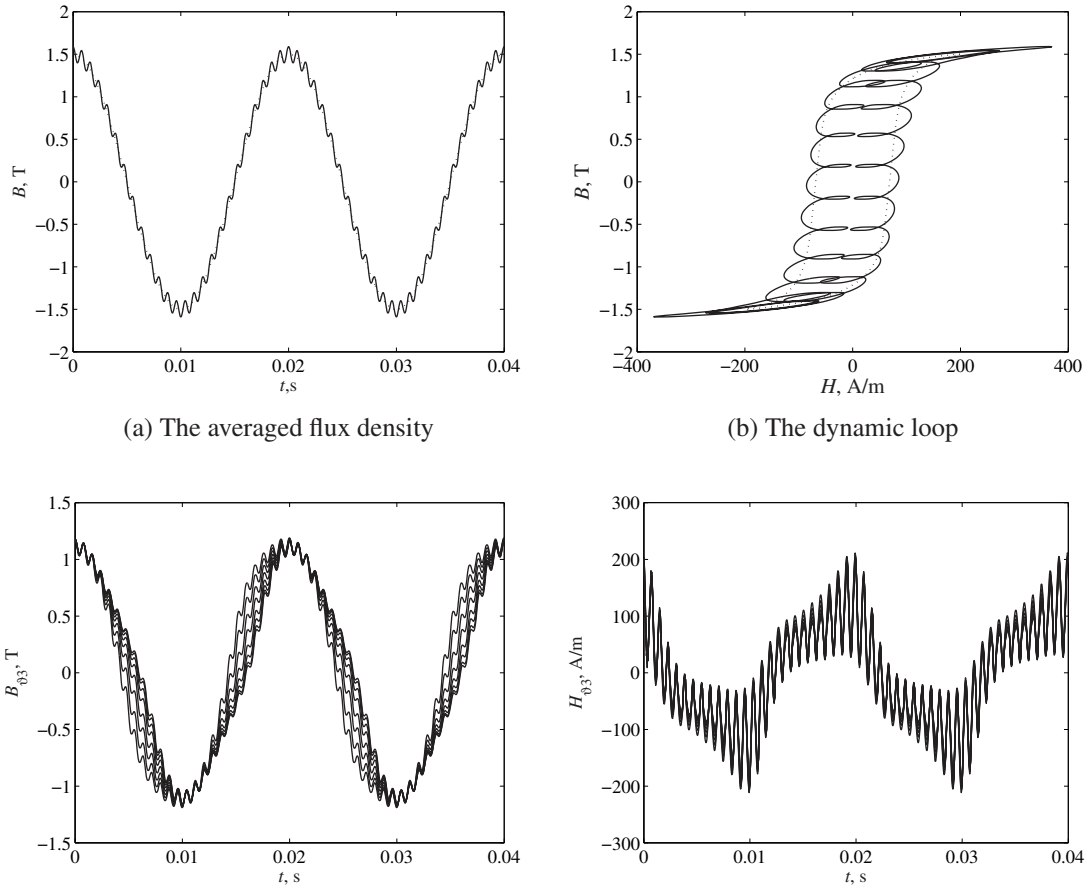

(a) The averaged flux density

(b) The dynamic loop

(c) B_{φ_3} in the lamination depth (finite elements)

(d) H_{φ_3} in the lamination depth (finite elements)

Figure 3.8: Effects of harmonics on iron losses with a fundamental frequency of 50 Hz (dotted): A 40% iron loss increase in this case.

drop at saturation and the phase lag α tends to go to zero. In the quasi-static case when $f = 0.01$ Hz, the hysteresis loss represented the total losses and dropped rapidly to zero at saturation. At the higher frequencies, the eddy-current and excess losses kept increasing slightly even at saturation, and thus the total iron loss did not reach zero. It is noticed that the peak value of the rotational losses does not necessarily correspond with the highest average value of the phase lag α because the magnitudes of the vectors $\boldsymbol{H}$ and $\boldsymbol{B}$ play a significant part. The highest average value of the phase lag α occurs when the hysteresis loops are largest.

Next, the effect of the constants w and ψ of Equation (3.7) on the quasi-static (hysteresis) rotational loss and the loop shapes will be investigated. It should be emphasized that these two constants have two distinct features. The coefficient w is more responsible for the magnitudes of the projected components. The phase lag ψ is, however, responsible for the directions of the projected components.

Let us first assign $\psi = 0$ and so examine only the coefficient w, which means that the generalized Mayergoyz model proposed by Adly and Mayergoyz (1993) is here being investigated. The calculated rotational hysteresis losses and the phase lags for different

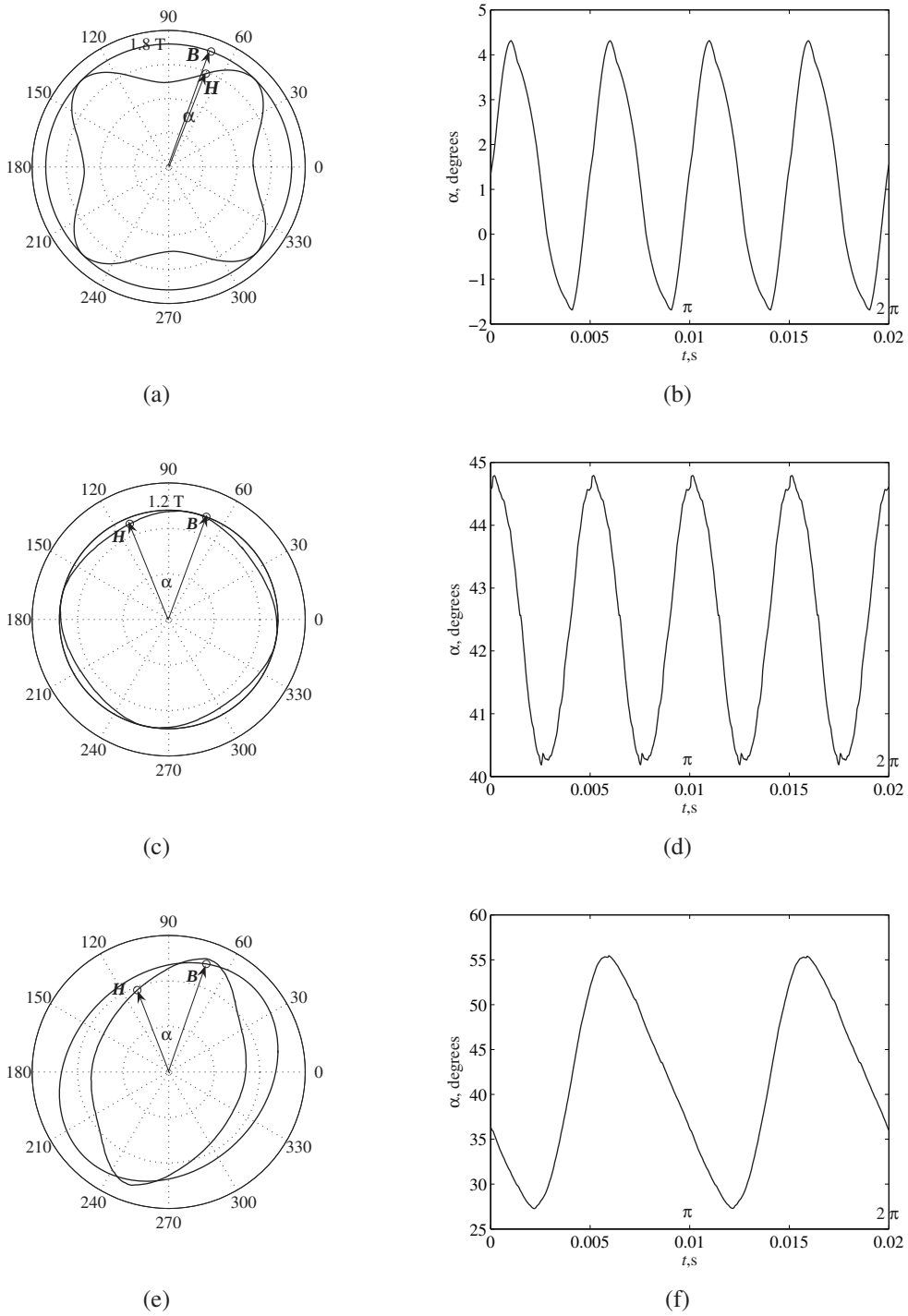

Figure 3.9: The loci of the vector fields rotating anticlockwise and their phase lag at 50 Hz.

values of w are shown in Figure 3.11. The rotational losses begin to be constant near saturation for most of the cases because the model simply oscillates over the major loop. The increase in w has led to no significant decrease in the rotational loss at saturation. On the other hand, the coefficient w has substantially changed the shapes of the B-H loops and thus the loci of the magnetic field strength (see Figure 3.12a). When $w = 1$, the model produced isotropic behavior. However, in the other two cases when $w = 2$ and

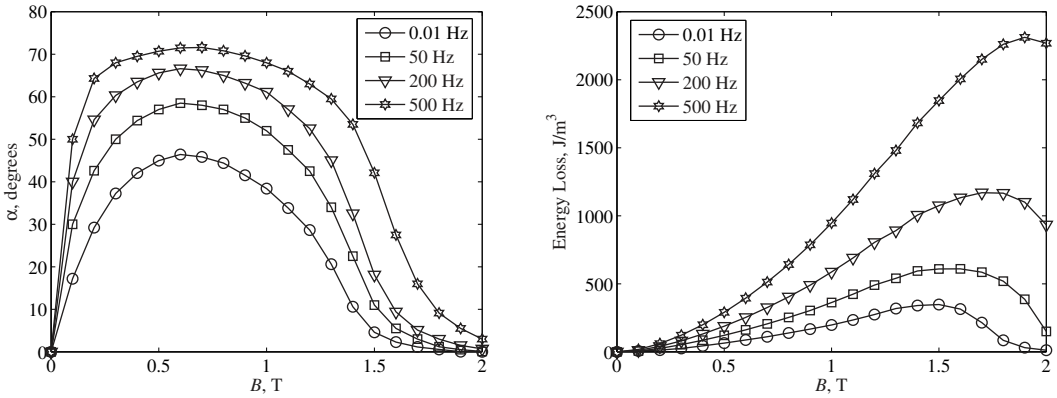

(a) Averaged phase lag (b) Rotational loss

Figure 3.10: The phase lag of the vector fields and their corresponding rotational losses of circular flux excitation at different frequencies.

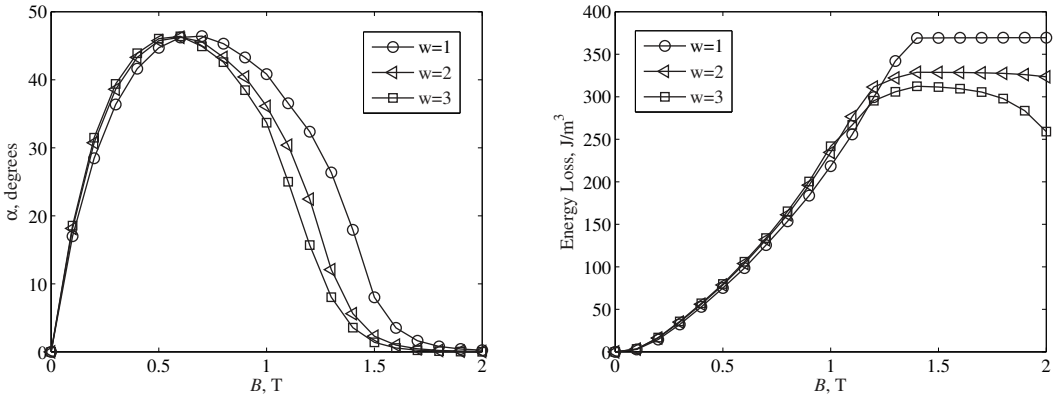

(a) Averaged phase lag (b) Rotational loss

Figure 3.11: The phase lag of the vector fields and the corresponding rotational losses of circular flux excitation when $f = 0.01$ Hz and $\psi = 0.0^{\circ}$.

$w = 3$, the model produced drastically non-circular magnetic field strengths that are not experimentally observed in non-oriented materials. This means that one has to be careful when choosing w and must pay attention not only to the loop area (iron loss) but also to the loci of the magnetic fields.

In theory, if the material is purely isotropic and homogenous, a circular flux excitation must result in a circular magnetic field strength, and vice versa. However, since there is always a degree of anisotropy in non-oriented materials, a circular flux excitation should result in a slightly non-circular magnetic field strength. In experiments, perfectly circular flux excitations cannot be easily achieved. Furthermore, the homogeneity and uniformity of the flux at the measuring points in the sheet is not ensured. The latter problems also affect the accomplishment of reliable experimental results. In the experimental setup constructed in this thesis, although the uniformity of the flux at the measuring points was targeted, uniformity in the flux cannot be said to have been certainly achieved, because

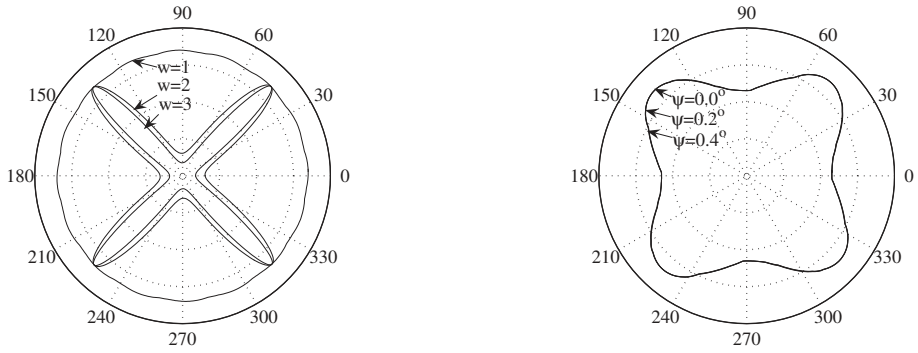

(a) When fixing $\psi = 0.0^{\circ}$ (b) When fixing $w = 1.15$

Figure 3.12: Normalized loci of the magnetic field strength of circular flux density $B = 1.5$ T and frequency $f = 0.01$ Hz.

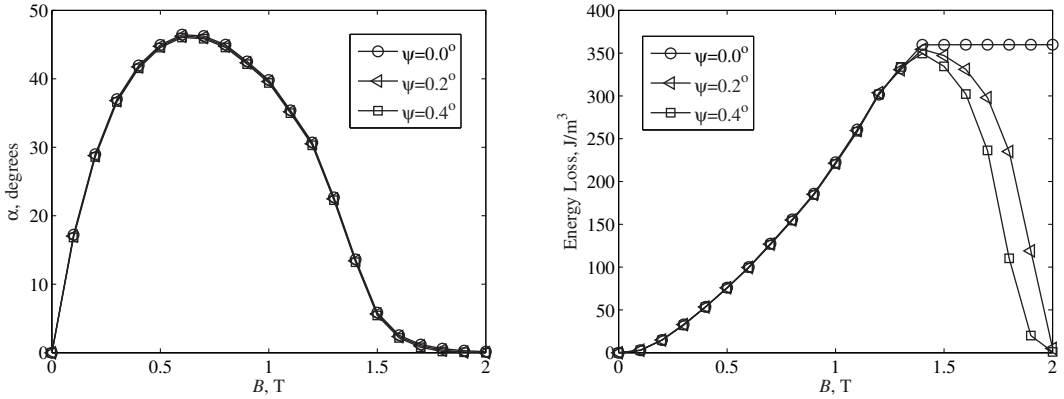

(a) Averaged phase lag (b) Rotational loss

Figure 3.13: The phase lag of the vector fields and their corresponding rotational losses of circular flux excitation when frequency $f = 0.01$ Hz and $w = 1.15$.

only two excitation coils were used. In the literature, most of the experimental methods are based on the arrangement of two excitation coils. For instance, in the work of Brix et al. (1984), the latter effects appear in the measured results of the loci of the magnetic fields. A circular flux excitation resulted in a flower-shaped non-circular magnetic field strength with four peaks [see Fig. 5 in Brix et al. (1984)].

In this work, during the identification procedure of the MDVH model, it is found that $w = 1.12$ or otherwise the calculated B-H loops would not fit to the experimental ones (Figure 3.6). This means that a very similar behavior to that in Brix et al. (1984) is observed here.

Introducing the phase shift ψ is an adequate solution to regulating the rotational losses without significant changes in the loop shapes. In Figure 3.13, different values of ψ were examined. The corresponding rotational hysteresis losses stay similar at peak flux density values below saturation and start to drop sharply at saturation. In the meantime, the loop

shapes are modified only slightly by varying ψ, as indicated in the loci of the magnetic field in Figure 3.12b, which conforms with the experimental results.

3.4 Conclusions

This chapter presented a general magnetodynamic vector hysteresis model for the prediction of iron losses in electrical steel sheets. The model is based upon the Mayergoyz notion of vector hysteresis modeling, but it is more general and is capable of reproducing the experimental data over a wide range of frequencies. The memory of the vector model is treated in the same way as in the Mayergoyz model. All projections of the vector model keep tracking of the history independently, but the vectorial sum of the projections combines these history properties.

The new idea of the vector model is to introduce a very small phase shift between the directions of the projected flux components and the directions of the calculated magnetic field components. In this way, the inadequate coupling of the perpendicular components can be compensated and accounted for by the delay that has been introduced. Thus, the rotational loss property becomes well satisfied. Moreover, the interesting properties of the Mayergoyz model remain the same provided that the introduced delay is small. The model presented here is simple and easy to implement. The identification problem of the Mayergoyz model is reduced to the estimation of a few parameters.

The numerical simulations conducted by the model revealed that the rotational losses under quasi-static circular flux excitations drop to zero at saturation and they remain more significant with an increase in the frequency. At saturation, the phase lag between the flux density vector and the magnetic field vector approaches zero and the vector fields become parallel. The rule of the phase lag ψ is associated with the rotational loss. On the other hand, the coefficient w is more responsible for the loop shapes in the material.

The applicability of the simplified magnetodynamic vector hysteresis model lies in the evasion of the iterative procedure needed for the solution of the nonlinear diffusion equations. This advantage is particularly important when incorporating the lamination model in the electrical machine model.

Chapter 4

Electrical Machine Model

This chapter focuses on the prediction of core losses in rotating electrical machines. In the first section, the 2D finite-element analysis of electrical machines is briefly described. The incorporation of the lamination model in the machine model and the resulting iterative procedure are dealt with. The power balance equation of the machine is shown. In the second section, the convergence of the fixed-point method is analyzed and a locally convergent scheme is proposed. Finally, the machine model is validated using experimental data from two induction motors and the results are discussed and analyzed.

4.1 The Machine Model

The lamination model is essentially useless if it cannot be applied to the prediction of the behavior of magnetic materials in electrical devices. The accurate solution of the magnetic field in a complicated geometry such as a rotating electrical machine requires a rigorous numerical treatment. The spatial discretization of the geometry is needed and here it is accomplished by the use of the 2D finite-element method. In the lamination model developed in Chapter 3, it was assumed that the flux density components, B_x and B_y, were known. Here they will be calculated by the machine model, using the 2D finite-element analysis coupled with the circuit equations [Arkkio (1987)]. Then the magnetic field strength components, H_x and H_y, are determined by the lamination model and entered back to the machine model. The coupling between the machine model and the lamination model is intricate and receives special attention in the thesis.

The initial angles or the reference coordinate systems of the vector hysteresis models are randomized over the entire mesh of the electrical machine. This is done in order to balance the anisotropic behavior of the non-oriented material, a measure that is also considered in practice by manufacturers of the laminations of electrical machines.

The machine model will not be elaborated on as a whole. More emphasis will be placed on the part concerning the laminations. For example, neither the electromagnetic equations of the windings and rotor bars nor the solid steel will be discussed in detail. Nevertheless, the complete overall system of equations will be briefly described.

4.1.1 Finite-Element Modeling

Applying the fixed-point method (3.3) with Maxwell equations results in the following formulation for the laminated core of the machine

$$\nabla \times \nu_{\mathrm{FP}}(\nabla \times \boldsymbol{A}) = -\nabla \times \boldsymbol{M} \tag{4.1}$$

where $\boldsymbol{A}$ is the magnetic vector potential.

If a 2D approach is performed, then one can write $A = \sum_{i=1}^{N_\mathrm{n}} \Lambda_i A_\mathrm{i}$ in which A is the z-component of $\boldsymbol{A}$, N_n is the total number of nodes in the mesh, and A_i is the vector potential in node i whose shape function is Λ_i. After making some mathematical manipulations, applying the Galerkin weighted-residual method over the entire solution region Ω (cross-section of the machine), and respecting the boundary conditions, the following system of differential equations of N_f (free nodes) unknowns results from (4.1)

$$\sum_{i=1}^{N_\mathrm{n}} \int_\Omega \nu_{\mathrm{FP}} \nabla\Lambda_i . \nabla\Lambda_j d\Omega \; A_i = -\int_\Omega (\nabla \times \boldsymbol{M})_z \Lambda_j d\Omega, \quad j = 1, ..., N_\mathrm{f} \tag{4.2}$$

or

$$\sum_{i=1}^{N_\mathrm{n}} S_{ij} A_i = -P_j, \quad j = 1, ..., N_\mathrm{f} \tag{4.3}$$

where $\boldsymbol{S} = [S_{ij}]$ is the assembly (coefficient) matrix and the column $\boldsymbol{P} = [P_j]$ is associated with the fixed-point formulation and has to be updated at each iteration step k.

4.1.2 Iterative Procedure

The flux density components, B_x and B_y, are calculated from the solution of the system of equations (4.3) and are used as the input of the lamination model. As the lamination model is nonlinear, the machine model will be nonlinear too. Therefore, the system of equations (4.3) is solved iteratively, as outlined in Figure 4.1.

In the case where the MDVH model plays the role of the lamination model, the flux density components, B_x and B_y, calculated by the machine model through (4.3) will be responsible for setting the boundary conditions of the MDVH model. Thus, in principle, two nested iteration loops are needed. The first is the local iteration loop of the lamination model and the second is the global iteration loop of the machine model. To circumvent this problem, the boundary conditions of the MDVH model may be kept fixed during iteration and thus one will end up with two more efficient iteration procedures that are not looped but rather made in series [Dlala et al. (2008a)]. The other option which appears to be more practical, and will be proven to be so, is the use of the simplified MDVH model, which has no requirement for an iterative solution. In this way, only one iteration loop is needed for the machine model. This simplification is useful not only for the efficiency of the iterative procedure and the time-stepping scheme but also for its stability.

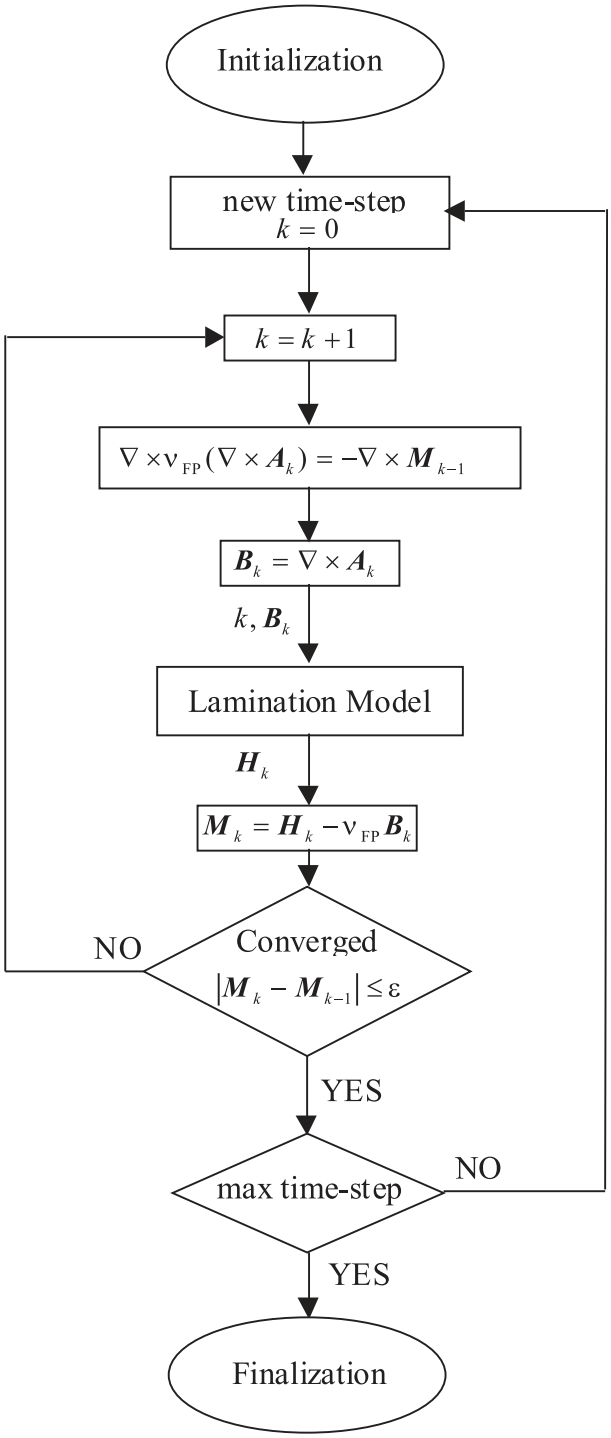

Figure 4.1: Iterative procedure of the machine model.

4.1.3 Overall System of Equations

Rotating electrical machines are constructed of two principal parts: a stationary part, called the stator, and a rotating part, called the rotor. Usually, the stator and the rotor are coupled through the air-gap, and the finite-element analysis must ensure that they are all well modeled together. The circuit equations of each part must be coupled with the 2D finite-element solution.

In a real case, the system of equations (4.3) associated with the laminations is not used alone. The 2D finite-element method is applied likewise to the other materials in the machine, such as the solid steel and rotor bars. The skin effect of the stator windings is not modeled in the field solution [Arkkio (1987); Islam et al. (2007)]. The complete overall system of equations of the rotating electrical machine is solved iteratively using the fixed-point method and discretized in time using the Crank-Nicholson time-stepping scheme as

$$\begin{bmatrix} \boldsymbol{S}^{n+1} & \boldsymbol{D}_{\mathrm{r}} & \boldsymbol{K}\boldsymbol{D}_{\mathrm{s}} \\ \boldsymbol{D}_{\mathrm{r}} & \boldsymbol{C}_{\mathrm{r}} & \boldsymbol{0} \\ \boldsymbol{K}\boldsymbol{D}_{\mathrm{s}} & \boldsymbol{0} & \boldsymbol{E}_{\mathrm{s}} \end{bmatrix} \begin{bmatrix} \boldsymbol{a}_{\mathrm{n}}^{n+1} \\ \boldsymbol{u}_{\mathrm{r}}^{n+1} \\ \boldsymbol{i}_{\mathrm{s}}^{n+1} \end{bmatrix} = \begin{bmatrix} \bar{\boldsymbol{S}}^{n}\boldsymbol{a}^{n} + \boldsymbol{D}_{\mathrm{r}}\boldsymbol{u}_{\mathrm{r}}^{n} + \boldsymbol{K}\boldsymbol{D}_{\mathrm{s}}\boldsymbol{i}_{\mathrm{s}}^{n} + \boldsymbol{P}^{n} + \boldsymbol{P}^{n+1} \\ \boldsymbol{D}_{\mathrm{r}}\boldsymbol{a}^{n} - \boldsymbol{C}_{\mathrm{r}}\boldsymbol{u}_{\mathrm{r}}^{n} - \boldsymbol{E}_{\mathrm{r}}\boldsymbol{i}_{\mathrm{s}}^{n} \\ \boldsymbol{K}\boldsymbol{D}_{\mathrm{s}}\boldsymbol{a}^{n} - \bar{\boldsymbol{E}}_{\mathrm{s}}\boldsymbol{i}_{\mathrm{s}}^{n} - \boldsymbol{C}_{\mathrm{s}}(\boldsymbol{V}_{\mathrm{s}}^{n+1} + \boldsymbol{V}_{\mathrm{s}}^{n}) \end{bmatrix} \tag{4.4}$$

where the solutions $\boldsymbol{a}_{\mathrm{n}}$, $\boldsymbol{u}_{\mathrm{r}}$, and $\boldsymbol{i}_{\mathrm{s}}$ are, respectively, the magnetic vector potential at the nodes, the voltages of the rotor circuit, and the currents of the stator phases. The matrices $\boldsymbol{C}_{\mathrm{r}}$, $\boldsymbol{D}_{\mathrm{r}}$, $\boldsymbol{D}_{\mathrm{s}}$, $\boldsymbol{E}_{\mathrm{s}}$, and $\bar{\boldsymbol{E}}_{\mathrm{s}}$ are associated with the rotor and stator circuits and the end windings. The subscripts r and s refer to the rotor and stator, respectively. The matrix $\boldsymbol{K}$ defines the type of connection of the stator winding. The elements of the coefficient matrix $\boldsymbol{S}$ and $\bar{\boldsymbol{S}}$ are given as

$$\begin{aligned} \boldsymbol{S} &= [S_{ij}] = \sum_{i=1}^{N_{\mathrm{n}}} \Big(\int_{\Omega} \nu_{\mathrm{FP}} \nabla\Lambda_i . \nabla\Lambda_j d\Omega + \frac{2\sigma}{\Delta t} \int_{\Omega} \Lambda_i \Lambda_j d\Omega \Big), \quad j = 1, ..., N_{\mathrm{f}} \\ \bar{\boldsymbol{S}} &= [\bar{S}_{ij}] = \sum_{i=1}^{N_{\mathrm{n}}} \Big(\int_{\Omega} \nu_{\mathrm{FP}} \nabla\Lambda_i . \nabla\Lambda_j d\Omega - \frac{2\sigma}{\Delta t} \int_{\Omega} \Lambda_i \Lambda_j d\Omega \Big), \quad j = 1, ..., N_{\mathrm{f}}. \end{aligned} \tag{4.5}$$

The system of equations (4.4) is sparse and here is efficiently solved using a direct method of sparse matrices.

4.1.4 The Power Balance and Core Losses

The power balance test is an adequate check of the errors that might exist in the numerical computations. Because the core losses are incorporated into the field solution, their effect on the input power of the electrical machine must appear.

The power balance of the electrical machine is applied to the average powers as follows:

$$P^{\mathrm{in}} = P^{\mathrm{out}} + P_{\mathrm{s}}^{\mathrm{res}} + P_{\mathrm{r}}^{\mathrm{res}} + P^{\mathrm{c}} \tag{4.6}$$

where P^{in} is the average input power of the stator, P^{out} is the average output power of the shaft, $P_{\mathrm{s}}^{\mathrm{res}}$ is the average resistive loss of the stator winding, $P_{\mathrm{r}}^{\mathrm{res}}$ is the average resistive loss of the rotor cage, and P^{c} is the average core losses. The methods for the determination and description of these powers can be found in Saitz (2001a). The term $\frac{\partial W}{\partial t}$ responsible for storing and releasing the energy in the machine is not apparent in (4.6) because the instantaneous powers are being averaged over several periods of the supply

frequency.

The output power is computed using the principle of virtual work [Coulomb (1983)]. The total core losses are computed using the Poynting vector theorem as

$$P^{\mathrm{c}} = \frac{1}{T}\int_T \boldsymbol{H}.\frac{\mathrm{d}\boldsymbol{B}}{\mathrm{d}t}\mathrm{d}t = \frac{1}{T}\int_T \left(H_x.\frac{\mathrm{d}B_x}{\mathrm{d}t} + H_y.\frac{\mathrm{d}B_y}{\mathrm{d}t}\right)\mathrm{d}t. \tag{4.7}$$

The core losses are separated into alternating and rotating components according to the theorem of Atallah and Howe (1993).

4.2 The Fixed-Point Method

None of the available iterative methods are sufficiently stable and efficient to solve nonlinear hysteresis. Indeed, although the standard Newton-Raphson method converges rapidly near the solution, it cannot always ensure convergence since it is fundamentally based upon the derivative and thus can easily suffer from instability.

The classical fixed-point method, on the other hand, can produce stable solutions but very slow ones [Hantila (1974a,b, 1975); Hantila et al. (2000)]. The fixed-point method is distinguished by its independence from calculating the derivative. In this thesis, it will be shown that applying the derivative to the fixed-point method can produce much faster iteration. It is important to remember that the Newton-Raphson method uses the derivative to find the solution and thus the method is highly sensitive to the derivative. On the other hand, the fixed-point method may apply the derivative to accelerate the convergence, and therefore, in the worst-case scenario, the derivative can even be approximated if it is difficult to determine.

4.2.1 Theory of the Fixed-Point Method

The conditions and criteria for the convergence of the fixed-point theory are well documented in mathematics [Olver and Shakiban (2005, 2007)]. Here, only the most relevant and important ones are summarized. In general, a nonlinear iterative system can be devised as

$$\boldsymbol{b}^{(k+1)} = \boldsymbol{G}(\boldsymbol{b}^{(k)}) \tag{4.8}$$

where $\boldsymbol{G} : \mathbb{R}^m \rightarrow \mathbb{R}^m$ is a real multidimensional function. The solution of (4.8), if one exists, is a fixed-point vector $\boldsymbol{b}^* = \boldsymbol{G}(\boldsymbol{b}^*)$, which is a discrete collection of points $\boldsymbol{b}^{(k)} \in \mathbb{R}^m$, which start at a specified initial iterate $\boldsymbol{b}^{(0)}$.

The fixed-point iteration is based on the contraction mapping principle. This principle guarantees the existence and uniqueness of fixed points and provides a constructive method to find those fixed points. A function $\boldsymbol{G} : \mathbb{R}^m \rightarrow \mathbb{R}^m$ is a contraction on a domain $\boldsymbol{G} : \boldsymbol{U} \rightarrow \boldsymbol{U}$ at a point $\boldsymbol{b}^* \in \boldsymbol{U}$ if there exists a constant $0 \leq \beta < 1$ such that

$$||\boldsymbol{G}(\boldsymbol{b}) - \boldsymbol{G}(\boldsymbol{b}^*)|| \leq \beta||\boldsymbol{b} - \boldsymbol{b}^*||. \tag{4.9}$$

Here, since $\boldsymbol{G}$ is a contraction, $\boldsymbol{b}^*$ is an asymptotically stable fixed point. In general, condition (4.9) can be perceived for multidimensional functions by using the power of linear algebra. If the spectral radius of the Jacobian matrix $\rho(\boldsymbol{G}^{'}(\boldsymbol{b}^*)) < 1$, then $\boldsymbol{G}$ is a contraction at $\boldsymbol{b}^*$. Hence, the fixed point $\boldsymbol{b}^*$ is asymptotically stable and a basin of attraction exists. The spectral radius is defined as

$$\rho = \max_{1 \leq i \leq m}(|\lambda_i|) \tag{4.10}$$

where λ_i are the eigenvalues of $\boldsymbol{G}^{'}$.

The smaller the spectral radius (or matrix norm) of the Jacobian matrix at the fixed point, the faster the iterates will converge to it. The quadratic convergence estimate is given by

$$||\boldsymbol{b}^{(k+1)} - \boldsymbol{b}^*|| \leq \tau ||\boldsymbol{b}^{(k)} - \boldsymbol{b}^*||^2 \tag{4.11}$$

for some constant $\tau > 0$.

In practical numerical systems, the norm or spectral radius of the Jacobian matrix cannot be known because one does not know in advance where the fixed point is. This apparent difficulty can be circumvented by requiring that $||\boldsymbol{G}^{'}(\boldsymbol{b})||$ be < 1 for all $\boldsymbol{b}$.

4.2.2 Analysis of the Fixed-Point Method in Magnetic Systems

There is freedom associated with the choice of the fixed-point coefficient ν_{FP} since only the convergence matters here. Therefore, the basis of choosing ν_{FP} is the contraction of the fixed-point iteration.

The use of Maxwell equations with the fixed-point method results in

$$\nabla \times \nu_{\mathrm{FP}} \boldsymbol{B} = -\nabla \times \boldsymbol{M}. \tag{4.12}$$

Equation (3.3) can also be written as

$$\boldsymbol{M}(\boldsymbol{B}) = \boldsymbol{H}(\boldsymbol{B}) - \nu_{\mathrm{FP}} \boldsymbol{B}, \tag{4.13}$$

where $\boldsymbol{H}(\boldsymbol{B})$ may be a hysteretic or single-valued function and must be Lipschitz continuous. Then, the following iterated function is obtained:

$$\nabla \times \boldsymbol{B} = \frac{-1}{\nu_{\mathrm{FP}}}(\nabla \times \boldsymbol{M}(\boldsymbol{B})). \tag{4.14}$$

Equation (4.14) is analogous to (4.8) since it represents the magnetic problem in the form of the fixed-point method as

$$\boldsymbol{B} \equiv \boldsymbol{G}(\boldsymbol{B}) \equiv \frac{\boldsymbol{H}(\boldsymbol{B})}{\nu_{\mathrm{FP}}} - \boldsymbol{B}. \tag{4.15}$$

For 3D problems ($m = 3$), the three components of (4.15) in the x-, y-, and z-directions

can be written as

$$\begin{aligned} G_x(B_x, B_y, B_z) &= \frac{H_x(B_x, B_y, B_z)}{\nu_{\mathrm{FP}}} - B_x \\ G_y(B_x, B_y, B_z) &= \frac{H_y(B_x, B_y, B_z)}{\nu_{\mathrm{FP}}} - B_y \\ G_z(B_x, B_y, B_z) &= \frac{H_z(B_x, B_y, B_z)}{\nu_{\mathrm{FP}}} - B_z \end{aligned}$$

and the Jacobian matrix of $\boldsymbol{G}$ follows as

$$\boldsymbol{G}^{'}(\boldsymbol{B}) = \begin{pmatrix} \frac{1}{\nu_{\mathrm{FP}}}\frac{\partial H_x}{\partial B_x} - 1 & \frac{1}{\nu_{\mathrm{FP}}}\frac{\partial H_x}{\partial B_y} & \frac{1}{\nu_{\mathrm{FP}}}\frac{\partial H_x}{\partial B_z} \\ \frac{1}{\nu_{\mathrm{FP}}}\frac{\partial H_y}{\partial B_x} & \frac{1}{\nu_{\mathrm{FP}}}\frac{\partial H_y}{\partial B_y} - 1 & \frac{1}{\nu_{\mathrm{FP}}}\frac{\partial H_y}{\partial B_z} \\ \frac{1}{\nu_{\mathrm{FP}}}\frac{\partial H_z}{\partial B_x} & \frac{1}{\nu_{\mathrm{FP}}}\frac{\partial H_z}{\partial B_y} & \frac{1}{\nu_{\mathrm{FP}}}\frac{\partial H_z}{\partial B_z} - 1 \end{pmatrix}. \tag{4.16}$$

The Jacobian matrix (4.16) contains the most important information about the convergence of the 3D function $\boldsymbol{G}(\boldsymbol{B})$. As stated earlier, the spectral radius (or the norm) of the Jacobian matrix (4.16) must be less than one so that the 3D function $\boldsymbol{G}(\boldsymbol{B})$ is convergent. For the sake of simplicity, the off-diagonal entries in (4.16) will be assigned to zero; the mutual magnetic field effects of the three components, B_x, B_y, and B_z, are small enough and the latter assumption can be appreciated. Therefore, one has to deal only with the diagonal elements (which are the eigenvalues of the matrix) to investigate the convergence of the function $\boldsymbol{G}(\boldsymbol{B})$. In such a case, the zero matrix can be enforced on the Jacobian matrix only in the following special case:

$$\nu_{\mathrm{FP}} = \frac{\partial H_x}{\partial B_x} = \frac{\partial H_y}{\partial B_y} = \frac{\partial H_z}{\partial B_z}.$$

This desirable case ensures quadratic convergence but is achieved only at certain instants if the magnetized body is purely isotropic and magnetized under a purely circular flux. Another special case, but an undesirable one, arises when any of the partial derivatives, $\frac{\partial H_x}{\partial B_x}$, $\frac{\partial H_y}{\partial B_y}$, $\frac{\partial H_z}{\partial B_z}$, equals zero, i.e., $\rho(\boldsymbol{G}^{'}) = 1$. This case makes the fixed-point iteration stable but not asymptotically stable, meaning that the iterates will remain oscillating around the fixed point, not converging or diverging. The borderline case ($\rho(\boldsymbol{G}^{'}) = 1$) will not be further analyzed here because of the assumption that it will not take place, and one is mostly interested in the general case. The problem that arises next is how to generally determine the optimal value of ν_{FP} that can permit the smallest norm of the Jacobian matrix, and hence the fastest convergence possible. This optimization problem can be approached by different techniques, including Lagrange multipliers, but here a simpler analytical technique is sought.

There is a constraint emerging immediately from the Jacobian matrix (4.16), affirming

that for every diagonal element, the following inequality must hold

$$\Big|\frac{1}{\nu_{\mathrm{FP}}}\frac{\partial H}{\partial B}-1\Big|<1$$

and hence

$$\frac{1}{\nu_{\mathrm{FP}}}\frac{\partial H}{\partial B}<2. \tag{4.17}$$

This inequality must hold for the three partial derivatives $\frac{\partial H_x}{\partial B_x}, \frac{\partial H_y}{\partial B_y}, \frac{\partial H_z}{\partial B_z}$ and must be always respected. The inequality is useful and will be the basis for finding the optimum of ν_{FP}. The inequality (4.17) is satisfied only when the three partial derivatives $\frac{\partial H_x}{\partial B_x}, \frac{\partial H_y}{\partial B_y}, \frac{\partial H_z}{\partial B_z}$ have the same sign and only when the following condition is applied:

$$\Big|\frac{1}{\nu_{\mathrm{FP}}}\frac{\partial H}{\partial B}\big|_{\min}-1\Big|=\Big|\frac{1}{\nu_{\mathrm{FP}}}\frac{\partial H}{\partial B}\big|_{\max}-1\Big|. \tag{4.18}$$

This condition is implied from the diagonal entries of the Jacobian matrix. The only components that play direct roles are the maximum and minimum of the three partial derivatives, and the one in the middle has no effect and does not contribute. The only case that permits (4.17) is when the condition (4.18) is imposed. Therefore, the optimal coefficient ν_{FP} that gives the fastest convergence is found as

$$\nu_{\mathrm{FP}}=\frac{\frac{\partial H}{\partial B}\big|_{\min}+\frac{\partial H}{\partial B}\big|_{\max}}{2}, \tag{4.19}$$

where

$$\frac{\partial H}{\partial B}\big|_{\min}=\min\{\frac{\partial H_x}{\partial B_x},\frac{\partial H_y}{\partial B_y},\frac{\partial H_z}{\partial B_z}\},$$
$$\frac{\partial H}{\partial B}\big|_{\max}=\max\{\frac{\partial H_x}{\partial B_x},\frac{\partial H_y}{\partial B_y},\frac{\partial H_z}{\partial B_z}\}.$$

In 2D problems, because there are two partial derivatives only for the x- and y-directions, the optimal coefficient ν_{FP} is found as

$$\nu_{\mathrm{FP}}=\frac{\frac{\partial H_x}{\partial B_x}+\frac{\partial H_y}{\partial B_y}}{2}. \tag{4.20}$$

In 1D problems, the optimal coefficient ν_{FP} is obtained when

$$\frac{1}{\nu_{\mathrm{FP}}}\frac{\mathrm{d}H}{\mathrm{d}B}-1=0$$

and the optimal value of ν_{FP}, which ensures quadratic convergence in this case, is found as

$$\nu_{\mathrm{FP}}=\frac{\mathrm{d}H}{\mathrm{d}B}. \tag{4.21}$$

The validity of (4.19) is also checked for the two special cases mentioned above, particularly when $\rho(\boldsymbol{G}')=0$ and $\rho(\boldsymbol{G}')=1$. Interestingly, the optimal coefficient ν_{FP} of (4.19)

was observed in a totally different way by Hantila et al. (2000). Because, in practice, the partial derivatives cannot be known prior to the fixed-point solution, Hantila suggested precalculating ν_{FP} and keeping it fixed throughout the computations. In this classical way, a global coefficient is used for the whole analysis and, thus, the method is referred to as the global-coefficient method (GCM). The resultant spectral radius from the GCM is often close to one, $\rho(\boldsymbol{G}') \approx 0.99$, consistently leading to slow convergence.

4.2.3 Locally Convergent Fixed-Point Scheme

In time-stepping analysis, the initial value $\boldsymbol{B}^{(k=0)}$ for time step n is known from the first solution of the current time step and is sufficiently close to the fixed point. Thus, a basin of attraction that contains $\boldsymbol{B}^{(0)}$ and fulfills (4.9) can be found by rewriting (4.19), (4.20), and (4.21), for the 3D, 2D, and 1D problems, respectively, as

$$\nu_{\mathrm{FP}}^{(n)}|_{3\mathrm{D}} = C\frac{\frac{\partial H}{\partial B}^{(k=0)}\big|_{\min} + \frac{\partial H}{\partial B}^{(k=0)}\big|_{\max}}{2}, \tag{4.22}$$

$$\nu_{\mathrm{FP}}^{(n)}|_{2\mathrm{D}} = C\frac{\frac{\partial H_x}{\partial B_x}^{(k=0)} + \frac{\partial H_y}{\partial B_y}^{(k=0)}}{2}, \tag{4.23}$$

$$\nu_{\mathrm{FP}}^{(n)}|_{1\mathrm{D}} = C\frac{\mathrm{d}H}{\mathrm{d}B}^{(k=0)}, \tag{4.24}$$

where C is a constant that must be conveniently chosen to ensure fast convergence so that the function $\boldsymbol{G}(\boldsymbol{B})$ is strictly attractive in some interval containing $\boldsymbol{B}^{(0)}$. The constant C is necessary and must be greater than one because the derivative at the present time step has been approximated from the first iteration. C is dependent on the size of the time step and on the temporal behavior of the system involved. A simple method using linear search was adopted in this work and was found to be effective. For any problem, one may start by giving C some value slightly greater than one and then testing the convergence for a complete simulation. If converged, the value of C is fixed; if not, C is increased by a small value until an appropriate value of C is obtained. For simple problems, it is generally found that C takes values in the range of $1 < C < 2$. On the other hand, in more complicated situations, such as in electrical machines, the factor C is usually greater than 2. In these types of problems, a time-stepping scheme such as Crank-Nicholson's is often used. The initial values resulted by the time-stepping scheme from the previous time step cannot always be close to the fixed-point solution because of the system dynamics. Therefore, the interval $\boldsymbol{U}$ is enlarged by increasing C in order to account for these effects.

The methods used above in Equations (4.22), (4.23), and (4.24) compute local coefficients ν_{FP} at each time step and produce locally convergent iterations. Thus, the methods are referred to as local-coefficient methods (LCM). The LCMs are well suited to solving nonlinear time-domain discretized partial differential equations. For example, solving Maxwell equations by the time-stepping finite-element method will result in calculating local coefficients ν_{FP} as a function of time and space $\nu_{\mathrm{FP}}(t, x, y, z)$. This means that ef-

ficient iteration is achieved because all the finite elements in the mesh are optimized to produce the fastest convergence at each time step.

It should be noted that the LCMs make use of the information about the differential reluctivities at each time step. This is similar to the Newton-Raphson method (NRM), which updates the differential reluctivity at each iteration step. However, the NRM is principally based on calculating the derivative while the fixed-point iteration is not. Therefore, the LCMs are not sensitive to non-differentiability, even in case of hysteresis.

4.3 Implementation

The finite-element model of the electrical machine developed in Section 4.1 is implemented in a Fortran program. The model is general and can be used for both synchronous and asynchronous machines. In this thesis, a squirrel-cage induction motor, referred to as Motor I, and a high-speed induction motor, referred to as Motor II, are studied using the models that were developed. The characteristics of the motors are given in Appendices B and C.

For the purpose of comparison, the lamination model in the 2D time-stepping finite-element model (Figure 4.1) was represented by three different models: the MDVH model, the simplified MDVH model, and a single-valued model. In the latter, the core losses were computed posteriorly using the two-component method of Lavers et al. (1978). In the case of Motor I, the manufacturer delivered a sample of the electrical steels but was not exactly sure that the machine was made of these specific steels. Nonetheless, it is believed that the properties of the steel sample that was delivered are very closely related to those of the machine, if not the same.

To avoid modeling the transient of the motor start-up, a time-harmonic model was applied to provide the initial values of the steady-state solution before the time-stepping model was used. Then the time-stepping analysis was run over several periods T of the supply voltage to ensure that the steady state was reached. In all the following simulations 10 periods were used. Second-order finite elements were used for the machine model. The locally convergent method (4.23) of the fixed-point iteration developed in Section 4.2 was used in the model.

4.3.1 Validation of the Machine Model

The core losses of the motors were measured at no load with various voltage levels and they were segregated from the total electromagnetic losses using a rigorous method described in detail by Dlala and Arkkio (2007). The measurement was based on the same principle used in determining the hysteresis torque [Saitz (2001a)]. The hysteresis torque changes sign at the synchronous speed (no load) and causes a jump in the input power of the machine. The only torque or loss component that changes significantly and abruptly when passing the synchronous speed is assumed to correspond to the hysteresis torque.

Near the synchronous speed, the torque components associated with the harmonics and friction are approximately constant. The jump of power, which is associated with the hysteresis torque, is determined by operating the machine at small slips in motoring and generating modes and then extrapolating to the synchronous speed. The average power loss obtained from these two modes corresponds to the core loss and the resistive losses.

The advantage of this method is that the motor is enforced to run near the synchronous speed, ensuring that no friction or windage mechanical losses are apparent in the measurements. Furthermore, the method suppresses the negative torque caused by the harmonics. The iron losses are then separated from the total electromagnetic losses by subtracting the resistive loss of the stator. The result of the subtraction is believed to be associated with the core losses.

For the sake of measurement convenience, Motor II was not operated under the nominal conditions because it is a high-speed machine. The motor was run at 50 Hz instead of its nominal frequency of 500 Hz. Nevertheless, the measured core loss data can be used for validating the numerical models. The precision of the measuring devices used in the experiments can be found in Saitz (2001a).

Motor I

Figure 4.2a shows the computed total core losses of Motor I compared with the experimental ones obtained from the synchronous no-load test. The MDVH model and its simplified version gave relatively accurate results over the whole range of supply voltages. The small discrepancies between the experimental and modeled results are believed to be associated with the harmonics. The harmonic losses induced in the iron and copper of the rotor are modeled in the field solution; thus, their effect is considered.

The single-valued model gives relatively acceptable results at lower voltage levels (lower flux densities) but becomes remarkably inaccurate at higher flux densities. The main reason for this is the inadequacies of the single-valued model and the two-component method in taking the rotational flux and eddy currents into account.

In Figure 4.2b, the total core losses of the motor calculated by the MDVH model are separated into alternating and rotating components.

It is observed that even though the voltage in the stator increases, the core losses decrease because at saturation the rotational losses start to drop. The hysteresis loss is predominant in the stator. However, the eddy-current losses are predominant in the rotor core and they increase sharply with an increase in the supply voltage. The high harmonics resulting from slotting have a direct influence on the eddy-current losses. The rotational loss component contributes 30% of the total core losses at the rated voltage.

The influence of the proper modeling of magnetic materials on the input power can be seen from Figure 4.3. The use of the magnetodynamic models gave better results because the current is proportional to the magnetic field strength. Furthermore, the power balance and the electromagnetic power losses of Motor I were computed at no load using the simplified MDVH model, as illustrated in Table 4.1.

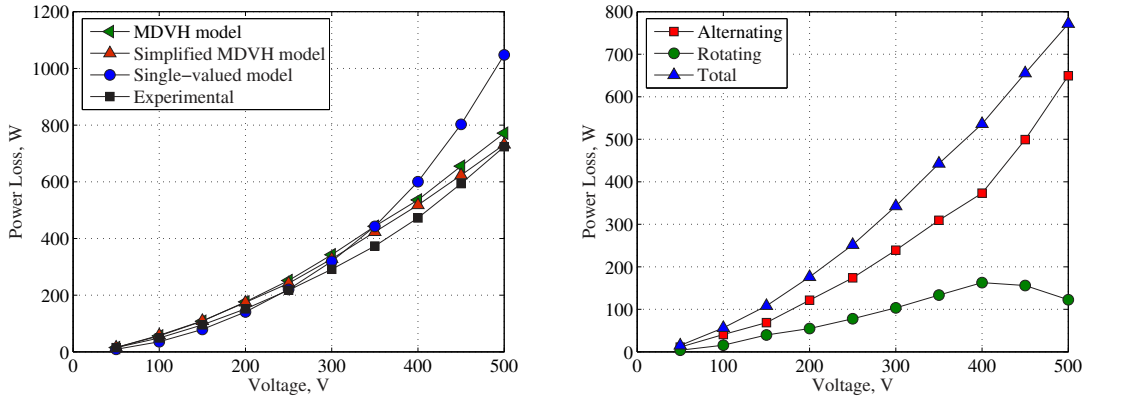

(a) Total core losses

(b) Alternating and rotational losses separated by the MDVH

Figure 4.2: No-load core losses of Motor I predicted by the MDVH model, the simplified MDVH model, the single-valued model, and compared with experimental data.

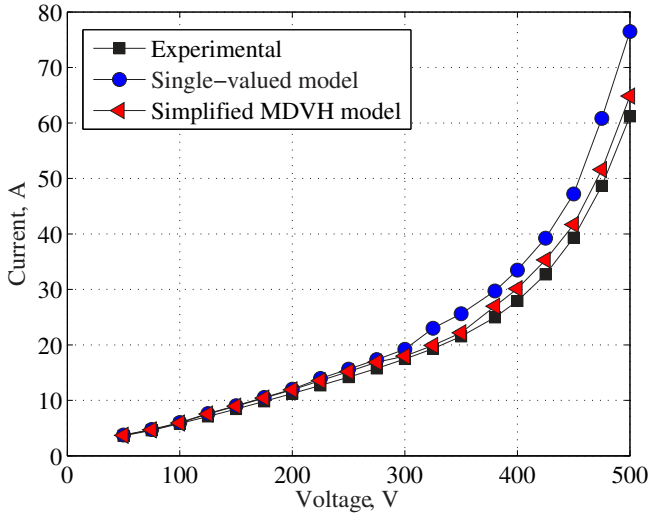

Figure 4.3: The effect of the magnetic material modeling on the characteristics of Motor I.

Motor II

Figure 4.4 shows the computed total core losses of Motor II compared with the experimental ones obtained from the synchronous no-load test. It is shown that the MDVH model and its simplified version gave relatively the same results over the whole range of supply voltages. On the other hand, the single-valued model has underestimated the experimental results.

4.3.2 Simulation Results

The validated machine model was used to develop further interesting results. The waveforms of the flux density and magnetic field strength, as well as the dynamic B-H loops

Table 4.1: The power balance and electromagnetic power losses of Motor I calculated by using the simplified MDVH model.

Power type	Value (W)
Input power	464.76
Shaft power	-143.83
Resistive loss	153.19
Hysteresis loss (stator)	171.23
Hysteresis rotor (rotor)	9.20
Classical eddy-current loss (stator)	135.81
Classical eddy-current loss (rotor)	103.45
Excess loss (stator)	34.34
Excess loss (rotor)	11.12
Total core losses	465.34

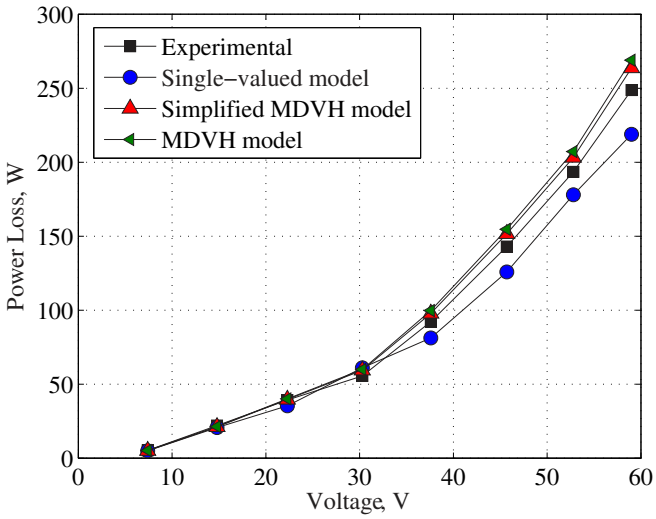

Figure 4.4: No-load core losses of Motor II predicted by the MDVH model, the simplified MDVH model, the single-valued model, and compared with experimental data.

and their loci at a point in the stator yoke of Motor I where the flux is noticeably rotational, are shown in Figures 4.5 and 4.6. The sum of the area of the B-H loops in the x- and y-directions represents the core losses dissipated at that point.

Furthermore, the same graphs at a point of on the rotor tooth are shown in Figures 4.7 and 4.8. In Figure 4.9, the periodicity of the flux in the rotor is shown in the magnified part of Figures 4.7a and 4.7b. This means that the minor loops are repeated at each time period T of the supply frequency. In a loaded machine, the slip, s, introduces an additional low-order harmonic, sf, that will mean the minor loops are not exactly repeated at the period T of the supply frequency f but rather at the period of the slip frequency $\frac{1}{sf}$. Thus, the accurate prediction of the iron loss in the rotor may require the simulation of at least one period of $\frac{1}{sf}$, which means relatively tedious work. From a statistical point of view, the effect of the harmonic $\frac{1}{sf}$ on the total core loss of the rotor is insignificant, and thus the

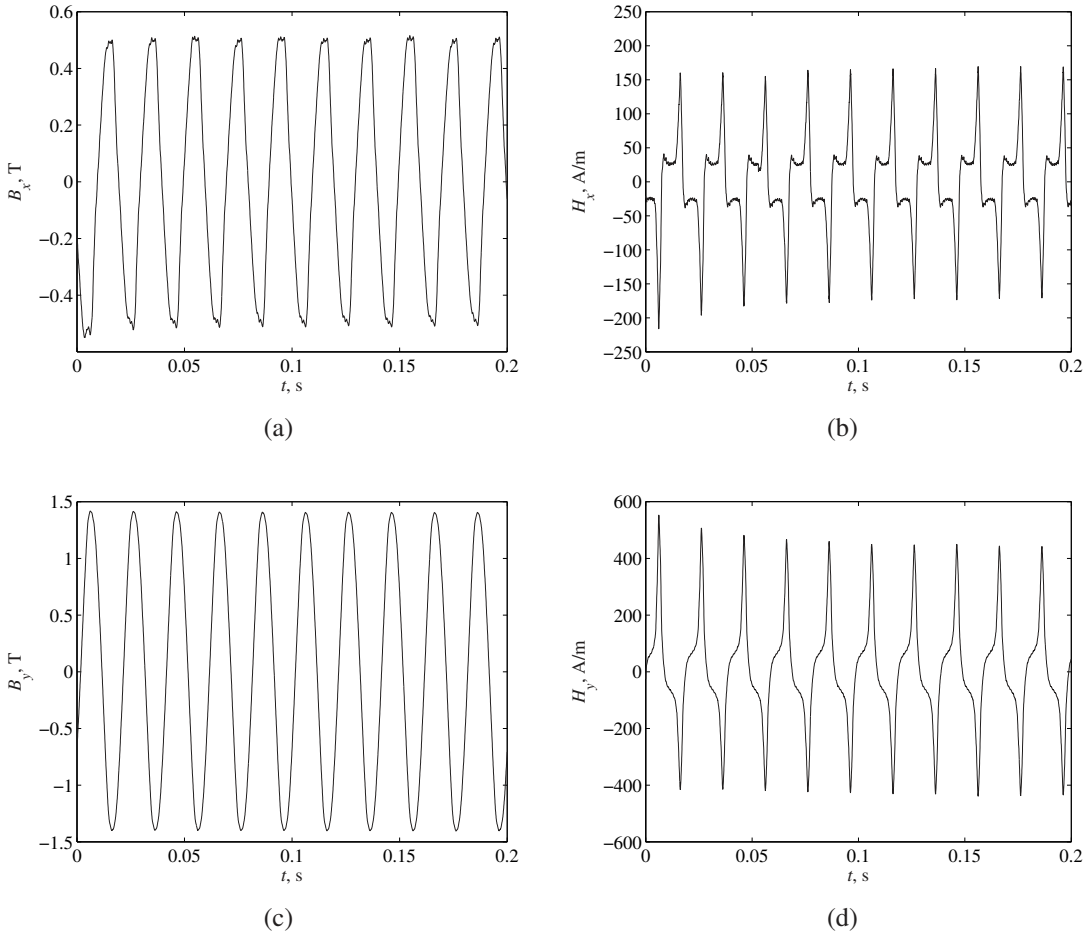

Figure 4.5: The waveforms of the magnetic fields at a point in the tooth root of the stator yoke of Motor I.

simulation of a few periods of T can be sufficient. Moreover, in general, the field of a loaded induction machine is not exactly periodic in time.

4.3.3 Numerical Problems and Computation time

The flux density in the rotor of Motor I is highly distorted, containing high-order harmonics (see Figure 4.9). When the MDVH model was being used, these high harmonics caused significant problems for the stability of the iterative procedure. On the other hand, since the simplified MDVH model does not require the solution of a nonlinear equation, the stability of the iterative procedure was guaranteed. The MDVH model imposed the use of a time-step size five times smaller than that of the simplified model in order to obtain stable, accurate results. It was observed that the eddy-current losses in the rotor were heavily dependent on the time-step size in the case of the MDVH model and their accurate prediction required the use of more than 1000 time steps per period. In the case of the simplified MDVH model, the dependence of the eddy-current loss of the rotor on the time-step size nearly vanished after 400 time steps per period were used. The flux density in the rotor of Motor II is less distorted because of the slotless geometry of the

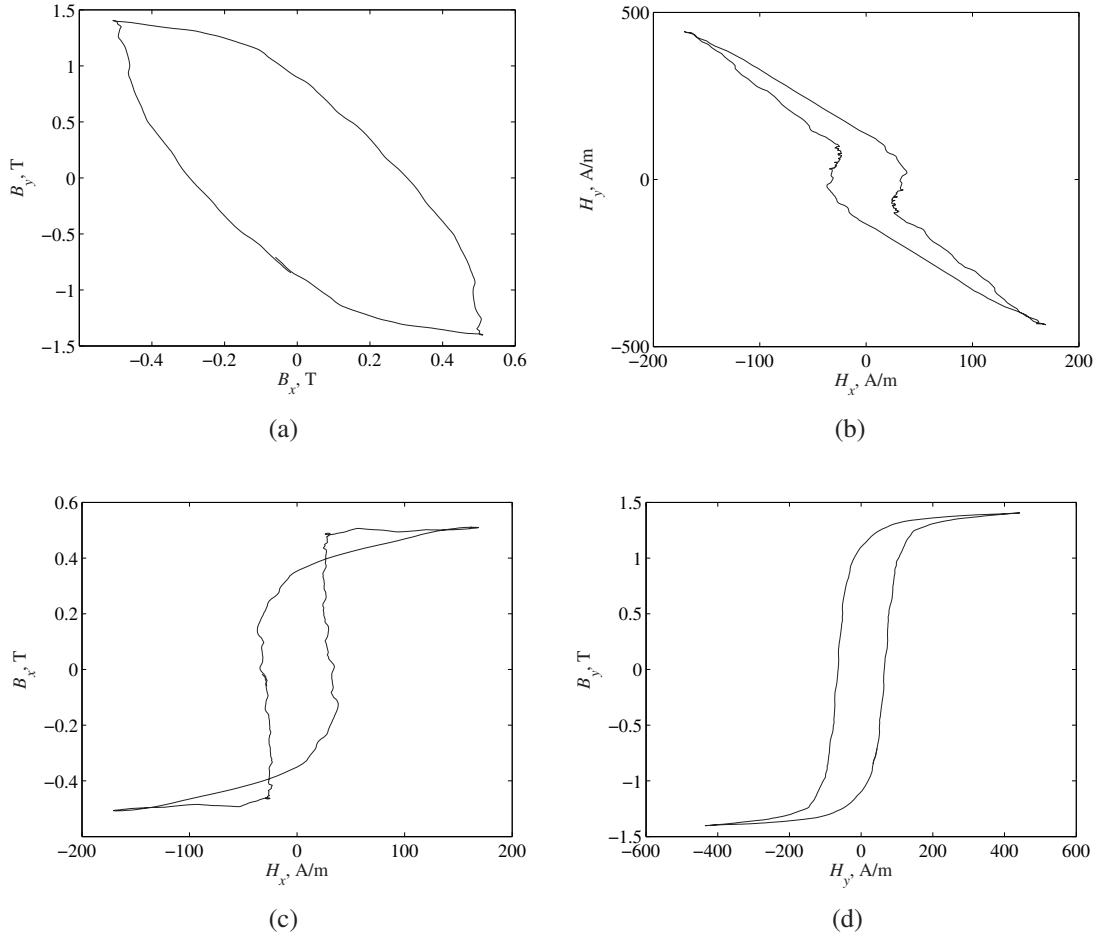

Figure 4.6: The dynamic hysteresis loops and the loci of the magnetic fields at a point in the tooth root of the stator yoke of Motor I.

rotor, and thus fewer numerical problems were met.

Table 4.2: The computation time results of Motor I.

Test results	Model type	LCM	GCM
Number of iterates per time step	MDVH	65	276
	Simplified MDVH	17	78
	Single-valued	15	79
CPU time per time step (sec)	MDVH	6.71	23.49
	Simplified MDVH	0.73	3.13
	Single-valued	0.29	1.34
CPU time per period (min)	MDVH	113.7	392.2
	Simplified MDVH	12.4	52.6
	Single-valued	5.2	22.6

Table 4.2 shows the comparative computational-time results of Motor I obtained by implementing the fixed-point methods, the GCM and LCM, in the 2D finite-element procedures, using the MDVH and the simplified MDVH models. The average number of

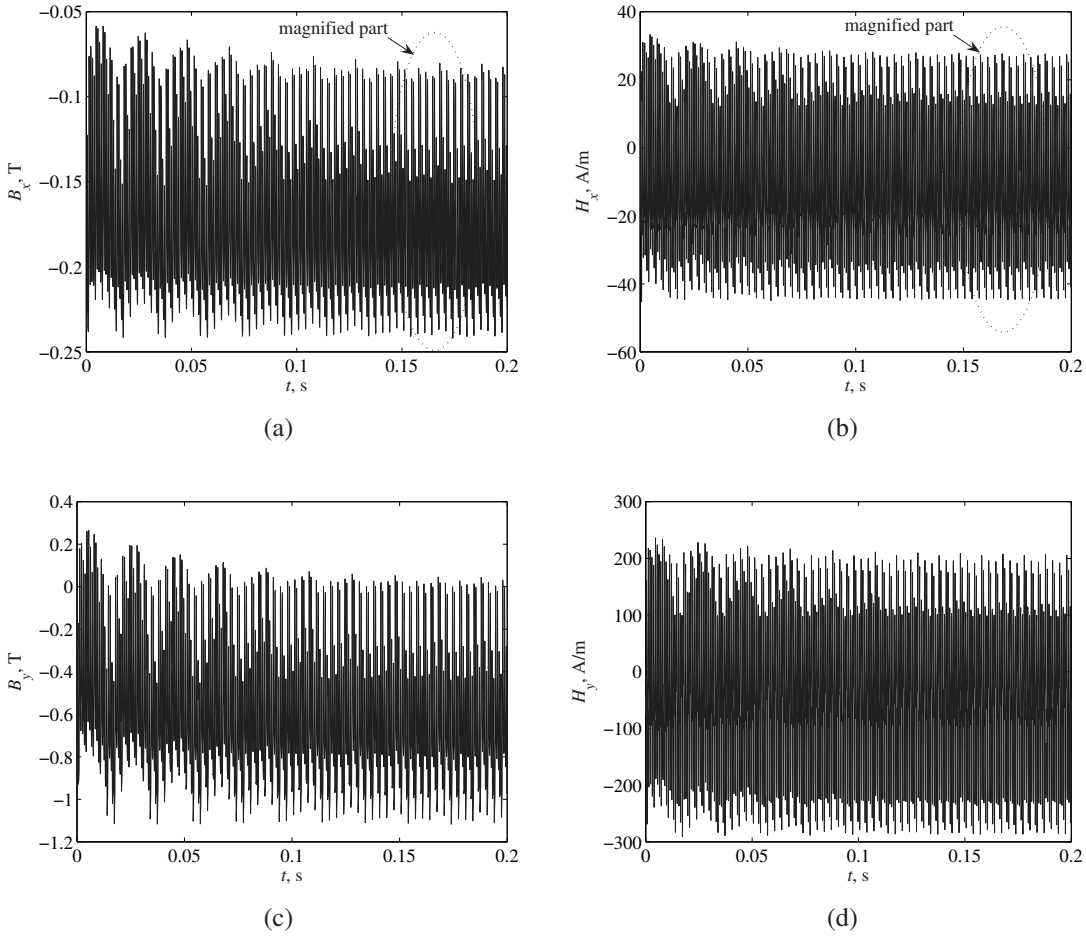

Figure 4.7: The waveforms of the magnetic fields at a point in the surface of a rotor tooth of Motor I (magnified parts are shown in Figure 4.9).

iterates per time step, the average CPU time spent on a time step, and the total CPU time spent on a period are tabulated. The computations were carried out using the same computer. The number of time steps per period, the number of second-order finite elements in the mesh, and the optimized values of the convergence factor C were fixed in all simulations, as shown in Table 4.3.

Table 4.3: The simulation input data and problem size of Motor I and Motor II.

Data	Motor I	Motor II
Convergence constant C	3.8	2.1
Number of second-order finite elements	1516	3194
Number of nodes	3085	6463
Number of integration points per element	6	6
Number of time steps per period	1000	1000

For the MDVH and the simplified MDVH models, the LCM was converging faster than the GCM. The problem that significantly affected the speed of the GCM is that the maximum differential reluctivity calculated from the maximum flux density in the mesh

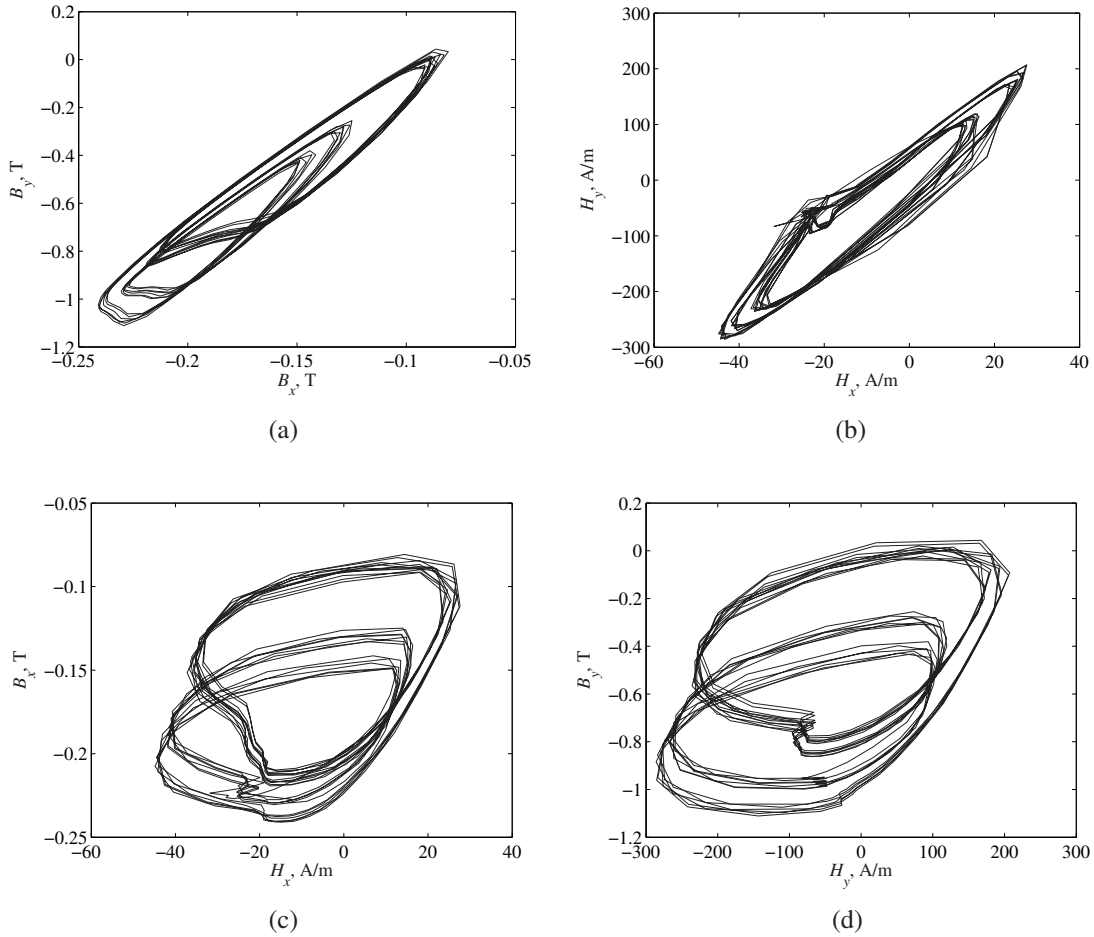

Figure 4.8: The dynamic hysteresis loops and the loci of the magnetic fields at a point in the surface of a rotor tooth of Motor I.

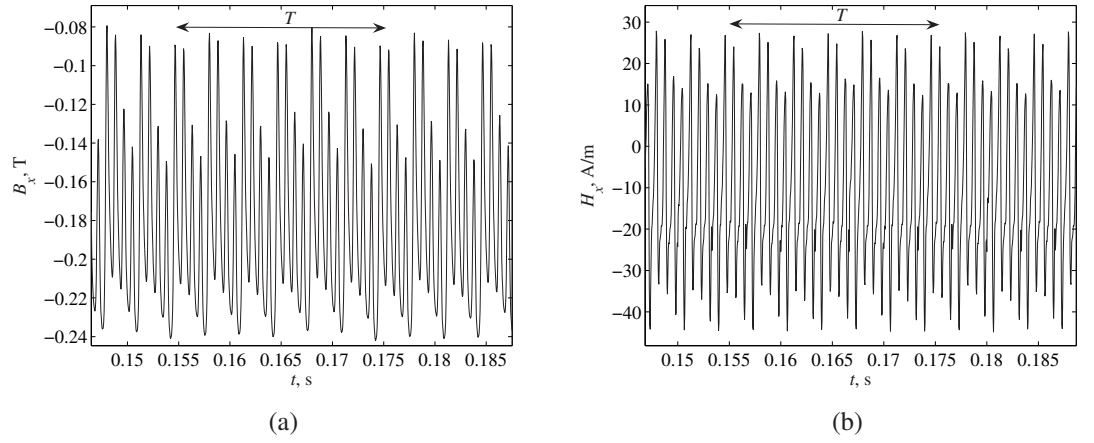

Figure 4.9: A magnified part of the waveforms shown in Figure 4.7.

has to be imposed on the entire mesh even for the elements with low flux densities. The number of iterates needed for the convergence in the case of the MDVH model increases the computation time significantly. Furthermore, the field solution of the 1D model adds

to the overall computational time.

It is observed that the convergence in the case of Motor II is significantly faster for all the methods. Motor II has a relatively large air-gap and its rotor is slotless. The maximum flux density in this motor is rather low especially in the stator core (less than $1\ \mathrm{T}$). On the other hand, the flux density in Motor I reaches over $1.7\ \mathrm{T}$ as a result of the rotor-slot openings being closed. In motors of this type, the torque can be significant only when the iron of the rotor-slot opening is saturated.

4.4 Conclusions

This chapter dealt with the incorporation of the lamination models into the 2D finite-element analysis of rotating electrical machines. The MDVH model was integrated into the machine model, using two iterative procedures, a local one for the 1D model and a global one for the 2D model.

The simplified MDVH model was also integrated into the 2D finite-element analysis. The advantages of the model lie in various aspects. Most importantly, the simplified MDVH model does not require a local iterative procedure. In this way, the efficiency of the 2D machine model is improved remarkably. Second, the simplified MDVH model is not as sensitive to the high harmonics as the MDVH model, which can be vulnerable to instability because of the harmonics. In electrical machines, high harmonics are mainly present as a result of slotting.

The simulations of the induction motors revealed that the models that were developed are appropriate for the prediction of core losses in electrical machines. On the other hand, the results showed that the conventional single-valued model can easily over- or underestimate the core losses, especially at high flux density levels.

The test of the efficiency of the models showed that the simulations carried out by the simplified MDVH model were more than 10 times faster than those carried out by the MDVH model. Moreover, the simplified MDVH model maintains the stability of the iterative procedure.

The LCM method has shown remarkable success in accelerating the convergence of the fixed-point iteration used for solving time-stepping hysteretic field problems. The computational time was reduced by more than 5 times in all the cases.

Chapter 5

Discussion and Conclusions

This chapter discusses the proposals developed in the thesis and where they fit in in global terms. The ideas, aspects, and applications of the work are synthesized and evaluated. Matters such as the accuracy, stability, and efficiency of the core loss models are brought up. The main conclusions of the dissertation are drawn.

5.1 Accuracy of the Models

Ferromagnetic materials are used to shape and direct the magnetic fields that act as a medium in the energy conversion process. Energy losses are inevitably dissipated in such a process. To estimate these losses accurately, advanced material modeling is required.

The methods developed in the thesis for the prediction of the core losses were based upon modeling the magnetization behavior and hence the magnetization curves and the ensuing core losses. The hysteresis, classical eddy-current, and excess losses, known as the magnetodynamic effects, were determined accordingly. The magnetodynamic vector hysteresis behavior was rigorously modeled, and thus the idea of using the concept of modeling the dynamic loop shapes proved to be fruitful in producing accurate estimates of the core losses.

Commonly, vector hysteresis models are tested only against their accuracy of the rotational losses. What distinguishes the proposed models most is not only their accuracy of calculating the rotational losses, but also their reproducibility of the experimental dynamic loop shapes obtained under alternating or rotational field excitations. The developed models are able to control both the loop shapes and the iron losses under different field patterns and in a wide range of frequencies. In this way, the generality of obtaining accurate estimation of iron losses under different magnetization behaviors is more feasible. For instance, under circular flux excitation, a decrease in the rotational losses at saturation is accomplished while maintaining the desired loop shapes, a property that none of the existing models in the literature has shown.

Validating the magnetodynamic vector hysteresis model by using only the sum of the areas enclosed by the loops (the iron loss) is a misconception and can lead to an unexpect-

edly different magnetization behavior from that observed in measurement. For example, the utilization of the generalized Mayergoyz model to relax the rotational loss property has shown non-physical anisotropic behaviors.

In electrical devices, such problems may significantly affect the electrical current drawn by the device. When the electrical machine is supplied by a voltage source, the flux linkage in the machine is basically defined by the voltage. The waveforms of the electrical current, however, are dependent on the waveforms of the magnetic field strength. Therefore, modeling the magnetic material inadequately can result in detrimental effects and will force the machine to draw non-physical amounts of input power.

It should be noted that the imperfections of the magnetic material models become blatant when the magnetic material in the machine is saturated and the flux is significantly rotational. In such cases, the use of the single-valued models can be described as inappropriate. Assuming collinearity between the magnetic flux density and the magnetic field strength is a gross approximation. Moreover, under saturated rotational fields, assigning the differential permeability to be equal to the permeability of the vacuum is another inappropriacy.

In the traditional methods used for the design and analysis of electrical machines (for example, finite-element analysis), the imperfections of the magnetic material models in the computation of iron losses may not appear as significant as they ought to be. The discretization of the geometry into finite elements leads to the application of the magnetic material models to each element in the mesh, or more specifically to each integration point in the mesh. In this manner, the inadequacy in the material modeling creates less noticeable effects because statistically, the material model would globally produce relatively reasonable results. Therefore, these gross models are still perceived as being acceptable. On the other hand, they should not be reliably used to localize the core losses in an electrical machine. Cooling system designers, who nowadays require the distribution of the losses in the machine, cannot rely on these simple models. The models developed in this thesis, however, can be appropriately applied in localizing the core losses because they are based upon the prediction of the magnetization behavior.

An alternative method is an intermediate approach, i.e. the computation of the flux patterns in the electrical machine is done using a single-valued model whereas a magnetodynamic model is applied posteriorly. Such an approach, which was not considered in the thesis, may estimate the core losses quite accurately, but it cannot incorporate the losses into the field computation.

5.2 Stability and Efficiency of the Models

Additional considerations that have been given equal importance in the thesis are the stability and efficiency of the models. A simulation model in numerical analysis must be robust and efficient; if it is not, it cannot be used as a design tool.

In the field of magnetic material modeling, the basis of the stable behavior of the mag-

netization curves begins with the static hysteresis model. The static hysteresis model must ensure the stability of the minor loops, which should be confined within the major loop. In this respect, the history-independent hysteresis model developed in the thesis has been found to be suitable for producing stable minor loops. The model is fast and computationally inexpensive because it does not store the previous reversal points.

The solution of the eddy-current problem has proven to be difficult and required a careful treatment, especially in electrical machines where the problem became more complicated because of the strong coupling between the 2D magnetic field solution and the eddy-current field solution. The idea of tackling the problem by using a simplified model, which is more stable and efficient, has considerably alleviated the overall iterative procedure. The simplified model is not only efficient from a computational viewpoint but also stable and adequate for modeling the eddy currents in a rotating electrical machine, where the flux is usually highly distorted.

The intrinsic freedom of the fixed-point method for creating different iterated functions has been utilized to obtain convergence with a high rate. In practice, the fixed-point solution cannot be predicted in advance, and thus constructing the optimal iterated functions that allow the fastest convergence is difficult. This difficulty has been circumvented in time-stepping analysis, where the solution of the current time step at the first iteration step was used to estimate the optimum of the iterated functions. This permits significantly fast local convergence.

5.3 Conclusions

This thesis dealt with the problems associated with the predictions of core losses in the laminations of rotating electrical machines. An appreciation and understanding of these problems is very desirable, if not essential. The objective was to seek a robust, accurate, and fast magnetic material model that is usable for the finite-element analysis of magnetic fields, with particular reference to rotating machines. Therefore, it was important that the magnetodynamic vector hysteresis behavior be modeled and the developed models be verified by experimental data.

Nowadays, as well as sinusoidal supplies, rotating electrical machines are supplied through frequency converters. The models developed in this thesis are general and can be used for this purpose. In the application examples studied in the thesis, the machines were fed from a sinusoidal supply. An investigation of the core losses of electrical machines supplied by frequency converters is very important, however.

In the factories where electrical machines are produced, the laminations are pressed, cut, and assembled. Each stack of laminations is bonded together by a dielectric material. The cutting and pressing effects of the laminations may damage the insulation, especially at the edges. These effects can result in the magnetic properties of the material being changed. The models developed here do not consider such effects. On the other hand, the generalization of the models may be accomplished through a statistical approach. Fur-

thermore, the mechanical stress, caused by the magnetic forces, and the magnetostriction, which can have an important impact on the properties of magnetic materials, have not been considered in the analysis of the thesis. Such problems require more comprehensive studies [Belahcen (2005)].

From the research conducted in this thesis, the following conclusions may be drawn:

- In the literature, the methods commonly used for computing core losses in electrical machines are based upon simple techniques that posteriorly exploit the field solution using statistical laws or empirical equations. Despite their imperfections and inaccuracies, the common tendency to use such techniques is mainly attributed to the lack of more concrete methods that can be easily implemented and reliably used.

- In this thesis, predicting the loop shapes, including the minor loops, has shown its effectiveness in reproducing the experimental data on core losses. To be adequate, a core loss model must reproduce not only the core losses accurately, as a sum of the loop areas enclosed, but also must predict the loop shapes accurately. This point has been well emphasized in the thesis because of its importance in affecting the characteristics of the electrical machine. The magnetodynamic model developed here meets these requirements rigorously.

- The stability of the magnetic material model is another crucial factor for the success and popularity of the model and has received sufficient treatment here. An accurate model that is not robust may be applied only to certain problems or may be useful only for academic studies in which these problems are often solved manually. For instance, the eddy current in the laminations of the rotor, in particular, can easily lead to significant problems in the time-stepping scheme and the iterative procedure involved. The proposed simplified eddy-current model was found to be consistently stable, accurate, and efficient.

- Since solving hysteretic eddy-current field problems is a difficult task, iterative schemes, which are often computationally costly and problematic, must be used to cope with nonlinearity. The local-coefficient method proposed in this work showed excellent improvements in speeding up the convergence of the fixed-point technique. The local-coefficient method seeks a solution in a local contractive interval at which the contraction factor is smaller than at all other feasible intervals in its vicinity.

References

Adly, A. A. and Abd-El-Hafiz, S. K. (1998), 'Using neural networks in the identification of Preisach-type hysteresis models', *IEEE Trans. Magn.*, **34**, 629–635.

Adly, A. A. and Abd-El-Hafiz, S. K. (2006), 'Efficient implementation of vector Preisach-type models using orthogonally coupled hysteresis operators', *IEEE Trans. Magn.*, **42**, 1518–1525.

Adly, A. A. and Mayergoyz, I. D. (1993), 'A new vector Preisach-type model of hysteresis', *J. Appl. Phys.*, **73**, 5824.

Alinejad-Beromi, Y. and Moses, A. J.and Meydan, T. (1992), 'New aspects of rotational field and flux measurement in electrical steel', *J. Magn. Magn. Mater.*, **112**, 135–138.

Alkar, K. (2007), 'Measuring power losses of electrical steel sheets in one- and two-dimensional magnetic fields', Master's thesis, Helsinki University of Technology, Finland, Available at: http://lib.tkk.fi/Dipl/2007/urn010204.pdf.

Amar, M. and Kaczmarek, R. (1995), 'A general formula for prediction of iron losses under nonsinusoidal voltage waveform', *IEEE Trans. Magn.*, **31**, 2504–2509.

Arkkio, A. (1987), *Analysis of induction motors based on the numerical solution of the magnetic field and circuit equations*, Ph.D. thesis, Helsinki University of Technology, Finland, Available at: http://lib.tkk.fi/Diss/198X/isbn951226076X/.

Arkkio, A., Niemenmaa, A., and Saitz, J. (1998), 'Hysteresis torque in a cage induction motor', ICEM, Istanbul, Turkey.

Atallah, K. and Howe, D. (1993), 'Calculation of the rotational power loss in electrical steel laminations from measured H and B', *IEEE Trans. Magn.*, **29**, 3547–3549.

Atallah, K., Zhu, Z. Q., and Howe, D. (1992), 'An improved method for predicting iron losses in brushless permanent magnet DC drives', *IEEE Trans. Magn.*, **28**, 2997–2999.

Barbisio, E., Fiorillo, F., and Ragusa, C. (2004), 'Predicting loss in magnetic steels under arbitrary induction waveform and with minor hysteresis loops', *IEEE Trans. Magn.*, **40**, 1810–1819.

Basso, V., Bertotti, G., Bottauscio, O., Fiorillo, F., Pasquale, M., Chiampi, M., and Repetto, M. (1997), 'Power losses in magnetic laminations with hysteresis', *J. Appl. Phys.*, **81**, 5606–5608.

Bastos, J. and Sadowski, N. (2003), *Electromagnetic Modeling by Finite Element Methods*. Marcel Dekker, New York.

Bate, G. (1962), 'The Preisach diagram and interaction fields for assemblies of γ-Fe2-O3 particles', *J. Appl. Phys.*, **33**, 425–427.

Belahcen, A. (2005), 'Magnetoelastic coupling in rotating electrical machines', *IEEE Trans. Magn.*, **41**, 1624–1627.

Belahcen, A. and Arkkio, A. (2008), 'Comprehensive dynamic loss model of electrical steel applied to FE simulation of electrical machines', accepted for publication in IEEE Trans. Magn.

Benabou, A., Clenet, S., and Piriou, F. (2004), 'Comparison of Preisach and Jiles-Atherton models to take into account hysteresis phenomenon for finite element analysis', *COMPEL*, **23**, 825–834.

Bennett, L. H., Vajda, F., Atzmony, U., and Swartzendruber, L. J. (1996), 'Accommodation study of a nanograin iron powder', *IEEE Trans. Magn.*, **32**, 4493–4495.

Bergqvist, A. (1994), *On magnetic hysteresis modeling*, Ph.D. thesis, Royal Institute of Technology, Stockholm, Sweden.

Bergqvist, A. and Engdahl, G. (1994), 'A phenomenological differential-relation-based vector hysteresis model', *J. Appl. Phys.*, **75**, 5484.

Bertotti, G. (1988), 'General properties of power losses in soft ferromagnetic materials', *IEEE Trans. Magn.*, **24**, 621–630.

Bertotti, G. (1992), 'Dynamic generalization of the scalar Preisach model of hysteresis', *IEEE Trans. Magn.*, **28**, 2599–2601.

Bertotti, G. (1998), *Hysteresis in Magnetism*. Academic Press, Inc., California, USA.

Bertotti, G., Basso, V., and Pasquale, M. (1994), 'Application of the Preisach model to the calculation of magnetization curves and power losses in ferromagnetic materials', *IEEE Trans. Magn.*, **30**, 1052–1057.

Bertotti, G., Boglietti, A., Chiampi, M., Chiarabaglio, D., Fiorillo, F., and Lazzari, M. (1991), 'An improved estimation of iron losses in rotating electrical machines', *IEEE Trans. Magn.*, **34**, 5007–5009.

Bertotti, G., Fiorillo, F., and Pasquale, M. (1993), 'Measurement and prediction of dynamic loop shapes and power losses in soft magnetic materials', *IEEE Trans. Magn.*, **29**, 3496–3498.

Binesti, D. and Ducreux, J. P. (1996), 'Core losses and efficiency of electrical motors using new magnetic materials', *IEEE Trans. Magn.*, **32**, 4887–4889.

Biorci, G. and Pescetti, D. (1966), 'Some remarks on hysteresis', *J. Appl. Phys.*, **37**, 1313–1317.

Bishop, J. E. (1973), 'The analysis of eddy-current-limited magnetic domain wall motion, including severe bowing and merging', *J. Phys.D: Appl. Phys.*, **6**, 97–115.

Bishop, J. E. (1985), 'Enhanced eddy current loss due to domain displacement', *J. Magn. Magn. Mater.*, **49**, 241–249.

Boglietti, A., Cavagnino, A., Lazzari, M., and Pastorelli, M. (2003), 'Predicting iron losses in soft magnetic materials with arbitrary voltage supply: an engineering approach', *IEEE Trans. Magn.*, **39**, 981–89.

Boglietti, A., Chiampi, M., Repetto, M., Bottauscio, O., and Chiarabaglio, D. (1998), 'Loss separation analysis in ferromagnetic sheets under PWM inverter supply', *IEEE Trans. Magn.*, **34**, 1240–1242.

Boglietti, A., Ferraris, P., Lazzari, M., and Pastorelli, M. (1996), 'Influence of the inverter characteristics on the iron losses in PWM inverter-fed induction motors', *IEEE Trans. Ind. Appl.*, **39**, 1190–1194.

Bottauscio, O. and Chiampi, M. (2001), 'Laminated core modeling under rotational excitations including eddy currents and hysteresis', *J. Appl. Phys.*, **89**, 6728–6730.

Bottauscio, O., Chiampi, M., and Chiarabaglio, D. (2000a), 'Advanced model of laminated magnetic cores for two-dimensional field analysis', *IEEE Trans. Magn.*, **36**, 561 –573.

Bottauscio, O., Chiampi, M., Chiarabaglio, D., Raguso, C., and Repeto, M. (1999), 'Ferromagnetic hysteresis and magnetic field analysis', *ICS Newsletter*, **6**, 3–7.

Bottauscio, O., Chiampi, M., Chiarabaglio, D., and Repetto, M. (2000b), 'Preisach-type hysteresis models in magnetic field computation', *Physica B: Condensed Matter*, **275**, 34–39.

Bottauscio, O., Chiarabaglio, D., and Chiampi, M.and Repetto, M. (1995), 'A hysteretic periodic magnetic field solution using Preisach model and fixed-point technique', *IEEE Trans. Magn.*, **31**, 3548–3550.

Bozorth, R. M. (1951), *Ferromagnetism*. D. Van Nostrand Co. Inc. Princeton, New Jersey.

Brailsford, F. (1938), 'Rotational hysteresis loss in electrical sheet steels', *IEEJ*, **83**, 566–575.

Brix, W., Hempel, K., and Schroeder, W. (1982), 'Method for the measurement of rotational power loss and related properties in electrical steel sheets', *IEEE Trans. Magn.*, **18**, 1469–1471.

Brix, W., Hempel, K., and Schult, F. J. (1984), 'Improved method for the investigation of the rotational magnetization process in electrical steel sheets', *IEEE Trans. Magn.*, **20**, 1708–1710.

Brokate, M. (1989), 'Some mathematical properties of the Preisach model for hysteresis', *IEEE Trans. Magn.*, **25**, 2922–2924.

Cardelli, E., Torre, E. D., and Tellini, B. (2000), 'Direct and inverse Preisach modeling of soft materials', *IEEE Trans. Magn.*, **36**, 1267–1271.

Cecchitti, A., Ferrari, G., Masoli, F., and Soardo, G. P. (1978), 'Rotational power losses in 3% SiFe as a function of frequency', *IEEE Trans. Magn.*, **14**, 356–358.

Charap, S. and Ktena, A. (1993), 'Vector Preisach modeling', *J. Appl. Phys.*, **73**, 5818.

Chiampi, M., Chiarabaglio, D., and Repetto, M. (1994), 'An accurate investigation on numerical methods for nonlinear magnetic field problems', *J. Magn. Magn. Mater.*, **133**, 591–595.

Chiampi, M., Chiarabaglio, D., and Repetto, M. (1995), 'A Jiles-Atherton and fixed-point combined technique for time periodic magnetic field problems with hysteresis', *IEEE Trans. Magn.*, **31**, 4306–4311.

Chiampi, M., Negro, A., and Tartaglia, M. (1980), 'A finite element method to compute three-dimensional magnetic field distribution in transformer cores', *IEEE Trans. Magn.*, **16**, 1413–1419.

Cirrincione, M., Miceli, R., Galluzzo, G. R., and Trapanese, M. (2002), 'Preisach function identification by neural networks', *IEEE Trans. Magn.*, **38**, 2421–2423.

Coulomb, J. L. (1983), 'A methodology for the determination of global electromechanical quantities from a finite element analysis and its application to the evaluation of magnetic forces, torques and stiffness', *IEEE Trans. Magn.*, **19**, 2514–2519.

Cramer, H. A. (1990), 'A moving Preisach vector hysteresis model for magnetic recording media', *J. Magn. Magn. Mater.*, **88**, 194–204.

Cullity, B. D. (1972), *Introduction to Magnetic Materials*. Addison-Wesley, Reading, MA.

Davino, D., Giustiniani, A., and Visone, C. (2008), 'Properties of hysteresis models relevant in electromagnetic fields numerical solvers', *Physica B: Condensed Matter*, **403**, 414–417.

Del Vecchio, R. (1980), 'An efficient procedure for modeling complex hysteresis processes in ferromagnetic materials', *IEEE Trans. Magn.*, **16**, 809–811.

Del Vecchio, R. (1982a), 'The calculation of eddy current losses associated with rotating magnetic fields in thin laminations', *IEEE Trans. Magn.*, **18**, 1707–1709.

Del Vecchio, R. (1982b), 'Computation of losses in nonoriented electrical steels from a classical viewpoint', *J. Appl. Phys.*, **53**, 8281–8286.

Del Vecchio, R. (1982c), 'The inclusion of hysteresis processes in a special class of electromagnetic finite element calculations', *IEEE Trans. Magn.*, **18**, 275–284.

Delince, F., Nicolet, A., Henrotte, F., Genon, A., and Legros, W. (1994), 'Influence of hysteresis on the behaviour of coupled finite element-electric circuit models', *IEEE Trans. Magn.*, **30**, 3383–3386.

Della Torre, E. (1966), 'Effect of interaction on the magnetization of single domain particles', *IEEE Trans. Audio Electroacoust*, **14**, 86–93.

Della Torre, E. (1987), 'Hysteresis modeling II: accommodation', *IEEE Trans. Magn.*, **23**, 2823.

Della Torre, E. (1994), 'A Preisach model for accommodation', *IEEE Trans. Magn.*, **30**, 2701–2707.

Della Torre, E. (1998), 'A simplified vector Preisach model', *IEEE Trans. Magn.*, **34**, 495–501.

Della Torre, E. (2000), *Magnetic Hysteresis*. Wiley-IEEE Press, Piscatway, NJ.

Della Torre, E. and Kadar, G. (1988), 'Vector Preisach and the moving model', *J. Appl. Phys.*, **63**, 3004.

Della Torre, E., Pinzaglia, E., and Cardelli, E. (2006a), 'Vector modeling-Part I: Generalized hysteresis model', *Physica B: Condensed Matter*, **372**, 111–114.

Della Torre, E., Pinzaglia, E., and Cardelli, E. (2006b), 'Vector modeling-Part II: Ellipsoidal vector hysteresis model. Numerical application to a 2D case', *Physica B: Condensed Matter*, **372**, 115–119.

Diaz, G., Gonzalez-Moran, C., Arboleya, P., and Gomez-Aleixandre, J. (2007), 'Analytical interpretation and quantification of rotational losses in stator cores of induction motors', *IEEE Trans. Magn.*, **43**, 3861–3867.

Dlala, E. and Arkkio, A. (2006), 'A neuro-fuzzy-based Preisach approach on hysteresis modeling', *Physica B: Condensed Matter*, **372**, 49–52.

Dlala, E. and Arkkio, A. (2007), 'Measurement and analysis of hysteresis torque in a high-speed induction machine', *Electric Power Applications, IET*, **1**, 737–742.

Dlala, E., Belahcen, A., and Arkkio, A. (2007), 'Locally convergent fixed-point method for solving time-stepping nonlinear field problems', *IEEE Trans. Magn.*, **43**, 3969–3975.

Dlala, E., Belahcen, A., and Arkkio, A. (2008a), 'Efficient magnetodynamic lamination model for twodimensional field simulation of rotating machines', accepted for publication in J. Magn. Magn. Mater.

Dlala, E., Belahcen, A., and Arkkio, A. (2008b), 'A fast fixed-point method for solving magnetic field problems in media of hysteresis', accepted for publication in IEEE Trans. Magn.

Dlala, E., Belahcen, A., and Arkkio, A. (2008c), 'Magnetodynamic vector hysteresis model of ferromagnetic steel laminations'.

Dlala, E., Saitz, J., and Arkkio, A. (2005), 'Hysteresis modeling based on symmetric minor loops', *IEEE Trans. Magn.*, **41**, 2343–2348.

Dlala, E., Saitz, J., and Arkkio, A. (2006), 'Inverted and forward Preisach models for numerical analysis of electromagnetic field problems', *IEEE Trans. Magn.*, **42**, 1963–1973.

Dular, P., Gyselinck, J., Geuzaine, C., Sadowski, N., and Bastos, J. (2003), 'A 3D magnetic vector potential formulation taking eddy currents in lamination stacks into account', *IEEE Trans. Magn.*, **39**, 1147–1150.

Dupre, L., Bertotti, G., and Melkebeek, J. (1998a), 'Dynamic Preisach model and energy dissipation in soft magnetic materials', *IEEE Trans. Magn.*, **34**, 1168–1170.

Dupre, L., Bottauscio, O., Chiampi, M., Fiorillo, F., Lo Bue, M., Melkebeek, J., Repetto, M., and Von Rauch, M. (1998b), 'Dynamic Preisach modelling of ferromagnetic laminations under distorted flux excitations', *IEEE Trans. Magn.*, **34**, 1231–1233.

Dupre, L., Bottauscio, O., Chiampi, M., Repetto, M., and Melkebeek, J. (1999), 'Modeling of electromagnetic phenomena in soft magnetic materials under unidirectional time periodic flux excitations', *IEEE Trans. Magn.*, **35**, 4171–4184.

Dupre, L., De Wulf, M., Makaveev, D., Permiakov, V., Pulnikov, A., and Melkebeek, J. (2003), 'Modelling of electromagnetic losses in asynchronous machines', *COMPEL*, **22**, 1051–1065.

Dupre, L., Fiorillo, F., Appino, C., Rietto, M., and Melkebeek, J. (2000), 'Rotational loss separation in grain-oriented Fe-Si', *J. Appl. Phys.*, **87**, 6511–6513.

Dupre, L. and Malkebeek, J. (2003), 'Electromagnetic hysteresis modeling: From material science to finite element analysis of devices', *ICS Newsletter*, **10**, 4–14.

Dupre, L., Van Keer, R., and Melkebeek, J. (1996), 'On a magnetodynamic model for the iron losses in nonoriented steel laminations', *J. Phys. D: Appl. Phys.*, **29**, 855–861.

Dupre, L., Van Keer, R., and Melkebeek, J. (1997), 'An iron loss model for electrical machines using the Preisach theory', *IEEE Trans. Magn.*, **33**, 4158–4160.

Dupre, L., Van Keer, R., and Melkebeek, J. (1998c), 'A computational model for the iron losses in rotating electrical machines', *Int. J. Eng. Sc.*, **39**, 699–709.

Dupre, L., Van Keer, R., Melkebeek, J., Moroz, Y. I., and Zirka, S. E. (2001), 'Hysteresis models for transient simulation', *Springer-Verlag*, **18**, 105–112, in Lecture Notes in Computer Science and Engineering.

Enokizono, M., Suzuki, T., and Sievert, J. D. (1990), 'Measurement of dynamic magnetostriction under rotating magnetic field', *IEEE Trans. Magn.*, **26**, 2067–2069.

Everett, D. H. (1954), 'A general approach to hysteresis', *Trans. Faraday Soc.*, **50**, 1077–1096.

Fallah, E. and Moghani, J. (2008), 'A new identification and implementation procedure for the isotropic vector Preisach model', *IEEE Trans. Magn.*, **44**, 37–42.

Feliachi, M. and Meunier, G. (1985), 'Two dimensional hysteresis model using finite element method', *IEEE Trans. Magn.*, **21**, 2362–2365.

Findlay, R. D., Stranges, N., and Mackay, D. K. (1994), 'Losses due to rotational flux in three phase induction motors', *IEEE Trans. Energy Convers*, **9**, 543–549.

Fiorillo, F., Dupre, L., Appino, C., and Rietto, A. M. (2002), 'Comprehensive model of magnetization curve, hysteresis loops, and losses in any direction in grain-oriented Fe-Si', *IEEE Trans. Magn.*, **38**, 1467–1476.

Fiorillo, F. and Novikov, A. (1990), 'An improved approach to power losses in magnetic laminations under nonsinusoidal induction waveform', *IEEE Trans. Magn.*, **26**, 2904–2910.

Fiorillo, F. and Rietto, A. M. (1988), 'Extended induction range analysis of rotational losses in soft magnetic materials', *IEEE Trans. Magn.*, **24**, 1960–1962.

Fiorillo, F. and Rietto, A. M. (1990), 'Rotational and alternating energy loss vs. magnetising frequency in SiFe laminations', *J. Magn. Magn. Mater.*, **83**, 402–404.

Flanders, P. J. (1967), 'The rotating-sample magnetometer', *J. Appl. Phys.*, **38**, 1293–1294.

Friedman, G. and Mayergoyz, I. D. (1989), 'Computation of magnetic field in media with hysteresis', *IEEE Trans. Magn.*, **25**, 3934–3936.

Fuzi, J. (1999), 'Computationally efficient rate dependent hysteresis model', *COMPEL*, **18**, 445–457.

Fuzi, J. and Ivanyi, A. (2001), 'Features of two rate-dependent hysteresis models', *Physica B: Condensed Matter*, **306**, 278–280.

Fuzi, J. and Kadar, G. (2003), 'Frequency dependence in the product Preisach model', *J. Magn. Magn. Mater.*, **254-255**, 278–280.

Gillott, D. H. and Calvert, J. F. (1965), 'Eddy current loss in saturated solid magnetic plates, rods, and conductors', *IEEE Trans. Magn.*, **1**, 126–137.

Guo, Y., Zhu, J. G., Lin, Z. W., and Zhong, J. J. (2005), 'Measurement and modeling of core losses of soft magnetic composites under 3-D magnetic excitations in rotating motors', *IEEE Trans. Magn.*, **41**, 3925–3927.

Guo, Y., Zhu, J. G., Zhong, J., Lu, H., and Jin, J. X. (2008), 'Measurement and modeling of rotational core losses of soft magnetic materials used in electrical machines: A Review', *IEEE Trans. Magn.*, **44**, 279–291.

Gyselinck, J., Melkebeek, J., and Dupre, L. (1998), 'Complementary finite element methods in 2D magnetics taking into account a vector Preisach model', *IEEE Trans. Magn.*, **34**, 3048–3051.

Hameyer, K. and Belmans, R. (1999), *Numerical Modeling and Design of Electrical Machines and Devices*. WIT Press, Bath,UK.

Hantila, F. (1974a), 'Mathematical models of the relation between B and H for non-linear media', *Rev. Roum. Sci. Techn.-Electrotechn. et Energ.*, **19**, 429–448.

Hantila, F. (1974b), 'An overrelaxation method for the computation of the fixed-point of a contractive mapping', *Rev. Roum. Sci. Techn.-Electrotechn. et Energ.*, **27**, 395–398.

Hantila, F. (1975), 'A method of solving stationary magnetic field in non-linear media', *Rev. Roum. Sci. Techn.-Electrotechn. et Energ.*, **20**, 397–407.

Hantila, F., Preda, G., and Vasiliu, M. (2000), 'Polarization method for static fields', *IEEE Trans. Magn.*, **36**, 672–675.

Henrotte, F. and Hameyer, K. (2006), 'A dynamical vector hysteresis model based on an energy approach', *IEEE Trans. Magn.*, **42**, 899–902.

Henrotte, F., Nicolet, A., Delince, F., Genon, A., and Legros, P. (1992), 'Modeling of ferromagnetic materials in 2D finite element problems using Preisach's model', *IEEE Trans. Magn.*, **28**, 2614–2616.

Hodgdon, M. L. (1988), 'Application of a theory of ferromagnetic hysteresis', *IEEE Trans.Magn.*, **24**, 218–221.

Ionel, D. M., Popescu, M., Dellinger, S. J., Miller, T. J. E., Heideman, R. J., and McGilp, M. I. (2006), 'On the variation with flux and frequency of the core loss coefficients in electrical machines', *IEEE Trans. Ind. Appl.*, **42**, 658–667.

Islam, M. J., Pippuri, J., Perho, J., and Arkkio, A. (2007), 'Time-harmonic finite-element analysis of eddy currents in the form-wound stator winding of a cage induction motor', *Electric Power Applications, IET*, **1**, 839–846.

Ivanyi, A. (1997), *Hysteresis Models in Electromagnetic Computation*. Akadémia kiadó, Budapest, Hungary.

Jiles, D. C. (1992), 'A self consistent generalized model for the calculation of minor loop excursions in the theory of hysteresis', *IEEE Trans. Magn.*, **28**, 2602–2604.

Jiles, D. C. (1998), *Introduction to Magnetism and Magnetic Materials*. CRC Press.

Jiles, D. C. and Atherton, D. (1984), 'Theory of ferromagnetic hysteresis', *J. Appl. Phys.*, **55**, 2115.

Jiles, D. C. and Atherton, D. (1986), 'Theory of ferromagnetic hysteresis', *J. Appl. Phys.*, **61**, 48–60.

Jordan, H. (1924), 'Ferromagnetic constants for weak fields', *Elek. Nachr. Tech.*, pp. 7–29.

Kadar, G. and Della Torre, E. (1987), 'Hysteresis modeling I: noncongruency', *IEEE Trans. Magn.*, **23**, 2820.

Kahler, G. R. and Della Torre, E. (2003), 'Comparison of measurements with simplified vector Preisach model computations', *IEEE Trans. Magn.*, **39**, 1385–1388.

Kahler, G. R., Della Torre, E., and Patel, U. D. (2005), 'Properties of vector Preisach models', *IEEE Trans. Magn.*, **41**, 8–16.

Koehler, T. R. (1987), 'A computationally fast, two-dimensional vector hysteresis model', *J. Appl. Phys.*, **61**, 1568.

Kuczmann, M. (2004), *Neural network based vector hysteresis model and the nondestructive testing method*, Ph.D. thesis, University of Technology and Economics, Budapest, Hungary.

Lavers, J. and Biringer, P. (1976), 'A general formula for prediction of iron losses under nonsinusoidal voltage waveform', *IEEE Trans. Magn.*, **12**, 1053–1055.

Lavers, J., Biringer, P., and Hollitscher, H. (1978), 'A simple method of estimating the minor loop hysteresis loss in thin laminations', *IEEE Trans. Magn.*, **14**, 386–388.

Lei, M., Sanada, M., Morimoto, S., and Takeda, Y. (2003), 'Prediction of iron loss in rotating machines with rotational loss included', *IEEE Trans. Magn.*, **39**, 2036–2041.

Leite, J. V., Sadowski, N. P. K.-P., , Batistela, N., and Bastos, J. (2003), 'The inverse Jiles-Atherton model parameters identification', *IEEE Trans. Magn.*, **39**, 1397–1400.

Leonard, P., Marketos, P., Moses, A., and Lu, M. (2006), 'Iron losses under PWM excitation using a dynamic hysteresis model and finite elements', *IEEE Trans. Magn.*, **42**, 907–910.

Leonard, P., Rodger, D., Karagular, T., and Coles, P. (1995), 'Finite element modelling of magnetic hysteresis', *IEEE Trans. Magn.*, **31**, 1801–1804.

Loschner, K., Rischmuller, V., and Brokate, M. (2007), 'On a vectorial Preisach operator', Aachen, Germany. PA3-2, Compumag.

MacLean, W. (1954), 'Theory of strong electromagnetic waves in massive iron', *J. Appl. Phys.*, **25**, 1267.

Madelung, E. (1905), 'On the magnetization by fast currents and an operation principle of the magnetodetectors of Rutherford-Marconi', *Ann. Phys.*, **17**, 861–890.

Maeda, Y., Shimoji, H., Todaka, T., and Enokizono, M. (2007), 'Rotational power losses of magnetic steel sheets in circular rotational magnetic field in CCW/CW direction', B-012, Presented at the SMM conference, Cardiff, UK, and submitted for publication in J. Magn. Magn. Mater.

Matsuo, T. and Shimasaki, M. (2006), 'Simple modeling of the AC hysteretic property of a grain-oriented silicon steel sheet', *IEEE Trans. Magn.*, **42**, 919–922.

Matsuo, T. and Shimasaki, M. (2007a), 'Generalization of an isotropic vector hysteresis model represented by the superposition of stop models–identification and rotational hysteresis loss', *IEEE Trans. Magn.*, **43**, 1389–1392.

Matsuo, T. and Shimasaki, M. (2007b), 'Several isotropic vector play models and their rotational hysteresis losses', Aachen, Germany. PA3-6, Compumag.

Mayergoyz, I. D. (1986), 'Mathematical models of hysteresis', *IEEE Trans. Magn.*, **22**, 603–608.

Mayergoyz, I. D. (1987), 'Isotropic vector Preisach model of hysteresis', *J. Appl. Phys.*, **61**, 4022.

Mayergoyz, I. D. (1988a), 'Dynamic Preisach models of hysteresis', *IEEE Trans. Magn.*, **24**, 2925–2927.

Mayergoyz, I. D. (1988b), 'Generalized Preisach model of hysteresis', *IEEE Trans. Magn.*, **24**, 212–217.

Mayergoyz, I. D. (1988c), 'Vector Preisach hysteresis models', *J. Appl. Phys.*, **63**, 2995.

Mayergoyz, I. D. (1991a), 'Dynamic vector Preisach models of hysteresis', *J. Appl. Phys.*, **69**, 4829.

Mayergoyz, I. D. (1991b), *Mathematical Models of Hysteresis*. Springer-Verlag, New York.

Mayergoyz, I. D. (1998), *Nonlinear Diffusion of Electromagnetic Fields: with Applications to Eddy Currents and Superconductivity*. Aca. Pre. Ser. Elect., New York.

Mayergoyz, I. D. (2003), *Mathematical Models of Hysteresis and Their Applications*. Aca. Pre. Ser. Elect., New York.

Moses, A. J. and Thomas, B. (1973), 'The spatial variation of localized power loss in two practical transformer T-joints', *IEEE Trans. Magn.*, **4**, 655–659.

Muller, D. E. (1956), 'A method for solving algebraic equations using an automatic computer', *Math. Comp.*, **10**, 208–215.

Naidu, S. R. (1990), 'Simulation of the hysteresis phenomenon using Preisach's theory', *IEE Proc.*, **137**, 73–79.

Neel, L. (1944), 'Les lois de l'aimantation et de la subdivision en domaines élémentaires d'un monocristal de fer (i)', *J. Phys. Radium*, **5**, 241–251.

O'Kelly, D. (1972), 'Flux penetration in a ferromagnetic material including hysteresis and eddy-current effects', *J. Phys.D:Appl. Phys.*, **5**, 203–213.

Olver, P. and Shakiban, C. (2005), *Applied Linear Algebra*. Prentice Hall.

Olver, P. and Shakiban, C. (2007), 'Fundamentals of applied mathematics', Available at: http://www.math.umn.edu/ olver/appl.html.

Ossart, F. and Meunier, G. (1991), 'Results on modeling magnetic hysteresis using the finite-element method', *J. Appl. Phys.*, **69**, 4835.

Ossart, F., Phung, T. A., and Meunier, G. (1990), 'Comparison between various hysteresis models and experimental data', *J. Appl. Phys.*, **67**, 5379.

Park, G., Hahn, S., Lee, K., and Jung, H. (1993), 'Implementation of hysteresis characteristics using the Preisach model with M-B variables', *IEEE Trans. Magn.*, **29**, 1542–1545.

Pasquale, M., Basso, V., Bertotti, G., Jiles, D. C., and Bi, Y. (1998), 'Domain-wall motion in random potential and hysteresis modeling', *J. Appl. Phys.*, **83**, 6497–6499.

Pasquale, M., Bertotti, G., Jiles, D. C., and Bi, Y. (1999), 'Application of the Preisach and Jiles-Atherton models to the simulation of hysteresis in soft magnetic alloys', *J. Appl. Phys.*, **85**, 4373–4375.

Philips, D., Dupre, L., Cnops, J., and Melkebeek, J. (1994a), 'The application of the Preisach model in magnetodynamics: theoretical and practical aspects', *J. Magn. Magn. Mater.*, **133**, 540–543.

Philips, D., Dupre, L., and Melkebeek, J. (1994b), 'Magneto-dynamic field computation using a rate-dependent Preisach model', *IEEE Trans. Magn.*, **30**, 4377–4379.

Philips, D., Dupre, L., and Melkebeek, J. (1995), 'Comparison of Jiles and Preisach hysteresis models in magnetodynamics', *IEEE Trans.Magn.*, **31**, 3551–3553.

Pinto, M. A. (1991), 'Vectorial aspects of ferromagnetic hysteresis', *J. Magn. Magn. Mater.*, **98**, 221–229.

Pippuri, J. and Arkkio, A. (2006), 'Combined 2D-1D time-harmonic model for analysis of rotating electrical machines'. PTA3-17, ICEM, Chania, Greece.

Pokrovskii, A. and Kransoselskii, M. (1983), *Systems with Hysteresis*. Nauka, Moscow.

Poritsky, H. and Butler, J. M. (1964), 'AC flux penetration into magnetic materials with saturation', *IEEE Trans. Commun. Elect.*, **83**, 99–111.

Preisach, F. (1935), 'Über die magnetische nachwirkung', *Zeitschrij fur Physik*, **94**, 277–302.

Saitz, J. (1997), 'Calculation of iron losses in electrical machines', Tech. rep., Report 51, Helsinki University of Technology, Finland.

Saitz, J. (2000), 'Computation of the core loss in an induction motor using the vector Preisach hysteresis model incorporated in finite element analysis', *IEEE Trans. Magn.*, **36**, 1243–1246.

Saitz, J. (2001a), *Magnetic field analysis of electric machines taking ferromagnetic hysteresis into account*, Ph.D. thesis, Helsinki University of Technology, Finland, Available at: http://lib.tkk.fi/Diss/2001/isbn9512256908/.

Saitz, J. (2001b), 'Magnetic field analysis of induction motors combining Preisach hysteresis modeling and finite element techniques', *IEEE Trans. Magn.*, **37**, 3693–3697.

Salon, S. J. (2000), *Finite Element Analysis of Electrical Machines*. Kluwer Academic Publ.

Serpico, C. and Visone, C. (1998), 'Magnetic hysteresis modeling via feed-forward neural networks', *IEEE Trans. Magn.*, **34**, 623–628.

Serpico, C., Visone, C., Mayergoyz, I. D., Basso, V., and Miano, G. (2000), 'Eddy current losses in ferromagnetic laminations', *J. Appl. Phys.*, **87**, 6923–6925.

Sievert, J., Ahlers, H., Enokizono, M., Kauke, S., Rahf, L., and Xu, J. (1992), 'The measurement of rotational power loss in electrical sheet steel using a vertical yoke system', *J. Magn. Magn. Mater.*, **112**, 91–94.

Silvester, P. P. and Ferrari, R. L. (1983), *Finite Elements for Electrical Engineers*. Cambridge University Press, UK.

Spomic, S., Moussaoui, D., Kedous-Lebouc, A., and Cornut, B. (1996), 'Frequency magnetic behaviour of SiFe sheets in a rotational field', *J. Magn. Magn. Mater.*, **160**, 147–148.

Steinmetz, C. P. (1984), 'On the law of hysteresis', *Proceedings of the IEEE*, **72**, 197–221.

Stoner, E. C. and Wohlfarth, E. P. (1948), 'A mechanism of magnetic hysteresis in heterogeneous alloys', *Phil. Trans. Roy. Soc.*, **240**, 599–642.

Stranges, N. and Findlay, R. D. (2000), 'Methods for predicting rotational iron losses in three phase induction motor stators', *IEEE Trans. Magn.*, **36**, 3112–3114.

Strattant, R. D. and Young, F. J. (1962), 'Iron losses in elliptical rotating fields', *J. Appl. Phys.*, **33**, 1285–1286.

Stumberger, B., Gorican, V., Stumberger, G., Hamler, A., Trlep, M., and Jesenik, M. (2003), 'Accuracy of iron loss calculation in electrical machines by using different iron loss models', *J. Magn. Magn. Mater.*, **254-255**, 269–271.

Suzuki, K. (1976), 'Theoretical study of vector magnetization distribution using rotational magnetization model', *IEEE Trans. Magn.*, **12**, 224–229.

Takahashi, N., Fukum, A., and Miyagi, D. (2005), 'Analysis of iron loss under distorted elliptical rotating flux of SPM motor', *COMPEL*, **24**, 385–395.

Visintin, A. (1994), *Differential Models of Hysteresis*. Springer, Berlin.

Wakui, G., Kurihara, K., and Kubota, T. (1987), 'Radial flux type hysteresis motor with reaction torque–numerical analysis of hysteresis motor using finite element method', *IEEE Trans. Magn.*, **23**, 3845–3852.

Wiesen, K. and Charap, S. (1987), 'Vector Preisach modeling', *J. Appl. Phys.*, **61**, 4019.

Wiesen, K. and Charap, S. (1988), 'A better scalar Preisach algorithm', *IEEE Trans. Magn.*, **24**, 2491–2493.

Wiesen, K., Charap, S., and Krafft, C. S. (1990), 'A rotational vector Preisach model for unoriented media', *J. Appl. Phys.*, **67**, 5367.

Yamazaki, K. (2004), 'Loss calculation of induction motors considering harmonic electromagnetic field in stator and rotor', *IEEJ-Trans. IA*, **147**, 63–73.

Young, F. J. and Schenk, H. L. (1960), 'Method for measuring iron losses in elliptically polarized magnetic fields', *J. Appl. Phys.*, **31**, 194.

Young, F. J. and Schenk, H. L. (1966), 'Iron losses due to elliptically polarized magnetic fields', *J. Appl. Phys.*, **37**, 1210.

Zhai, Y. and Vu-Quoc, L. (2005), 'Analysis of power magnetic components with nonlinear static hysteresis: finite-element formulation', *IEEE Trans. Magn.*, **41**, 2243–2256.

Zhu, J. G. and Ramsden, V. S. (1998), 'Improved formulations for rotational core losses in rotating electrical machines', *IEEE Trans. Magn.*, **34**, 2234–2242.

Zirka, S. E. and Moroz, Y. I. (1999), 'Hysteresis modeling based on similarity', *IEEE Trans. Magn.*, **35**, 2090–2096.

Zirka, S. E., Moroz, Y. I., and Della Torre, E. (2005a), 'Combination hysteresis model for accommodation magnetization', *IEEE Trans.Magn.*, **41**, 2426–2431.

Zirka, S. E., Moroz, Y. I., Marketos, P., and Moses, A. J. (2002), 'Modeling losses in electrical steel laminations', *IEE Proc.-Sci. Meas. Technol.*, **149**, 218–221.

Zirka, S. E., Moroz, Y. I., Marketos, P., and Moses, A. J. (2004a), 'Congruency-based hysteresis models for transient simulations', *IEEE Trans. Magn.*, **40**, 390–399.

Zirka, S. E., Moroz, Y. I., Marketos, P., and Moses, A. J. (2004b), 'Dynamic hysteresis modeling', *Physica B: Condensed Matter*, **343**, 90–95.

Zirka, S. E., Moroz, Y. I., Marketos, P., and Moses, A. J. (2004c), 'Properties of dynamic Preisach models', *Physica B: Condensed Matter*, **343**, 85–89.

Zirka, S. E., Moroz, Y. I., Marketos, P., and Moses, A. J. (2005b), 'A viscous-type dynamic hysteresis model as a tool of loss separation in conducting ferromagnetic laminations', *IEEE Trans. Magn.*, **41**, 1109–1111.

Zirka, S. E., Moroz, Y. I., Marketos, P., and Moses, A. J. (2006a), 'Measurement and modeling of B-H loops and losses of high silicon nonoriented steels', *IEEE Trans. Magn.*, **42**, 3177–3179.

Zirka, S. E., Moroz, Y. I., Marketos, P., and Moses, A. J. (2006b), 'Viscosity-based magnetodynamic model of soft magnetic materials', *IEEE Trans. Magn.*, **42**, 2121–2132.

Zirka, S. E., Moroz, Y. I., Marketos, P., and Moses, A. J. (2007), 'Comparison of engineering methods of loss prediction in thin ferromagnetic laminations', O-06, Presented at the SMM conference, Cardiff, UK, and submitted for publication in J. Magn. Magn. Mater.

Zurek, S., Marketos, P., Meydan, T., and Moses, A. J. (2005), 'Use of novel adaptive digital feedback for magnetic measurements under controlled magnetizing conditions', *IEEE Trans. Magn.*, **41**, 4242–4249.

Zurek, S. and Meydan, T. (2006a), 'Errors in the power loss measured in clockwise and anticlockwise rotational magnetisation. Part 1: Mathematical study', *IEE Proceedings*, **153**, 147–151.

Zurek, S. and Meydan, T. (2006b), 'Errors in the power loss measured in clockwise and anticlockwise rotational magnetisation. Part 2: Physical phenomena', *IEE Proceedings*, **153**, 152–157.

Appendix A

Measurement Setup of Dynamic Hysteresis Loops

The measurement of the B-H loops under rotational flux excitations was accomplished by using a vertical yoke setup (see Figure A-1). The sensing coils for the B and H fields were placed in the x- and y-directions. The measuring device consisted of two pairs of double U-shaped yokes. Each yoke is built of 520 thin electrical steel sheets with a thickness of 0.2 mm and wound with 400 turns of exciting coils. The arrangement of the exciting coils made it possible to apply a high flux density through the yokes to the sample sheets.

The $\boldsymbol{H}$ sensors were sandwiched between two sheets (sample sheets) in order to eliminate the effect of the gradient resulting from the fact that the magnetic field strength on the surface of the sheet may vary with the distance. The signals of $\boldsymbol{B}$ and $\boldsymbol{H}$ were acquired using a data acquisition card (PCI-7831R) and Labview FPGA module (see Figure A-2 and Alkar (2007) for more details.)

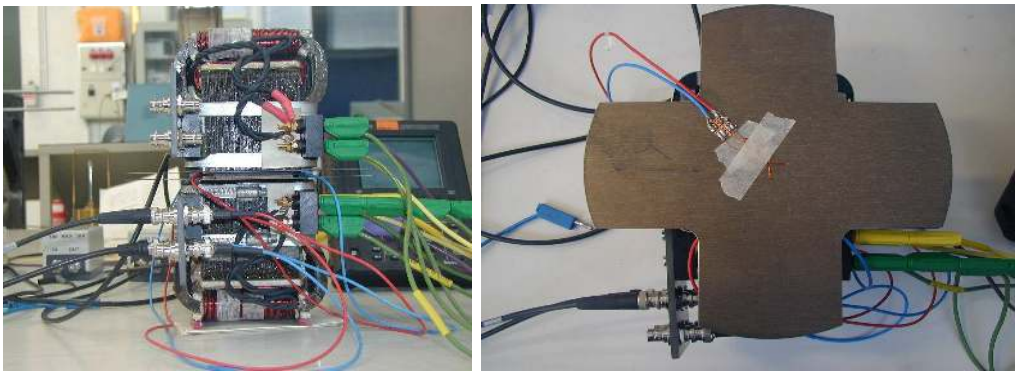

(a) Vertical yoke (b) Sample

Figure A-1: Measurement setup of the dynamic hysteresis loops.

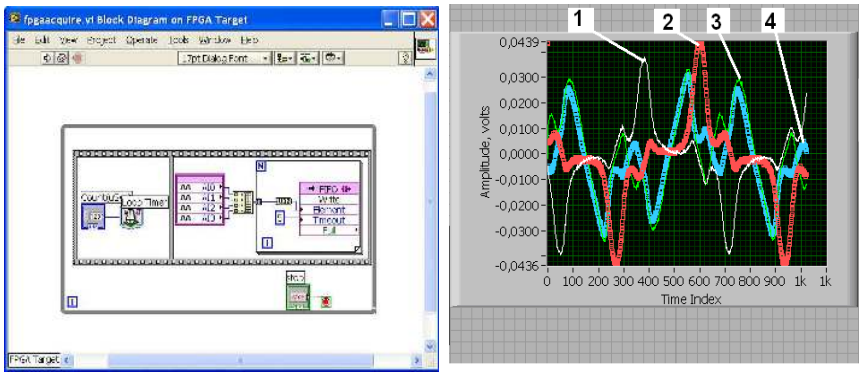

(a) Labview FPGA module (b) Acquired waveforms

Figure A-2: Computer Labview program of the measuring setup.

Appendix B

Characteristics of Motor I

Table B-1: The main parameters of the squirrel-cage induction motor referred to as Motor I.

Parameter	Value
Number of poles	4
Number of phases	3
Outer diameter of the stator core [mm]	310
Inner diameter of the stator core [mm]	200
Number of the stator slots	48
Number of rotor slots	40
Rated voltage [V]	400
Rated power [kW]	37
Rated frequency [Hz]	50
Connection	Star

The magnetic materials of the stator and rotor are fully processed non-oriented steel sheets.

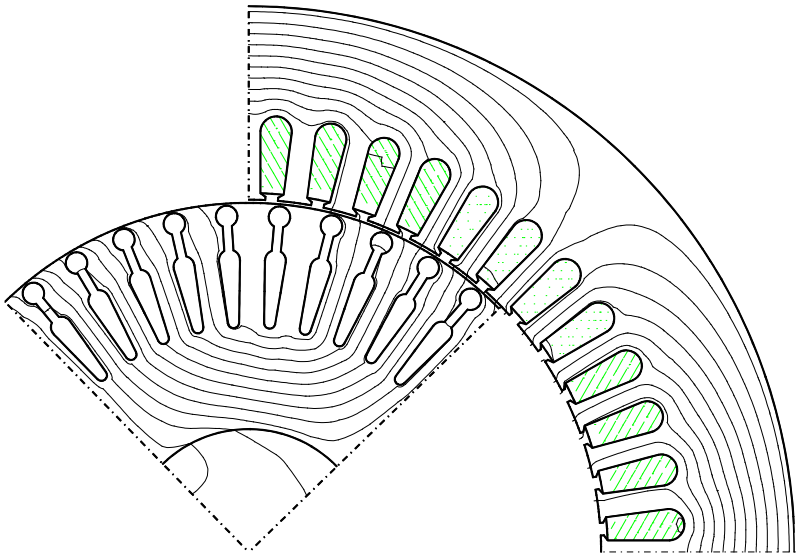

Figure B-1: The geometry of the squirrel-cage induction motor (Motor I) and the distribution of the flux at the rated load.

Appendix C

Characteristics of Motor II

Table C-1: The main parameters of the high-speed induction motor referred to as Motor II.

Parameter	Value
Number of poles	2
Number of phases	3
Outer diameter of the stator core [mm]	290
Diameter of the solid iron of the rotor [mm]	123
Number of the stator slots	36
Rated voltage [V]	400
Rated power [kW]	200
Rated frequency [Hz]	500
Connection	Delta

The magnetic materials of the stator are fully processed non-oriented steel sheets. The rotor is made of solid steel (semi-hard magnetic material).

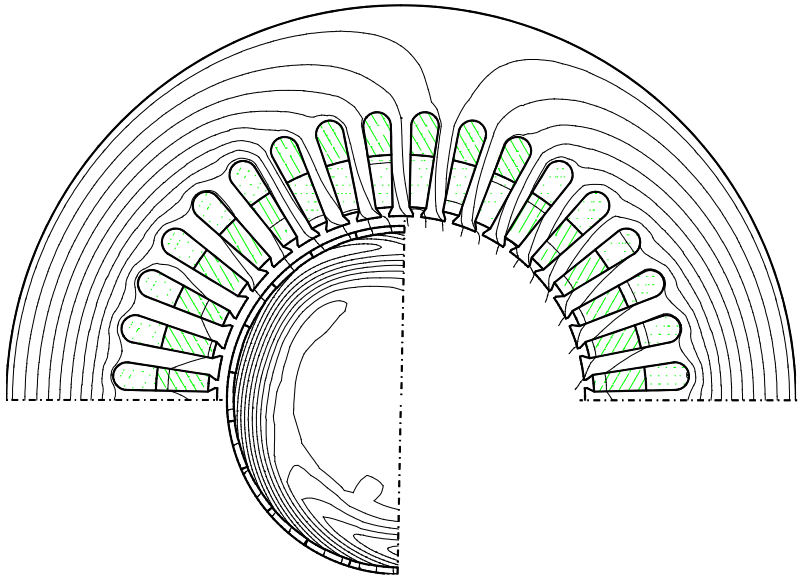

Figure C-1: The geometry of the high-speed induction motor (Motor II) and the distribution of the flux at the rated load.

ISBN 978-951-22-9276-9
ISBN 978-951-22-9277-6 (PDF)
ISSN 1795-2239
ISSN 1795-4584 (PDF)